Targeting Oncogenic Transcription Factors in Alveolar Rhabdomyosarcoma

Dissertation
zur
Erlangung der naturwissenschaftlichen Doktorwürde
(Dr. sc. nat.)

vorgelegt der
Mathematisch-naturwissenschaftlichen Fakultät
der
Universität Zürich
von

Verena Thalhammer

aus
Deutschland

Promotionskomitee

Prof. Dr. Beat Schäfer (Vorsitz und Leitung der Dissertation)
Prof. Dr. Ian Frew
Prof. Dr. Alex Hajnal
Prof. Dr. Carola Ponzetto

Zürich, 2015

The experimental work presented in this thesis was performed at the Department of Oncology and Children's Research Center, University Children's Hospital Zurich. The supervision of this thesis was conducted by Prof. Dr. Beat Schäfer (University Children's Hospital Zurich), Prof. Dr. Ian Frew (University of Zurich), Prof. Dr. Alex Hajnal (University of Zurich), and Prof. Dr. Carola Ponzetto (University of Torino).

Zurich, 2015

Verena Thalhammer

To my parents

Table of contents

1 Summary

Various different tumors are characterized by oncogenic addiction to transcription factors, which are frequently mutated and aberrantly expressed. These transcription factors represent ideal therapeutic targets supposing that specific inhibition might improve therapeutic outcome and minimize treatment related side effects. While direct targeting of transcription factors remains a pharmaceutical challenge due to unfavorable structure, we developed an efficient strategy to impair their activity in fusion positive alveolar rhabdomyosarcoma (aRMS). This aggressive pediatric tumor is mainly driven and maintained by the tumor-specific chimeric transcription factor PAX3-FOXO1. As the PAX3-FOXO1-underlaying translocation is often the sole genetic alteration detected in aRMS biopsies, this tumor is highly addicted to the emerging oncogenic transcription factor and consequently its depletion induces apoptosis of cancer cells. Hence, we believe that establishing a targeting approach to antagonize activating posttranslational modifications of the PAX3-FOXO1 fusion protein might improve aRMS treatment to overcome resistance to conventional therapy.

In fact, utilizing mass spectrometric analysis, we detected multiple phosphorylation sites in PAX3-FOXO1. Having established a two-armed activity reporter system to screen for druggable upstream regulatory kinases in aRMS cells, we applied a kinome siRNA library as well as a small-molecule library and identified polo-like kinase 1 (PLK1) and casein kinase 1α (CK1α) as modulators of PAX3-FOXO1. We could further demonstrate binding of PLK1, likely induced by CDK1 priming, and cooperation of PLK1 and CK1α in direct phosphorylation of PAX3-FOXO1 at the novel phospho-site S503, respectively in phosphorylation within the previously characterized octapeptide. Phosphorylation of S503 led to protein stabilization, whereas phosphorylation of the octapeptide mediated fusion protein transactivation.

With promising PLK1 inhibitors in clinical studies, such as BI 2536 and BI 6727, we first of all focused on antagonizing PLK1. PLK1 inhibition resulted in ubiquitination and proteasomal degradation of the fusion protein, subsequent reduction of target gene expression and induction of apoptosis. We believe that objective responses observed in aRMS xenograft mouse models are the result of different mechanisms induced by PLK1 inhibition, with a central, dominant role of the novel PLK1 - PAX3-FOXO1 axis. In addition, mechanistic data imply, next to PAX3-FOXO1 and NMYC oncogene reduction, a cell cycle arrest that potentiates PAX3-FOXO1 degradation.

Moreover, tissue microarray analysis of human aRMS tumor biopsies showed PLK1 overexpression and multivariate analysis offered prognostic significance of PLK1 for event-free and overall survival of aRMS patients. As one of the first markers at all, PLK1 might therefore be used for prognosis of fusion positive RMS and thus have major implications on risk stratification and treatment options.

However, monotherapy with kinase inhibitors can induce escape mechanisms and cause drug resistance as observed in our *in vivo* studies. Thus, we propose different rational combinations with PLK1 inhibitors based on our screening results. Our findings highlighted phosphatidylinositol and MAPK signaling as well as cell cycle regulation to exert impact on PAX3-FOXO1 activity. Moreover, we discovered cooperating functions of PLK1, PLK4 and CK1α, which might be relevant for prevention of resistance to PLK1 inhibition. Especially, overexpression of PLK4 in fusion positive tumors suggests synergistic cytotoxicity by simultaneous inhibition of PLK1 and PLK4. Tumor specific treatment combination could furthermore enable the generation of a favorable therapeutic window, which is indispensable considering potential adverse effects of PLK1 inhibition.

In summary, we established a promising strategy to target oncogenic transcription factors. Our preclinical studies validated the PLK1 - PAX3-FOXO1 axis as a highly relevant target in alveolar rhabdomyosarcoma and our data suggest translation into clinical practice.

2 Zusammenfassung

Eine Vielfalt von Tumoren ist durch onkogene Abhängigkeit von Transkriptionsfaktoren charakterisiert, welche häufig mutiert sind und anomal exprimiert werden. Da sich diese Transkriptionsfaktoren deshalb ideal als therapeutische Angriffspunkte eignen, könnte deren spezifische Inhibition Therapieergebnisse verbessern und behandlungsbedingte Nebenwirkungen minimieren. Während die direkte Inhibition von Transkriptionsfaktoren aufgrund unvorteilhafter Struktur weiterhin eine pharmazeutische Herausforderung darstellt, haben wir eine effiziente Strategie zur Hemmung ihrer Aktivität im Fusions-positiven alveolären Rhabdomyosarkom (aRMS) entwickelt. Diese aggressive, pädiatrische Krebsart wird hauptsächlich durch den tumorspezifischen, chimären Transkriptionsfaktor PAX3-FOXO1 hervorgerufen, welchem eine Chromosomentranslokation zugrunde liegt und welcher das Überleben von Tumorzellen sichert. Somit ist aRMS von PAX3-FOXO1 hochgradig abhängig und folglich induziert die Schwächung von PAX3-FOXO1 Apoptose in Krebszellen. Daher glauben wir, dass die Etablierung eines gezielten Ansatzes zur Hemmung aktivierender posttranslationaler Modifikationen die Behandlungsaussichten für aRMS verbessern würde und so aRMS-Resistenzen gegenüber konventionellen Therapien überwunden werden könnten.

Tatsächlich haben wir durch massenspektrometrische Analyse mehrere Phosphorylierungsstellen detektiert. Nach der Entwicklung und Etablierung eines zweiarmiges Aktivitäts-Reportersystems, welches darauf abzielt, systematisch nach medikamentös behandelbaren, regulatorischen Kinasen zu suchen, setzten wir eine Kinom-siRNA-Bibliothek und eine Bibliothek sogenannter „kleiner Moleküle“ ein und identifizierten Polo-like Kinase 1 (PLK1) und Casein Kinase 1α (CK1α) als Modulatoren von PAX3-FOXO1. Wir konnten die Bindung von PLK1 - wahrscheinlich eingeleitet durch sogenanntes „CDK1 priming” - sowie die Kooperation von PLK1 und CK1α in direkter Phosphorylierung von PAX3-FOXO1 an der neuen Phosphorylierungsstelle S503, respektive innerhalb des im Vorfeld charakterisierten Oktapeptids nachweisen. Die Phosphorylierung von S503 führte dabei zu Proteinstabilisierung, während Phosphorylierung des Oktapeptids Transaktivierung des Fusionsproteins verursachte.

Aufgrund vielversprechender Studienresultate in Bezug auf PLK1 Inhibitoren wie etwa BI 2536 und BI 6727, konzentrierten wir uns in der Folge darauf, PLK1 zu hemmen. PLK1 Inhibierung verursachte Ubiquitinierung und proteasomale Degradierung des Fusionsproteins, anschließende Verringerung der Zielgen-Expression sowie die Einleitung von apoptotischen Mechanismen. Wir glauben, dass der erzielte Behandlungseffekt in Xenograft-Mausmodellen das Resultat verschiedener, durch PLK1 Inhibierung induzierter Mechanismen mit einer zentralen, dominanten Rolle der neuentdeckte PLK1 - PAX3-FOXO1 Achse ist. Mechanistische Daten implizieren neben der Abnahme der Onkogene PAX3-FOXO1 und NMYC einen Zellzyklusarrest, welcher die PAX3-FOXO1 Degradierung verstärkt. Darüberhinaus zeigten Gewebeschnitts-Analysen von humanen Tumorbiopsien eine PLK1-Überexprimierung. Schlussendlich demonstrierten multivariate Analysen den signifikanten prognostischen Wert von PLK1 im Hinblick auf ereignisfreie und gesamte Überlebensraten von aRMS Patienten. Als einer der ersten Marker überhaupt könnte PLK1 deshalb für Prognosen von Fusions-positiven RMS Tumoren verwendet werden und somit zukünftig bedeutende Auswirkungen auf die Risiko-Stratifizierung und auf Behandlungsoptionen haben.

Dennoch kann entsprechend unserer Beobachtungen in *in vivo* Studien eine Monotherapie mit Kinase-Inhibitoren Ausweichmechanismen erzeugen und Medikamentenresistenz bewirken. Basierend auf unseren Screening-Resultaten schlagen wir deshalb konsequenterweise verschiedene Kombinationen mit PLK1 Inhibitoren vor. Unsere Ergebnisse zeigen auf, dass insbesondere Phosphatidylinositol- und MAPK-Signaltransduktion bedeutenden Einfluss auf die Aktivität von PAX3-FOXO1 ausüben. Zudem haben wir eine Kooperation von PLK1, PLK4 und CK1α entdeckt, welche relevant für Resistenzen gegenüber PLK1 Hemmung sein könnte. Insbesondere die Überexprimierung von PLK4 in Fusions-positiven Tumoren lässt synergistische Zytotoxizität durch gleichzeitige Inhibierung von PLK1 und PLK4 vermuten. Tumorspezifische Kombinationsbehandlung ermöglicht des Weiteren die Bildung eines bevorzugten therapeutischen Fensters, welches in Anbetracht potentieller Nebenwirkungen der PLK1 Hemmung, unabdingbar ist.

Zusammenfassend haben wir eine erfolgsversprechende Strategie zur gezielten Hemmung onkogener Transkriptionsfaktoren erarbeitet. Unsere präklinischen Studien konnten die PLK1 - PAX3-FOXO1 Achse als hochrelevantes Ziel im alveolären Rhabdomyosarkom validieren und unsere Daten legen eine Übertragung in die klinische Praxis nahe.

3 Abbreviations

14-3-3γ	Tyrosine 3-monooxygenase/tryptophan 5-monooxygenase activation protein, gamma
ABCB1	ATP-binding cassette sub-family B member 1
ABCG2	ATP-binding cassette sub-family G member 2
ACN	Acetonitrile
ADAM	Metalloproteinase; ADAM = a disintegrin and metalloproteinase
AKT	v-Akt murine thymoma viral oncogene homolog
ALK	Anaplastic lymphoma kinase
ALL	Acute lymphoblastic leukemia
AmBIC	Ammonium bicarbonate
AML	Acute myeloid leukemia
AP2β	Transcription factor AP2 beta
APC	Anaphase promoting complex
ARF	Alternate reading frame
aRMS	Alveolar rhabdomyosarcoma
ATP	Adenosine triphosphate
BALB/c	Albino laboratory-bred strain of mus musculus
BCL-XL	BCL2-like 1
BCL2	B-cell CLL/lymphoma 2
BCOR	BCL6 co-repressor
BET	Bromo and extra terminal family
BORA	Aurora kinase A activator
BRD4	Bromodomain containing 4
BSA	Bovine serum albumin

BUB1B	BUB1 mitotic checkpoint serine/threonine kinase B
CARD11	Caspase recruitment domain family, member 11
CCND	Cyclin D
CD44v6	CD44 molecule variant 6
CDC25	Cell division cycle 25
CDE	Cycle-dependent element
CDH3	P-cadherin
CDK	Cyclin-dependent kinase
CDKN2A	Cyclin-dependent kinase inhibitor 2A
cDNA	Complementary deoxyribonucleic acid
CHR	Cell cycle gene homology region
CHX	Cycloheximide
CI	Confidence interval
CIAP	Calf intestinal alkaline phosphatase
CID	Collision-induced dissociation
CK1	Casein kinase 1
CML	Chronic myeloid leukemia
CNR1	Cannabinoid receptor type 1
CNS	Central nervous system
CSNK1A1	Casein kinase 1, alpha 1
CTNNB1	Beta-catenin
CXCR4	CXC chemokine receptor type 4
DAPI	4',6-Diamidino-2-phenylindole
DMEM	Dulbecco's minimum essential medium
DMSO	Dimethyl sulfoxide
Dpn1	Restriction endonuclease to digest methylated GATC sites

DTT	Dithiothreitole
E2F1	Transcription factor E2F1
ECT2	Epithelial cell transforming 2
EDTA	Ethylene diamine tetraacetic acid
EFS	Event-free survival
EGR1	Early growth response 1
EMI1	Metazoan protein early mitotic inhibitor 1
ERK	Extracellular signal regulated kinase
eRMS	Embryonal rhabdomyosarcoma
EZH2	Enhancer of zeste 2 polycomb repressive complex 2 subunit
FACS	Fluorescence activated cell sorting
FBS	Fetal bovine serum
FBXW7	F-box/WD repeat-containing protein 7
FGFR4	Fibroblast growth factor receptor 4
Fig.	Figure
FLAG	Octapeptide DYKDDDDK
FOXM	Forkhead box M
FOXO	Forkhead box O
FRS2	Fibroblast growth factor receptor substrate 2
GAPDH	Glyceraldehyde 3-phosphate dehydrogenase
GFP	Green fluorescent protein
GSK3β	Glycogen synthase kinase 3 beta
GTP	Guanosine triphosphate
GTSE1	G2 and S-phase expressed 1
H2afx	H2A histone family, member X
HBSS	Hank's balanced salt solution

HEPES	4-(2-Hydroxyethyl)-1-piperazineethanesulfonic acid
HER2	v-ERB-B2 erythroblastic leukemia viral oncogene homolog 2
HPLC	High pressure liquid chromatography
HRAS	Harvey rat sarcoma viral oncogene homolog
HRP	Horseradish peroxidase
HsCYK4	Rac GTPase activating protein 1
HSP90	Heat shock protein 90
IAM	Iodoacetamide
IGF1R	Insulin-like growth factor 1 receptor
IGF2	Insulin-like growth factor 2
IGFBP2	Insulin-like growth factor binding protein 2
IgG	Immunoglobulin G
Il2rg	Interleukin 2 receptor, gamma chain
INK4	Inhibitor of cyclin-dependent kinase 4
INO80D	INO80 complex subunit D
IP	Immunoprecipitation
IRES	Internal ribosomal entry site
JARID2	Jumonji, AT rich interactive domain 2
KEGG	Kyoto Encyclopedia of Genes and Genomes pathway analysis
KIF11	Kinesin family member 11
KMT1A	Histone lysine N-methyltransferase
KRAS	Kirsten rat sarcoma viral oncogene homolog
LDS	Lithium dodecyl sulfate
LF/V	Luciferase activity / cell viability
LOH	Loss of heterozygosity
MAPK	Mitogen-activated protein kinase

MCL1	Myeloid cell leukemia 1
MCU/MICU1	Mitochondrial calcium uniporter/mitochondrial calcium uptake 1
MDM2	Mouse double minute 2 homolog
MEF	Mouse embryonic fibroblast
MEK	Dual specificity mitogen-activated protein kinase (MAPK) kinase
MET	Mesenchymal-epithelial transition factor
MIB1	Proliferation marker, antibody directed against Ki-67
MIR-17-92/ MIR17HG	Polycystronic microRNA encoding cluster
miRNA	Micro ribonucleic acid
MKLP2	Mitotic kinesin-like protein 2
MMP	Matrix metalloproteinase
mRNA	Messenger ribonucleic acid
MS	Mass spectrometry
MSC	Mesenchymal stem cell
mTOR	Mammalian target of rapamycine
mTORC1/2	mTOR complex 1 and 2
MYC	v-Myc avian myelocytomatosis viral oncogene homolog
MYF	Myogenic factor
MYL1	Myosin light chain 1
MYOD1	Myogenic differentiation 1
MYT1	Myelin transcription factor 1
NCOA1	Nuclear receptor and coactivator 1
NEK2	NIMA (never in mitosis gene a)-related kinase 2
NF1	Neurofibromin 1
NLP	Ninein-like protein
NMYC/MYCN	Neuroblastoma v-Myc avian myelocytomatosis viral oncogene

NOD	Non-obese diabetic
NRAS	Neuroblastoma rat sarcoma viral oncogene homolog
ORC2	Origin recognition complex, subunit 2
OS	Overall survival
p21	Cyclin-dependent kinase inhibitor 1A (p21, Cip1)
P3F	PAX3-FOXO1
p53	Tumor protein p53
p57KIP2	Cyclin-dependent kinase inhibitor p57
PARP	Poly (ADP-ribose) polymerase
PAX	Paired box protein
PBD	Polo-box binding domain
PBS	Phosphate buffered saline
PDGFRα	Platelet-derived growth factor receptor alpha
PDK1	3-Phosphoinositide dependent protein kinase 1
pGL4	Luciferase reporter vector
PI	Propidium iodide
PI3K	Phosphoinositide-3-kinase
PIK3CA	Phosphatidylinositol-4,5-bisphosphate 3-kinase alpha
PIPOX	Pipecolic acid oxidase
PKC	Protein kinase C
PKC412	Midostaurin
PKCA	Protein kinase C, alpha
PLK	Polo-like kinase
POU4F1	POU domain, class 4, transcription factor 1
PP	Protein phosphatase
PRC1	Protein regulator of cytokinesis 1

PRC2	Polycomb repressive complex 2
PRKAR2B	cAMP-dependent protein kinase type 2 beta
PTEN	Phosphatase and tensin homolog
qRT-PCR	Quantitative real-time polymerase chain reaction
RAF	RAF proto-oncogene serine/threonine protein kinase
RARA	Retinoic acid receptor, alpha
RAS	RAS GTPase; rat sarcoma viral oncogene homolog
RB	Retinoblastoma protein
RNA_i	RNA interference
ROS	Reactive oxygen species
SCC1	Sister chromatid cohesin protein 1
SCID	Severe combined immunodeficiency
SD	Standard deviation
SDS	Sodium dodecyl sulfate
siPF2	PAX3-FOXO1 directed siRNA
siRNA	Small interfering RNA
SRC	SRC proto-oncogene tyrosine kinase
STAT	Signal transducer and activator of transcription
STR	Short tandem repeat
TBS	Tris buffered saline
TERT	Telomerase reverse transcriptase
TET	Tetracycline
TFA	Trifluoroacetic acid
TMA	Tissue microarray
Tris	Tris(hydroxymethyl)-aminomethane
VSV-G	Vesicular stomatitis virus glycoprotein

WEE1	M phase inhibitor protein kinase
Wnt	Wingless type integration site
wt	Wild type
YES1	Yamaguchi sarcoma viral oncogene homolog 1
γ-TuRC	Gamma-tubulin ring complex

4 Introduction

4.1 Cancer

Cancer is a very complex disease with more than 100 different types, which can be further divided into different subtypes, again showing great heterogeneity. They are classified depending on the various kinds of normal tissue they arise from. Most of them develop from epithelial tissue and are called carcinomas. Non-epithelial tissue includes mesenchymal tissue giving rise to sarcomas, the hematopoietic system giving rise to leukemias or lymphomas, and the nervous system as tissue of origin. Furthermore, also atypical and mixed multi-lineage forms exist. Nevertheless, not only the tissue but also the age of onset of cancer development is used to distinguish between adult and pediatric cancer.

The development of cancer is a multi-step process reflecting genetic alterations leading to the transformation of a healthy to a malignant cell. These alterations include mainly point mutations, but also deletions, insertions, inversions, translocations and changes in chromosome numbers, which can result in the activation of oncogenes or the inactivation of tumor suppressor genes.

Despite complexity and heterogeneity between patients as well as between and even within metastatic lesions, underlying principles of transformation are common to probably most or all the different forms of cancer and have been summarized as the hallmarks of cancer by Hanahan and Weinberg (2000, 2011). These hallmarks describe transforming cells to sustain proliferative signaling, to evade growth suppression, to avoid immune destruction, to enable replicative immortality, to promote inflammation, to activate invasion and metastasis, to induce angiogenesis, to destabilize the genome, to resist cell death, and to deregulate cellular energetics (Fig. 1). Still, tumor progression is highly variable and cells take alternative pathways acquiring all the different capabilities as proven by exome and whole genome sequencing approaches allowing the generation of genomic landscapes to visualize genetic alterations for many of the most common cancer types. However, it is important to distinguish between driver and passenger alterations and also to consider epigenetic regulation, which can cause aberrant expression of driver genes. In total, Vogelstein and colleagues (2013) described 138 driver genes that lead to selective growth advantage. They can be summarized in 12 signaling pathways

spanning the core cellular processes cell survival, cell fate and genome maintenance (Fig. 2) (Vogelstein et al., 2013).

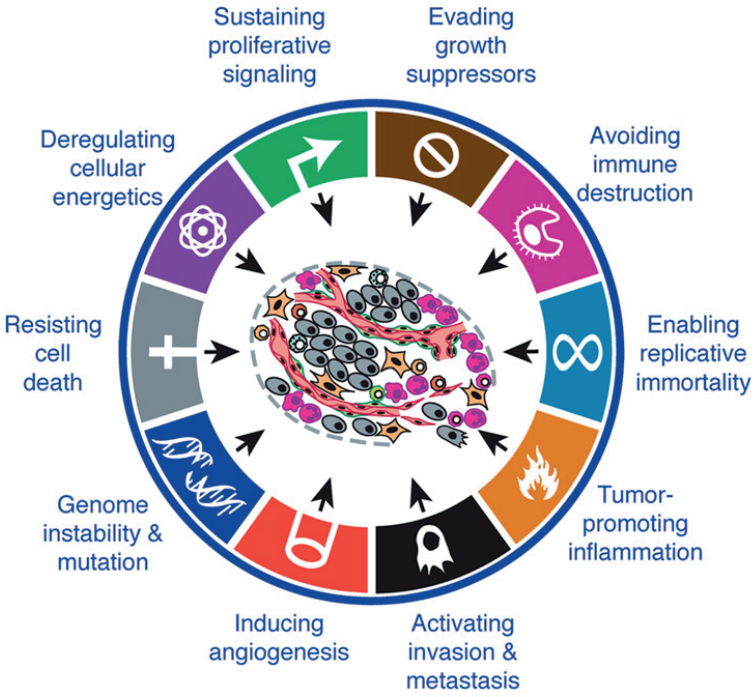

Fig. 1. Hallmarks of cancer. Cancer hallmark capabilities acquired during tumor development and progression are illustrated. Adapted from (Hanahan and Weinberg, 2011).

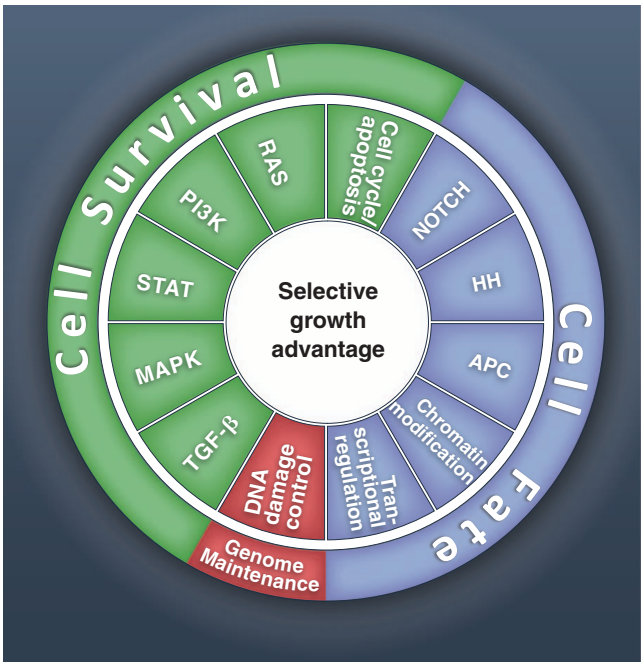

Fig. 2. Cancer cell signaling pathways and core processes. 138 driver genes identified in genetic landscapes of tumors have been classified into twelve pathways, which in turn mediate the regulation of the three core cellular processes cell survival, cell fate and genomic maintenance (Vogelstein et al., 2013).

4.2 Childhood cancer

Usually tumor evolution is a long-term process that needs time to acquire a series of mutations and thus the different cancer capabilities, meaning that the number of mutations is correlated with long-time exposure to potent mutagens like UV light or cigarette smoke, and also to age (Tomasetti et al., 2013). Consequently, pediatric tumors harbor fewer mutations than adult tumors (Fig. 3) (Vogelstein et al., 2013). Pediatric cancers often originate from non-self-renewing tissue or precursor cells with a shorter history of self-renewal in children than in adults, which reduces the probability for random mutations (Vogelstein et al., 2013). However, that does not mean that pediatric tumors do not fulfill all hallmarks of cancer. More likely, one single genetic event might simultaneously cause the acquisition of several different properties (Hanahan and Weinberg, 2000). Furthermore, pediatric cancers show a high frequency of mutations in genes encoding epigenetic regulators, which can affect transformation in multiple manners (Huether et al., 2014).

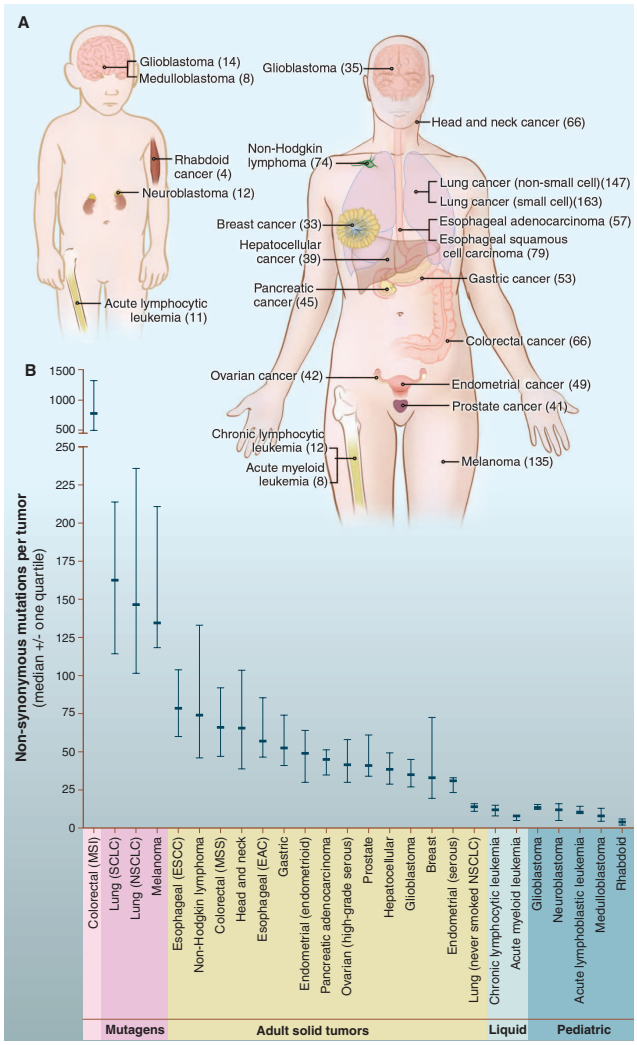

Fig. 3. Number of somatic mutations found in different cancer types. Indicated pediatric and adult cancers have been analyzed in genome-wide sequencing studies. Median numbers of mutations per tumor are shown in parenthesis in (A) and as graphic illustration in (B). Horizontal bars indicate the 25 and 75% quartiles. MSI, microsatellite instability; SCLC, small cell lung cancers; NSCLC, non-small cell lung cancers; ESCC, esophageal squamous cell carcinomas; MSS, microsatellite stable; EAC, esophageal adenocarcinomas (Vogelstein et al., 2013).

For these reasons and since pediatric cancers arise mainly in developing tissue, the spectrum of cancer types arising in childhood is very different from the one observed in the adult population. The most common types of childhood cancer are leukemias followed by CNS tumors and lymphomas. Carcinomas are very frequent in adults but not in the pediatric population, whereas many brain and solid tumors including medulloblastoma, neuroblastoma, rhabdomyosarcoma, Ewing sarcoma, osteosarcoma and Wilms tumor are almost exclusively found in children. Also, pediatric leukemias substantially differ from adult leukemias (Fig. 4) (Downing et al., 2012).

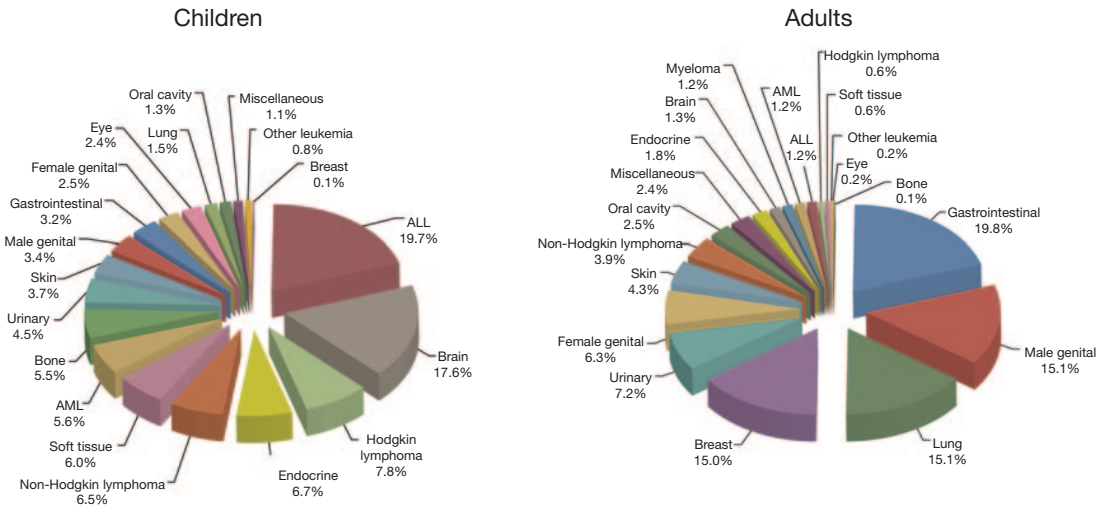

Fig. 4. Frequency of pediatric and adult cancer types. Graphics are based on 2012 Surveillance, Epidemiology and End Results (SEER) data. Adapted from (Downing et al., 2012).

Representing about 1% of all malignancies and an incidence rate of about 140 per million children aged younger than 14, childhood cancers are quite rare. However, incidence rates are increasing (Kaatsch, 2010; Ward et al., 2014). About 175,000 children younger than 15 years are annually diagnosed with cancer worldwide and in developed countries, cancer is actually the second most common cause of death in childhood (Ward et al., 2014). Although 5-year survival rates have improved with the discovery of cytotoxic chemotherapeutic agents and currently range at about 80%, aggressive pediatric tumors like rhabdomyosarcoma, Ewing sarcoma and osteosarcoma display resistance to conventional chemo- and radiotherapy leading to a 5-year survival rate of 60-65% (Linabery and Ross, 2008). Unfortunately, and in contrast to other pediatric malignancies, there has been no major improvement in mortality rates for these bone and soft tissue sarcomas during the last decades (Fig. 5). Despite a satisfying overall outcome and superior response rates to therapy in comparison to adults, future goals include development of innovative treatment of solid tumors as well as reduction of treatment side effects aiming at improvement in quality of life for long-term survivors (Smith et al., 2010).

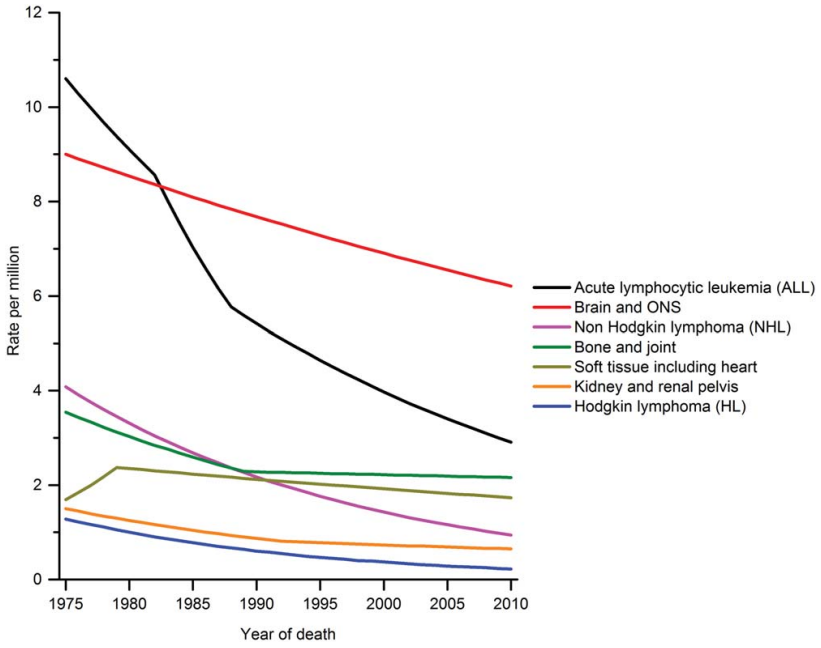

Fig. 5. Mortality rates for different pediatric cancer types. Children aged 0-19 years are included in the statistics from 1975 to 2010. Joinpoint fitted trends are shown. ONS, other nerve system (Ward et al., 2014).

4.3 Rhabdomyosarcoma

Rhabdomyosarcoma (RMS) accounts for 4-8% of all pediatric cancers and is the most common soft tissue sarcoma with an incidence rate of 4.3 per million and year. The two main subtypes embryonal (eRMS) and alveolar (aRMS) rhabdomyosarcoma share features of skeletal myogenesis and express embryonic or adult myogenic lineage markers but block terminal muscle differentiation. Both subtypes are first in line diagnosed by MYOD1 and myogenin expression controlling differentiation (De Giovanni et al., 2009). However, the origin of the two subtypes is probably not the same und is still under debate (Hettmer and Wagers, 2010). It was first of all suggested that RMS could originate from the myogenic lineage. eRMS might arise in myoblasts (Rubin et al., 2011), while aRMS could be experimentally induced in Myf6 expressing maturing muscle cells hypothesizing that dedifferentiation underlies the tumor formation (Fig. 6) (Keller and Capecchi, 2005). However, RMS can also occur in non-skeletal muscle sites like the biliary and the genitourinary tract. Furthermore, infiltration of bone marrow, which is reminiscent of acute leukemia, and cases without any detectably primary tumor have been reported (Lisboa et al., 2008). Hence, it has been suggested that aRMS could also originate from mesenchymal progenitors, which

are not committed to the myogenic lineage and can circulate to different organs and also be found in bone marrow (Hettmer and Wagers, 2010). Along these lines, also the adipogenic lineage or a non-myogenic neural crest-derived stem cell compartment are discussed as potential origins of eRMS (Hatley et al., 2012; Vogel et al., 1999).

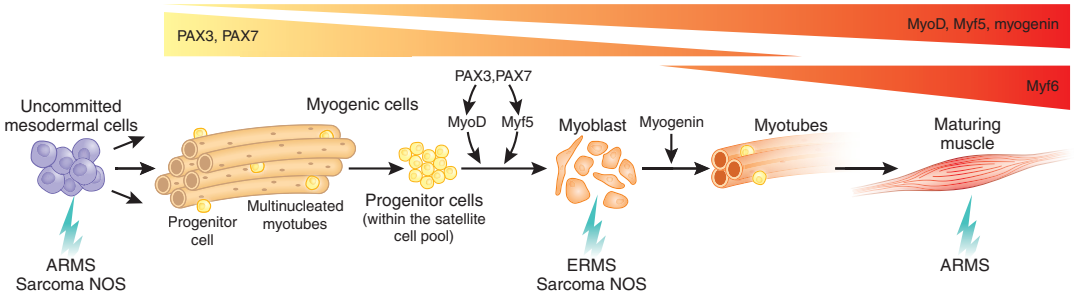

Fig. 6. Potential cellular origins of rhabdomyosarcoma subtypes during skeletal myogenesis. Expression of myogenic transcription factors PAX3, PAX7, MyoD, myogenin and Myf6, crucial for muscle specification, is indicated. Muscle progenitor cells are responsible for postnatal muscle maintenance and regeneration. Uncommitted MSCs could give rise to ARMS (aRMS) and undifferentiated sarcomas. A second hypothesis describes maturing muscles as the origin of ARMS. Myoblasts might generate ERMS (eRMS) and undifferentiated sarcomas. NOS, not otherwise specified (Hettmer and Wagers, 2010).

4.3.1 Clinical classification: Clinical features and therapy

eRMS and aRMS need to be distinguished not just in terms of origin but also regarding histology, incidence, age of onset, primary tumor localization, predestination of metastasis and outcome. With 60-70%, the majority of diagnosed RMS tumors compose the subgroup of embryonal RMS, which presents histologic features of immature skeletal muscle. eRMS predominately occurs in the head and neck as well as the genitourinary region of mainly 0-5 years old children. The 5-year overall survival is about 73% (Ognjanovic et al., 2009).

20% of RMS tumors are diagnosed as alveolar RMS, which gained its name due to the histological appearance resembling lung alveoli. aRMS mainly localizes to the trunk and the extremities and is more common in adolescents than in young children. It is more aggressive than eRMS, with a high tendency to metastasize, usually to lungs, bone marrow, lymph nodes and bones (Breneman et al., 2003). Thus, the 5-year overall survival of 48% is lower than in eRMS (Ognjanovic et al., 2009) and can even fall below 30% in metastatic cases (Malempati and Hawkins, 2012).

The very rare group of pleomorphic RMS tumors affects mainly adults with a 5-year overall survival rate of only 27% (Sultan et al., 2009).

Before therapy starts, patients are classified into different risk groups depending on clinical parameters and pathological features including histology, site, size, involvement of lymph nodes and metastases to receive risk-based multimodal treatment of different intensities (Malempati and Hawkins, 2012). Although protocols slightly differ in Europe and the United States, all patients undergo chemotherapy with standard regimens including vincristine, actinomycin-D and ifosfamide or cyclophosphamide. Topotecan and irinotecan are additionally used for intermediate and high-risk groups in US protocols. Furthermore, surgical intervention aims at complete resection of the primary tumor. Depending on group classification, radiotherapy is optionally applied for local control of the tumor (Van Gaal et al., 2012a). During the last decades, progress in treatment strategies led to improved outcomes of low and intermediate risk patients. Unfortunately, children with advanced RMS could not benefit so far, and clinical and pathologic features might not be sufficient to assign patients to different treatment protocols within the intermediate risk group (Chen et al., 2013; Dasgupta and Rodeberg, 2012).

4.3.2 Molecular classification: Genetic landscapes and aberrant signaling of rhabdomyosarcoma

Molecular classification and better understanding of RMS biology might help to develop novel targeted therapies, especially for the advanced RMS cases. At genetic level, the most prominent difference of eRMS and aRMS is the occurrence of specific chromosomal translocations. In about 70%-80% of aRMS, translocation of *PAX3* (60%-70%) or *PAX7* (10%) to *FOXO1* ((2;13)(q35;q14) or (1;13)(p36;q14)) results in the generation of a fusion protein. It consists of the PAX3/7 N-terminal paired domain and homeodomain encompassing the octapeptide motif, and the FOXO1 C-terminal transactivation domain (Fig. 7). In very rare cases translocations of *PAX3* to different genes like *NCOA1* or *INO80D* have been detected (Shern et al., 2014; Wachtel et al., 2004).

Translocation leads to higher expression, exclusive nuclear localization and enhanced activity of the emerging chimeric transcription factor compared to wild type PAX3 and FOXO1 (Olanich and Barr, 2013). Importantly, the fusion protein is also a highly relevant prognostic factor, especially comparing PAX3-FOXO1 expressing to fusion negative tumors (De Giovanni et al., 2009; Williamson et al., 2010). Sorensen et al.

(2009) reported a 4-year overall survival of only 8% for PAX3-FOXO1 positive tumors within the cohort of metastatic aRMS patients.

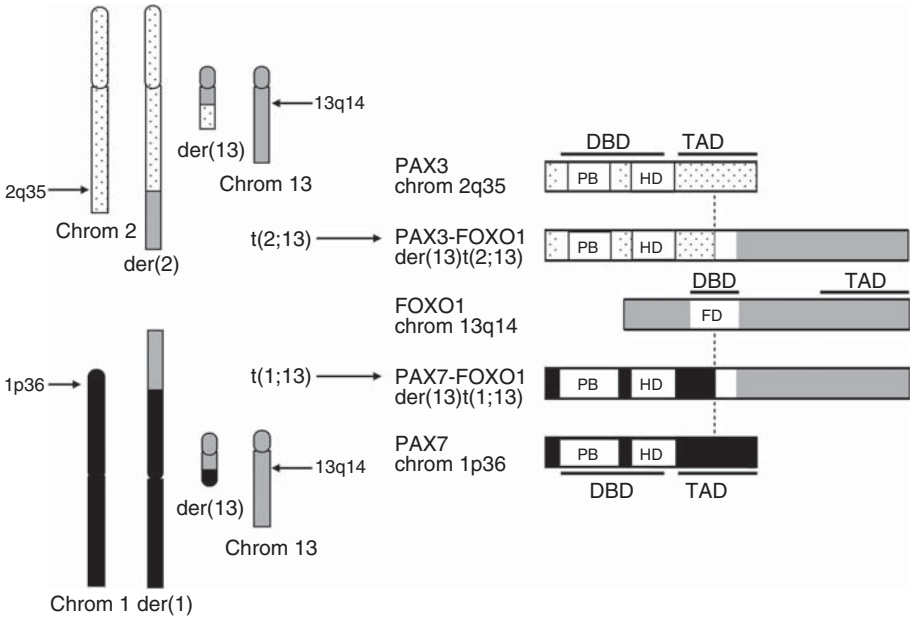

Fig. 7. Chromosomal translocations generating the chimeric fusion proteins PAX3-FOXO1 and PAX7-FOXO1. Translocation occurs between chromosome 2 and chromosome 13, respectively chromosome 1 and chromosome 13. Fusion proteins harbor complete paired domains and homeodomains of PAX3/7 and a complete transactivation domain of FOXO1. PB, paired domain; HD, homeodomain; FD, forkhead domain; DBD, DNA binding domain; TAD, transcriptional activation domain (Olanich and Barr, 2013).

The crucial role of determination of fusion protein status for classification of RMS types becomes further evident comparing genetic landscapes as well as gene expression analyses and regulation of differentiation of translocation positive and negative tumors. Sequencing approaches revealed that translocation negative tumors, including eRMS tumors, are characterized by a higher number of mutations and structural and copy number alterations than translocation positive RMS. Sequence analyses have identified mutations in the eight cancer consensus genes *NRAS, KRAS, TP53, NF1, RARA, CTNNB1, CARD11* and *PIK3CA* as well as recurrent alterations in *HRAS, FGFR4, FBXW7* and *BCOR* in patient-derived fusion negative tumors (Fig. 8) (Chen et al., 2013; Shern et al., 2014). Additionally, lesions could be detected in genes regulating cell cycle checkpoints (*BUB1B, FOXM1, CCND1* and *CCND2*). Apart from these mutations, eRMS tumors are characterized by a high frequency in loss of heterozygosity in 11p15.5 including *IGF2*. Also loss of imprinting at *IGF2* or

amplifications of *IGF1R* have been observed. Furthermore, *MDM2/FRS2* amplifications and *CDKN2A* deletions or loss of heterozygosity (LOH) as well as gain of chromosome 2, 8 and 13 were identified predominantly in fusion negative tumors. Overall, several studies showed that mutations were most commonly found in the RAS pathway (Chen et al., 2013; Paulson et al., 2011; Shern et al., 2014; Shukla et al., 2012), interestingly also significantly correlating with risk group classification (Chen et al., 2013). However, there was no significant increase in cytotoxicity of RAS pathway targeting drugs in primary orthotopic eRMS xenografts. This study further showed increased expression of p38MAPK pathway and decreased MCU/MICU1 expression implicated in oxidative stress suggesting it as therapeutically relevant pathway in eRMS.

In contrast, in fusion positive tumors neither cancer consensus genes, apart from the PAX3/7-FOXO1 translocation, nor any significantly enriched canonical pathway, could be identified. Very often the translocation was even the sole aberration detected (Fig. 8). The only mutation found in two independent studies was *PIKC3A* in 1 out of 17, respectively in only 1 out of 53 fusion positive aRMS patients next to just one tumor mutated in the transcriptional repressor *BCOR* in only one of the studies (Chen et al., 2013; Shern et al., 2014). However, amplifications of *CDK4* and *MYCN* were found with a slightly higher frequency (Shern et al., 2014). CDK4 is a regulator of G1/S cell cycle transition, whereas MYCN is an oncogenic transcription factor, regulating expression of TERT, MDM2 and IGF1R. Also, amplification of *MIR-17-92*, encoding a cluster of at least six miRNAs, was detected in a few cases and might be involved in cell survival, proliferation, differentiation, and angiogenesis. In addition, a further study showed that aberrations in ALK, a receptor tyrosine kinase activating the STAT3, AKT/PI3K and RAS/ERK pathways involved in proliferation, migration and survival are more commonly observed in aRMS than in eRMS (van Gaal et al., 2012b). Some aRMS tumors also depict loss of heterozygosity in 11p15.5 (Shern et al., 2014).

In conclusion, the low numbers of genetic lesions per tumor without any recognizable consensus indicate that mainly the fusion protein and expression of its target genes mediate tumor formation and progression of aRMS.

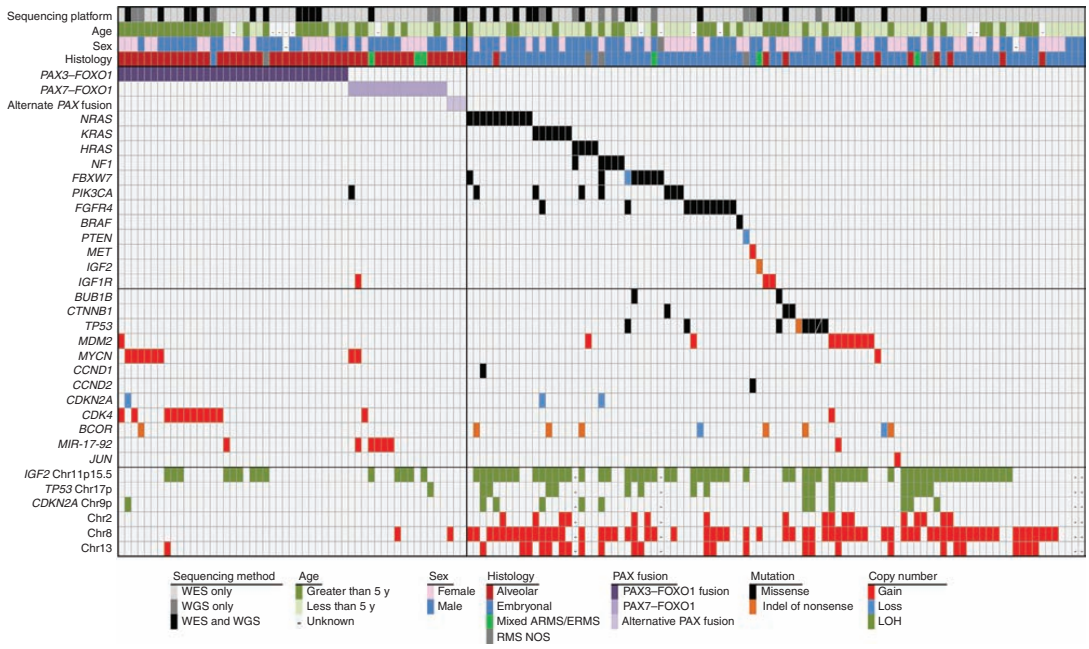

Fig. 8. Genomic landscape of rhabdomyosarcoma. Genomic alterations of 147 rhabdomyosarcoma cases identified by whole exome or whole genome sequencing are depicted. Age, years at diagnosis; WES, whole exome sequencing; WGS, whole genome sequencing; NOS, not otherwise specified (Shern et al., 2014).

4.3.3 Functions of PAX3-FOXO1

A number of studies have conducted gene expression and PAX3-FOXO1 binding site analysis. Comparing eRMS and aRMS tumors as well as introducing PAX3-FOXO1 into fusion negative RMS cells revealed a PAX3-FOXO1 dependent gene expression signature (Cao et al., 2010; Davicioni et al., 2006; De Pitta et al., 2006; Ebauer et al., 2007; Khan et al., 1998; Lae et al., 2007; Wachtel et al., 2004). Some of the most important and validated PAX3/7-FOXO1 targets include FGFR4, MET and CXCR4 involved in proliferation, migration and invasion, the oncogenic transcription factor MYCN, the anti-apoptotic BCL-XL, ADAM protease and elastase promoting metastasis, AP2β mediating cell survival, IGF2, CNR1 and CDH3 inducing migration and invasion as well as maintaining expression of the CDK4 cofactor cyclin D1 (Fig. 9) (Marshall and Grosveld, 2012; Olanich and Barr, 2013). Overall, it is very interesting that some of these target genes can additionally be impaired by genetic alterations.

Fig. 9. PAX3-FOXO1 target genes. Target genes contribute to development and progression of alveolar rhabdomyosarcoma promoting invasion, migration, proliferation, transformation, and survival. Adapted from (Marshall and Grosveld, 2012).

Although additional lesions like *p53* or *Ink4/Arf (Cdkn2A/B)* loss are necessary for the generation of aRMS mouse models and although the formation of aRMS-like tumors from human skeletal myoblasts requires expression of *TERT*, *MCYN* and loss *CDKN2A* next to PAX3-FOXO1 expression (Keller et al., 2004; Naini et al., 2008), the fusion protein is suggested to be the major oncogenic driver in fusion positive tumors. Accordingly and as stated earlier, alterations in exactly these genes or pathways were observed in sequenced tumors, including amplification of *CDK4,* the protein of which is directly inhibited by CDKN2A, amplification of *MYCN,* upstream of TERT, deletion of *CDKN2A*, and LOH at 11p15.5 encoding for the CDK inhibitor p57/KIP2 (Shern et al., 2014). Thus, these studies demonstrate the oncogenicity of PAX3/7-FOXO1 and suggest cooperation mainly by CDK4 and MYCN in tumorigenesis. In summary, considering the low frequency of genetic alterations apart from the translocation in aRMS reveals the biological relevance and the high potential of the fusion protein as therapeutic target.

Most interestingly, comparing genetic alterations of translocation positive and negative tumors demonstrates that many genes upregulated by the fusion protein are alternatively activated by genetic alteration in fusion negative tumors, including *FGFR4, CCND2, IGF2, MET, MYOD1,* and *CNR1*, which therefore likely contribute to tumor formation and progression (Fig. 10) (Shern et al., 2014).

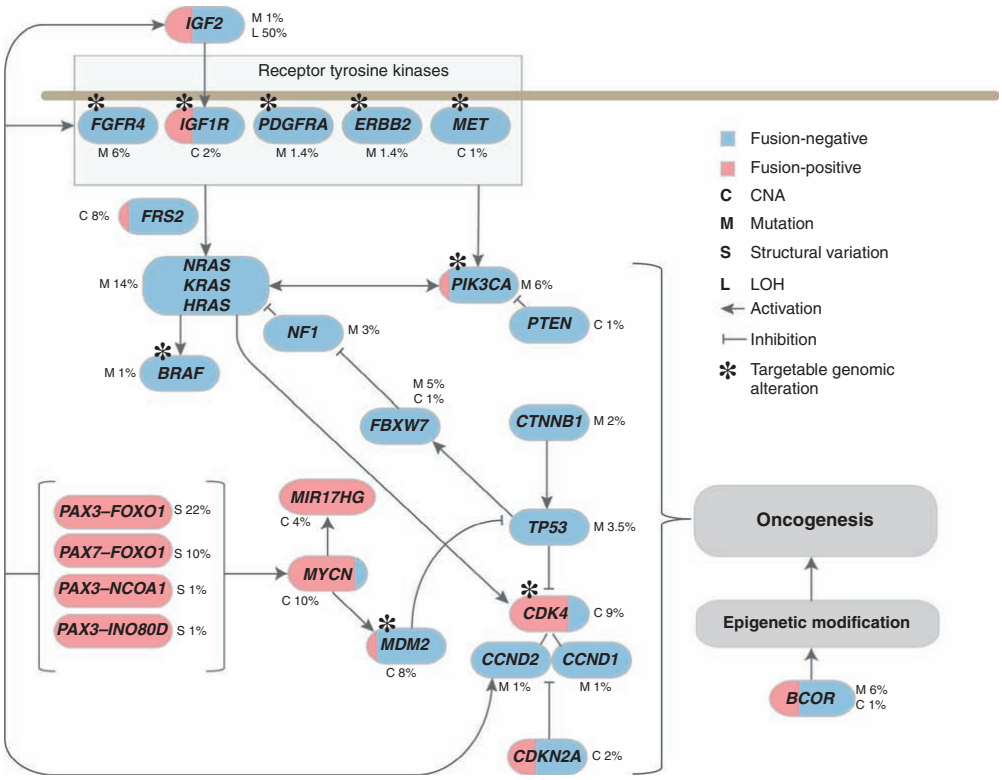

Fig. 10. Pathways altered in rhabdomyosarcoma. Model is based on genomic landscapes generated based on whole exome and whole genome sequencing. Alteration type and frequency of individual genes are depicted. CNA, copy number deletions and amplifications (Shern et al., 2014).

Fusion positive and negative tumors further share the common phenotype of impaired terminal differentiation, which is predominantly but not only mediated through suppressed activity of the myogenic transcription factor MYOD resulting in reduced expression of the muscle differentiation factor myogenin and the muscle specific differentiation mediator miR-206 (Keller and Guttridge, 2013). In eRMS, MYOD binding to E-box proteins is competed by musculin (Keller and Guttridge, 2013; Yang et al., 2009). In aRMS, myogenin transcription is epigenetically blocked by direct binding of the histone methyltransferase KMT1A to MYOD and by repression through the fusion target gene JARID2 in complex with PRC2 (Lee et al., 2011; Walters et al., 2014). Moreover, inhibition of MYOD target gene expression by PAX3-FOXO1 has been proposed as PAX3-FOXO1 expression diminished occupation of the myogenin promoter by RNA polymerase II and reduced histone H4 acetylation (Calhabeu et al., 2013). In addition, fusion target genes including FGFR4, IGF1R and MET further support proliferation while inhibiting differentiation (Keller and Guttridge, 2013).

Beyond its central role in oncogenic transformation and tumorigenesis, the fusion protein is also indispensable for maintenance of fusion positive tumor cells. Depletion of PAX3-FOXO1 leads to decreased proliferation, impaired motility, reduced invasion, and enhanced myogenic differentiation (Kikuchi et al., 2008). Furthermore, it is essential for tumor cell survival as its inhibition induces apoptosis (Bernasconi et al., 1996; Ebauer et al., 2007).

Summarizing all these facts, fusion protein function is mimicking different malignant abnormalities also found in eRMS. Importantly, translocation negative RMS tumors that have traditionally been classified as aRMS by histological features clustered with eRMS tumors when comparing genetic landscapes. Thus, genetic data suggest that the fusion protein status is more accurate for classification of rhabdomyosarcoma than histology.

4.3.4 Regulation of PAX3-FOXO1

Heterogeneity in Pax3-Foxo1 expression in primary and metastatic tumors of a genetically engineered conditional knock-in aRMS mouse model suggested that Pax3-Foxo1 is temporally regulated in a cell cycle dependent manner. Indeed, a dynamic regulation with an enhanced expression of mRNA and protein in G2, but not M phase, could be shown for mouse as well as human aRMS cells indicating its regulation at transcriptional level (Kikuchi et al., 2014). Furthermore, genome-wide expression analysis of 2N and 4N sorted cells, before and after Pax3-Foxo1 depletion, revealed several G2/M checkpoint adaptation genes including Plk1, Cdc25b, H2afx, and survivin to be downregulated upon knockdown of the fusion protein. In addition, radiation led to a higher percentage of DNA double-strand breaks in Pax3-Foxo1 expressing mitotic cells and lower induction of apoptosis indicating that the fusion protein facilitates G2/M transition before DNA damage repair is completed. Consequent genomic instability and aneuploidy due to checkpoint adaptation are strategies of tumor cell survival (Kikuchi et al., 2014).

As a principle of cell cycle progression proteins become posttranslationally modified and are controlled by the interplay of phosphorylation, dephosphorylation, ubiquitination, and subsequent proteolytic cleavage by the 26S proteasome. For its dynamic cell cycle regulation, also PAX3-FOXO1 might be actively degraded. Roeb et al. demonstrated ubiquitination of PAX3-FOXO1 and therefore its subjection to proteasomal degradation (Roeb et al., 2007). Surprisingly, this even caused co-

degradation of its binding partner EGR1 leading to impaired expression of the cell cycle regulators p57KIP2 as well as p21 and thus to maintenance of cell proliferation of myoblasts and interruption of myogenic differentiation (Hecker et al., 2010; Roeb et al., 2007; Roeb et al., 2008). These studies revealed a novel functional mechanism of PAX3-FOXO1 next to its role as transcription factor. Hence, it is likely that PAX3-FOXO1 also targets additional interaction partners by this mechanism. In conclusion, PAX3-FOXO1 is not just regulated during cell cycle but it actually actively overrides cell cycle checkpoints.

Phosphorylation can modulate different biological processes like cellular localization, enzymatic activation or repression in cellular signal transduction, transactivation of transcription factors, DNA binding, protein-protein interaction, stabilization or degradation to mediate cell cycle progression, growth, cell death, and differentiation. In PAX3-FOXO1, phosphorylation was identified at least at four out of six serines (S187, S193, S197, S201, S205 and S209) within the octapeptide region triggering DNA binding to mediate transcriptional activation. Moreover, PKC412, a broad-spectrum kinase inhibitor, demonstrated reduction of transcriptional activity. It was suggested that these phospho-sites work in concert, as only a combination of mutations at several of these sites was sufficient to partially rescue the inhibitory effect of PKC412 (Amstutz et al., 2008). PKC, represented within the target profile of PKC412, was discussed as one of the potential upstream kinases since its influence on PAX3 activity has also been shown in presomitic mesoderm (Fig. 11) (Brunelli et al., 2007).

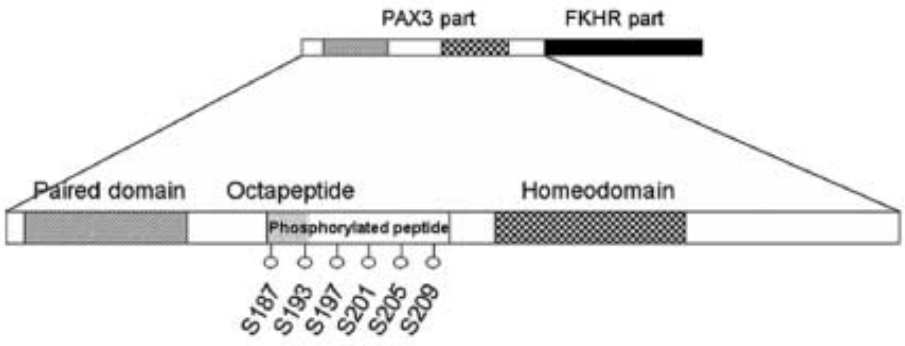

Fig. 11. Phosphorylation sites in PAX3. Localizations of phospho-sites as identified by mass spectrometry of PAX3 are schematically illustrated. FKHR = FOXO1. Adapted from (Amstutz et al., 2008).

Phosphorylation of wild type Pax3 was confirmed in a series of further studies showing phosphorylation of S205 in proliferating mouse myoblasts, whereas phosphorylation of S201 and S209 was demonstrated during early myogenic differentiation. In these studies GSK3β and CK2 were proposed as potential upstream kinases. Accordingly, also phosphorylation of PAX3-FOXO1 at S201 and S205, but not S209, could be observed in proliferating as well as differentiating myoblasts (Fig. 12) (Dietz et al., 2009; Dietz et al., 2011; Iyengar et al., 2012; Miller et al., 2008).

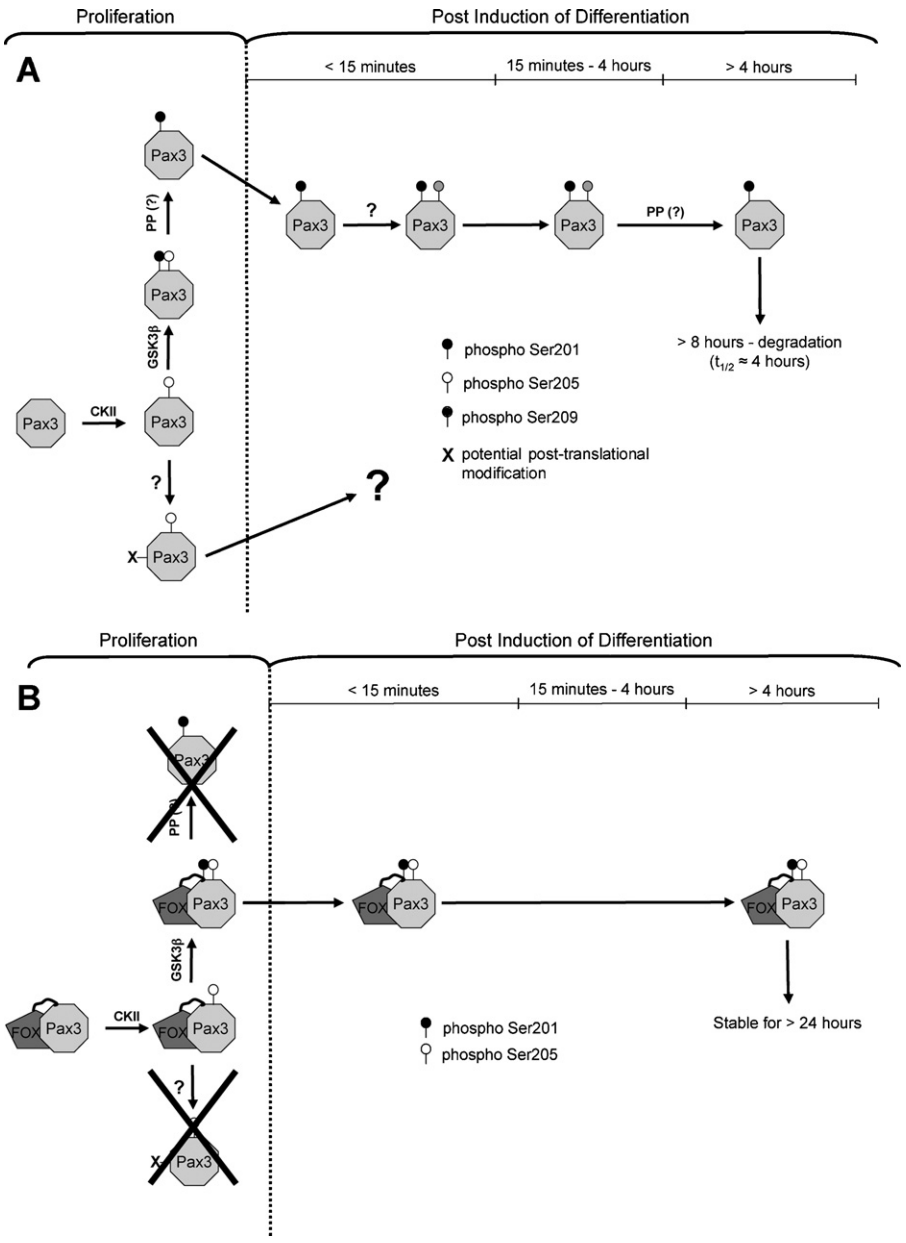

Fig. 12. Model for sequential phosphorylation events in Pax3 (A) and Pax3-FOXO1 (B) during early myogenic differentiation (Dietz et al., 2011).

Also Zeng et al. (2010) reported that GSK3 phosphorylates the fusion protein *in vitro* and that its inhibition by TWS119 or knockdown of either GSK3α or GSK3β reduced transcriptional activity of PAX3-FOXO1. However, specific sites have not been addressed in this study.

Furthermore, a small molecule library screen identified the compound fascaplysin, an inhibitor of CDK4/cyclin D1, to suppress PAX3-FOXO1 activity by increasing its cytoplasmic levels while total protein levels were not affected. Accordingly, CDK4 directly phosphorylated the fusion protein at S430 *in vitro* and enhanced PAX3-FOXO1 activity. However, additional CDK4 sites have been proposed, as mutation of this one site did not fully abolish phosphorylation by CDK4 (Liu et al., 2013). This is of special interest as gain of CDK4 was one of the few mutations observed in sequenced aRMS tumors and loss of *Ink4a/Arf* locus, leading to activation of the Cdk4 pathway, together with PAX3-FOXO1 expression induced *in vivo* tumor formation (Keller et al., 2004; Shern et al., 2014).

The role of phosphorylation by AKT is complex and remains controversial. AKT activation in aRMS was reported to correlate with poor prognosis (Cen et al., 2007; Guenther et al., 2013; Petricoin et al., 2007). On the one hand, its attenuated activity sustained PAX3-FOXO1 transactivation, whereas on the other hand, differentiation dependent hyperactivation of AKT inhibited PAX3-FOXO1 by phosphorylation under differentiation-permissible conditions and therefore blocked terminal myogenic differentiation by suppressing MyoD expression (Jothi et al., 2012). Thus, AKT was suggested to balance fusion protein activity (Jothi and Mal, 2012). Interestingly, thapsigargin, a sarco-/endoplasmic reticulum Ca^{2+} ATPase inhibitor, induced AKT to phosphorylate the fusion protein by affecting intracellular Ca^{2+} levels. This phosphorylation in turn inhibited DNA binding of PAX3-FOXO1 and subsequently induced its proteasomal degradation supporting an inhibitory function of AKT phosphorylation (Jothi et al., 2013). However, the exact mechanism of this inhibition remains unclear. One possibility is that the inhibition is directly mediated by phosphorylation of the two AKT consensus sites S437 and S500 but also an indirect effect was suggested, for example through blockade of downstream GSK3 reducing PAX3-FOXO1 transactivation (Jothi et al., 2013).

In summary, regulation of PAX3-FOXO1 by phosphorylation is highly complex and probably dynamic, also depending on cell cycle and myogenic differentiation state.

4.4 Polo-like kinase 1

4.4.1 PLK family and structure

The PLK family is comprised of five serine/threonine kinases (PLK1 - PLK5) with key roles in cell cycle control. PLK1 and PLK4 are widely considered as oncogenes while PLK2, PLK3 and PLK5 are primarily linked to tumor suppressive functions mainly involved in replication checkpoint signaling, DNA damage response signaling and apoptosis induction. Interestingly, compensatory balances of different family members have been described, which might be based on their highly homologous features (Craig et al., 2014; Mason et al., 2014).

PLK1 - PLK4 are characterized by an N-terminal kinase domain, which is truncated in PLK5. In addition, PLK1, PLK2, PLK3 and PLK5 possess two polo-box binding domains (PBD) functioning as phospho-recognition modules necessary for protein-protein interactions and subcellular localization, whereas the cryptic PBD domain of PLK4 forms homodimers (Fig. 13) (Lee et al., 2014).

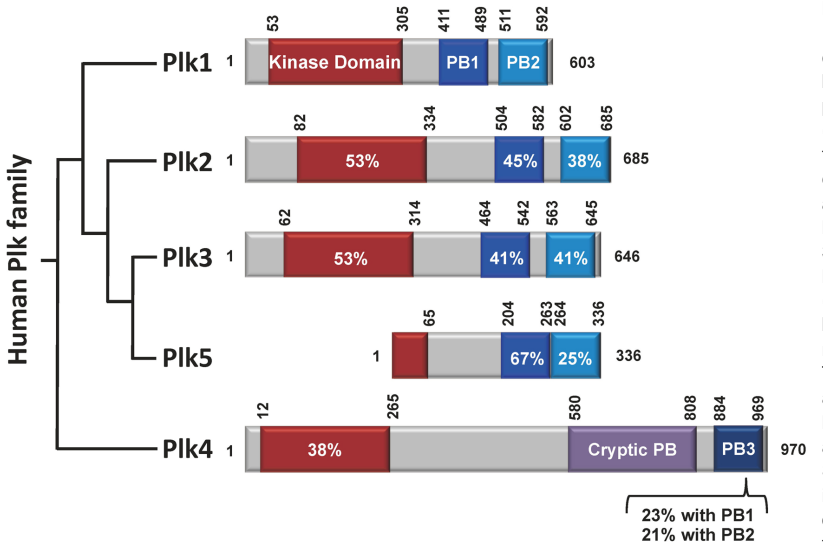

Fig. 13. Homology within the human PLK family. Percentages of sequence homologies of kinase and polo-box binding domains relative to PLK1 are depicted. PB, polo-box binding domain (Lee et al., 2014).

4.4.2 Regulation and functions of PLK1

PLK1 is regulated in a temporal but also in a spatial manner. It is mainly expressed starting at late S phase and peaking in G2/M phase. p53, p21, RB, E2F, and the CDE/CHR element (cell cycle dependent element/cell cycle gene homology region element) repress PLK1 expression, whereas FOXM1 induces its transcription. Interestingly, a positive feedback loop exists, as PLK1 itself is able to activate FOXM1. Furthermore, PLK1 is activated by T-loop phosphorylation at T210 by Aurora A/BORA or by Aurora B to relieve the suppressive interaction of polo-box binding domain and kinase domain (Archambault and Glover, 2009). PI3K/Akt dependent phosphorylation at S99 for 14-3-3γ binding is required for metaphase/anaphase transition (Kasahara et al., 2013). The polo-box binding domain is responsible for binding of interaction partners primed at consensus recognition motifs by proline-directed kinases such as CDKs or by self-priming. Substrate binding might further enhance kinase activity. On the contrary, deactivation is probably mediated by protein phosphatase 1 (PP1). Further inactivation is achieved by cell cycle dependent proteolysis in late M and G1 phase after ubiquitination by the E3 ligase APC^{Cdh1} (Cdh1 activated anaphase promoting complex) for degradation via the 26S proteasome (Archambault and Glover, 2009).

Mouse models have been generated to investigate Plk1 function. Homozygous knockout (*Plk1*$^{-/-}$) embryos were not viable and did not develop beyond the eight-cell stage indicating vital Plk1 functions during very early development. *Plk1*$^{+/-}$ mice developed lymphomas and pulmonary carcinomas suggesting that Plk1 haploinsufficiency might promote tumorigenesis. However, the sample size of this study was very small and Plk1 status has not been determined (Craig et al., 2014; Lu et al., 2008). A more recent study by Raab et al. (2011) used an inducible RNA_i system to knockdown Plk1 *in vivo* resulting in no significant phenotypic consequences. Nevertheless, teratomas formed by embryonic stem cells in which Plk1 has been depleted were significantly smaller than those formed by control embryonic stem cells indicating that Plk1 depletion inhibits tumor growth *in vivo* (Raab et al., 2011).

4.4.3 PLK1 as cell cycle regulator

PLK1 is a crucial regulator of several processes during cell cycle progression. It mediates mitotic entry, centrosome maturation, spindle assembly, APC/C regulation, as well as cytokinesis (Fig. 14).

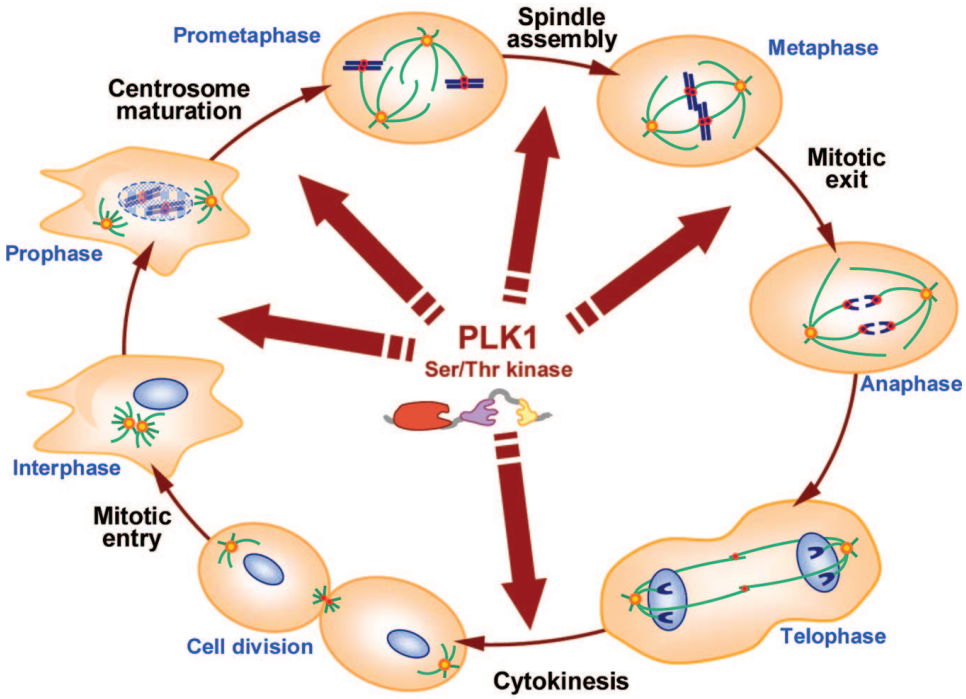

Fig. 14. Key functions of PLK1 in cell cycle regulation (Schoffski, 2009).

PLK1 is involved in centrosome maturation by taking over the function of ninein-like protein (NLP) in prophase to recruit the γ-tubulin ring complex (γ-TuRC) to centrosomes for microtubule nucleation. Furthermore, it phosphorylates kizuna suggested to function in mitotic centrosome architecture and localizes Aurora A to centrosomes (Fig. 15A). Before mitosis, CDK1 is phosphorylated by WEE1 and MYT1 to keep it inactive. PLK1 then induces mitotic entry by phosphorylating and activating the counteracting phosphatase CDC25 as well as by inhibiting WEE1 and MYT1. In addition, it also phosphorylates cyclin B1 promoting full activity of CDK1/cyclin B1 (Fig. 15B) (Strebhardt, 2010). Also RNA_i and PLK1 inhibitor studies indicate that PLK1 activity is important but not essential for mitotic entry while it is absolutely essential for mitotic progression (Lenart et al., 2007; van Vugt et al., 2004). PLK1 depletion was

shown to arrest cells in prometaphase. The metaphase/anaphase transition is controlled by the ubiquitin ligase anaphase promoting complex APC/C, which is kept in an inactive state until all chromosomes are properly aligned and kinetochors are bipolarly attached in metaphase. On the one hand, PLK1 phosphorylates the SA2 subunit of cohesin, a multi-protein ring complex surrounding the sister chromatids while shugoshin 1 and protein phosphatase 2A (PP2A) still protect them from separation. On the other hand, mitotic progression is guaranteed by activation of APC/C through PLK1 dependent phosphorylation of EMI1. Like this, PLK1 promotes the cleavage of cohesion protein 1 subunit (SCC1) by separase resulting in sister chromatid segregation (Fig. 15C). Finally, PLK1 is also involved in mitotic exit and cytokinesis. PLK1 phosphorylates and docks to MKLP2 and PRC1 localized at the spindle midzone in between the sister chromatids. This enables it to phosphorylate the Rho GTPase-activating protein HsCYK4 for recruitment of the rho GTP exchange factor ECT2 leading to assembly of the contractile ring and the generation of the cleavage furrow (Fig. 15D) (Chopra et al., 2010; Strebhardt, 2010).

Interestingly, in cancer cells PLK1 is also significantly expressed during interphase suggesting additional cell cycle functions. Indeed, it becomes more and more evident that PLK1 is also implicated in G1/S transition and DNA replication as well as in stress response to DNA damage in cancer cells (Cholewa et al., 2013). E2F regulates the transcription of cell cycle control and DNA synthesis genes such as PLK1. Frequent deregulation of E2F is associated with carcinogenesis and might cause PLK1 overexpression. PLK1 in turn promotes DNA replication under stress conditions in the presence of DNA damage by phosphorylation of ORC2 and therefore mediates checkpoint adaptation in S-phase potentially causing genomic instability (Cholewa et al., 2013).

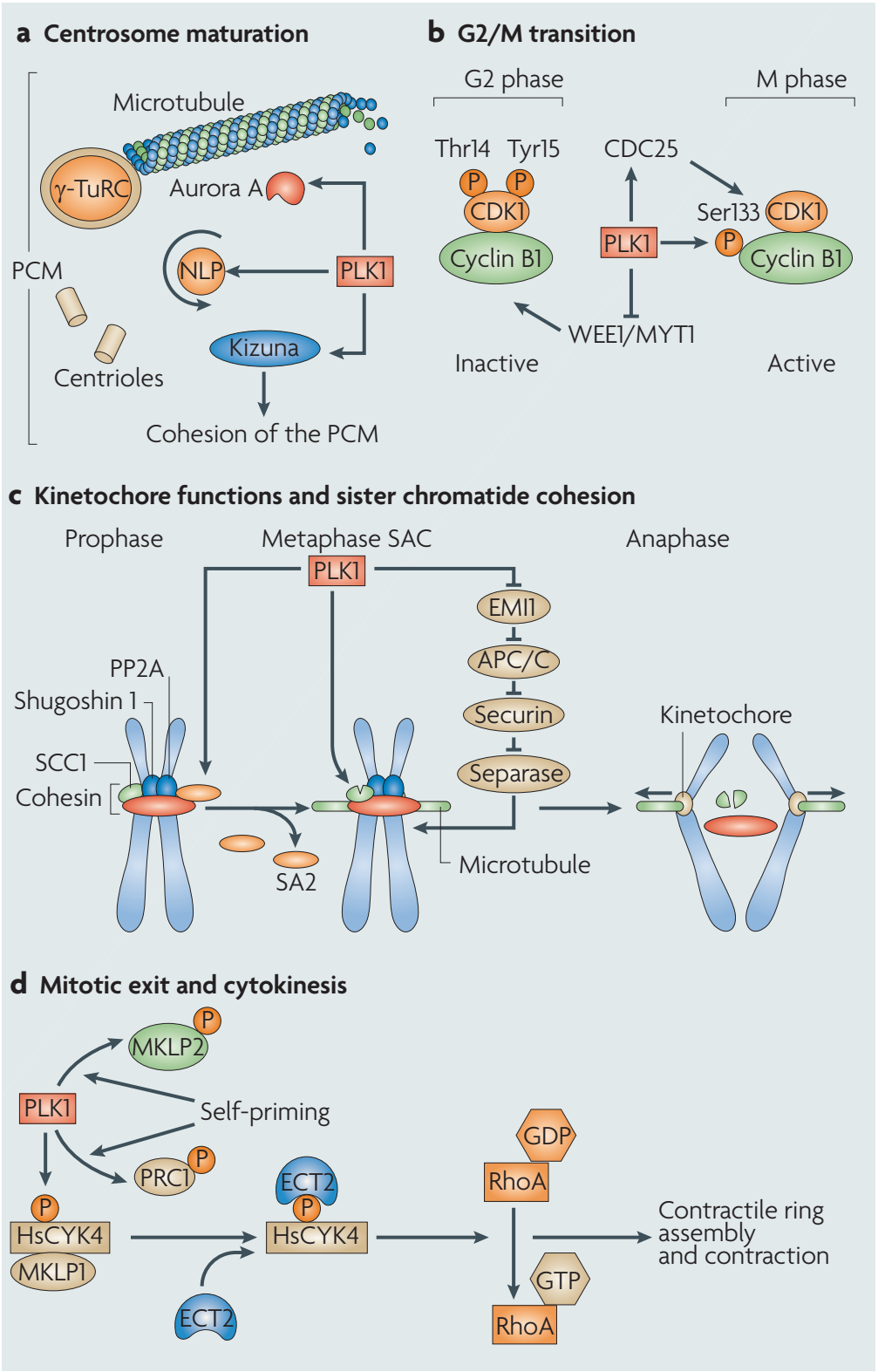

Fig. 15. Mitotic functions and targets of PLK1 (Strebhardt, 2010).

4.4.4 PLK1 in tumorigenesis

Overexpression of PLK1 causes malignant transformation of human fibroblasts leading to tumor growth when engrafted in nude mice, thus indicating a pivotal role in carcinogenesis (Smith et al., 1997). The tumorigenic potential of PLK1 can partly be explained by deregulation of the cell cycle. However, beyond its function in cell cycle regulation, PLK1 is directly associated with all three cancer core processes and eight out of twelve cancer cell signaling pathways, which have been described by Vogelstein et al. (2013) (Figs. 2 and 16) (Cholewa et al., 2013). Furthermore, several studies examined multiple interaction mechanisms of the oncogene PLK1 and the master tumor suppressor p53 demonstrating that the two proteins negatively regulate each other. p53 is defined as a stress response gene that induces cell cycle arrest or apoptosis. Along these lines, p53 can also inhibit the transcription of PLK1 and it is speculated that p53 loss of function, next to E2F deregulation, could be the basis for PLK1 overexpression in cancer. In addition p21, a transcriptional target of p53, can mediate repression via the CDE element or by direct binding to the *PLK1* promoter during oncogene-induced senescence. Generating feedback loops, also PLK1 is able to repress p21 expression and to control the activity of p53. First, PLK1 can reduce transcriptional activity and the pro-apoptotic function of p53 by direct binding. Second, PLK1 activity can induce degradation of p53 by promoting the p53-MDM2 association and by phosphorylation of the topoisomerase I binding protein topors, a combined ubiquitin and SUMO E3 ligase, inhibiting sumoylation while enhancing ubiquitination of p53. Third, PLK1 phosphorylates GTSE1 leading to nuclear export of p53 and therefore promoting its proteasomal degradation during DNA damage recovery (Fig. 16) (Cholewa et al., 2013). Overall, p53 inactivation by PLK1 is a central step of checkpoint termination leading to enhanced aneuploidy and genomic instability.

Further studies revealed an active function of PLK1 in invasion through the extracellular matrix by phosphorylation of vimentin regulating β1-integrin cell surface levels (Rizki et al., 2007). In addition, downregulation of PLK1 in thyroid carcinoma cells also resulted in downregulation of metalloproteases MMP-2 and MMP-9 and the adhesion protein CD44v6, which mediate cancer cell invasion (Zhang et al., 2012).

PLK1 is also suggested to protect against apoptosis as its expression was shown to maintain levels of anti-apoptotic survivin, BCL-2 and MCL1 (Feng et al., 2009).

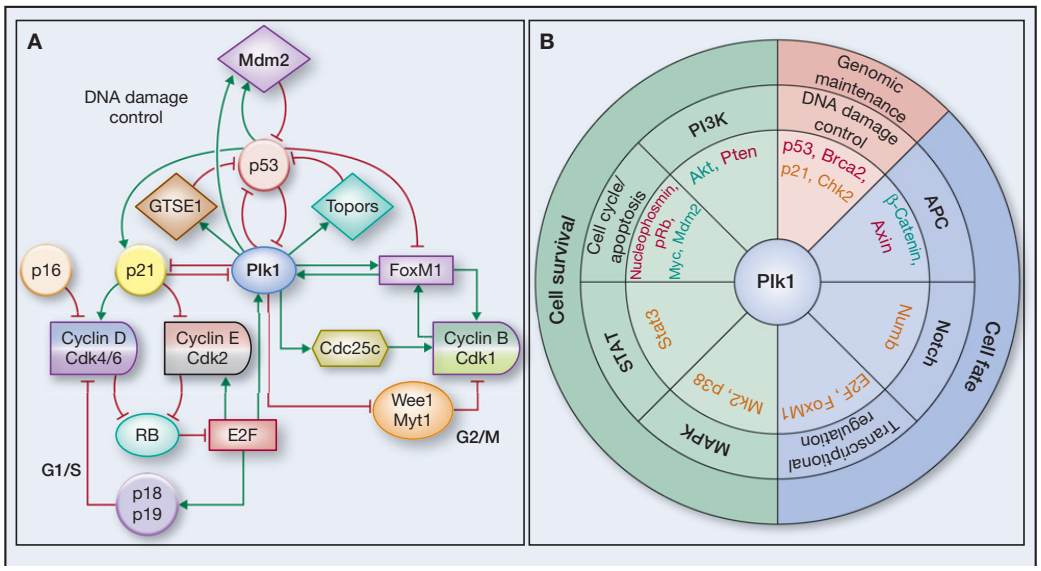

Fig. 16. PLK1 interactions with cancer associated pathways. (A) PLK1 is involved in G1/S and G2/M transition, and DNA damage control. It is regulated by multiple feedback loops. (B) Summary of direct PLK1 interactions with proteins associated with cancer promoting signaling pathways and core cellular processes. Green, transcribed by oncogenic driver genes; red, transcribed by tumor-suppressive driver genes (Cholewa et al., 2013).

4.4.5 PLK1 as cancer target

PLK1 was found to be overexpressed in a variety of different adult solid tumors and leukemias as well as in pediatric tumors including neuroblastoma, medulloblastoma, glioblastoma, osteosarcoma, and also alveolar rhabdomyosarcoma, which importantly has been shown to be unfavorable for outcome (Ackermann et al., 2011; Duan et al., 2010; Hu et al., 2009; Strebhardt and Ullrich, 2006; Triscott et al., 2013).

Depletion of PLK1 in cancer cells demonstrated strong effects on proliferation and cell viability, which could be explained by formation of mono-polar spindles, activation of the spindle assembly checkpoint, cell cycle arrest in G2/M called polo arrest, and induction of apoptosis (Liu and Erikson, 2003; Spankuch-Schmitt et al., 2002a; Spankuch-Schmitt et al., 2002b). These early studies provided the basis for pharmaceutical development and evaluation of PLK1 inhibitors. Available inhibitors are either targeting the ATP binding site or the polo-box binding domain and demonstrated high efficacies with relatively good specificity in preclinical studies (Craig et al., 2014).

One of the first compounds, BI 2536 has been tested in preclinical xenograft studies of childhood cancer. In neuroblastoma xenografts BI 2536 abrogated tumor growth and

resulted in steady tumor volume (Ackermann et al., 2011; Grinshtein et al., 2011). Treatment of osteosarcoma xenografts induced a reduction of tumor volume and for medulloblastoma xenografts an extended survival was observed (Liu et al., 2011; Triscott et al., 2013). The studies showed prevention of cell cycle progression and apoptosis. However, none of the studies demonstrated tumor-specific mechanisms at molecular level.

5 Aim of the thesis

Oncogenic transcription factors are frequently mutated and associated with aberrant gene expression in various different cancers. Thus, they are considered promising therapeutic targets, especially in aRMS, which represents a nearly perfect model of oncogene addiction as it is mainly driven and maintained by the chimeric transcription factor PAX3-FOXO1. Most aRMS studies concentrated rather on downstream functions of the fusion protein to investigate its functions than on upstream regulation. Subsequently, many target genes have been characterized and later suggested as therapeutic targets in aRMS. But certainly, for the development of improved therapies, distinguishing downstream driver pathways from passenger pathways remains a challenge. Therefore, we think that directly targeting the fusion protein on top of the oncogenic machinery is more efficient than interference with single downstream effectors. However, due to the lack of enzymatic activity, deep binding pockets, and their nuclear localization, transcription factors are less accessible to small-molecule inhibitors than for example active sites of kinases. Also, the structure of PAX3-FOXO1 has not been resolved and is likely to be intrinsically disordered impeding a biochemistry-based design of novel compounds. Unfortunately, cost-intense development of PAX3-FOXO1 specific compounds indicated for a rare malignancy and a small market is rather unlikely, especially from the economic perspective of the pharmaceutical industry. To circumvent the pharmacological challenge of direct compound binding, we first of all aimed at identifying kinases involved in PAX3-FOXO1 regulation. Working out biological processes and validating single kinases and their mechanisms create the basis for a model of the fusion protein regulatory environment. This enables the rational selection of drug targets such as kinases associated with the fusion protein and the choice of anti-cancer drugs that are developed for a broader range of cancer entities and applicable for preclinical *in vivo* treatment of xenograft tumors and prospective clinical trials in children. Furthermore, we aimed at investigating the clinical relevance of potential drug targets and their prognostic value in patient biopsies. Overall, our final goal is to improve treatment strategies and therapy outcome for alveolar rhabdomyosarcoma and to reduce treatment-related side effects.

6 Manuscript 1: PLK1 phosphorylates PAX3-FOXO1, the inhibition of which triggers regression of alveolar rhabdomyosarcoma

Accepted for publication in Cancer Research

Verena Thalhammer[1], Laura A. Lopez-Garcia[1], David Herrero-Martin[1], Regina Hecker[1], Dominik Laubscher[1], Maria E. Gierisch[1], Marco Wachtel[1], Peter Bode[2], Paolo Nanni[3], Bernd Blank[4], Ewa Koscielniak[4], and Beat W. Schäfer[1]

[1]Department of Oncology and Children's Research Center, University Children's Hospital Zurich, Zurich, Switzerland

[2]Department of Surgical Pathology, University Hospital Zurich, Zurich, Switzerland

[3]Functional Genomics Center Zurich, University of Zurich, Zurich, Switzerland

[4]Department of Oncology/Hematology/Immunology, Olgahospital, Klinikum Stuttgart, Stuttgart, Germany

Contributions:

Verena Thalhammer:	Figs. 1C, 1F
	Fig. 2
	Fig. 3
	Figs. 4C, 4D, 4E, 4G
	Fig. 5, with support of David Herrero und Peter Bode
	Fig. 6, with support of Peter Bode und Bernd Blank
	Tab. 1, with support of Bernd Blank
	Figs. S2B, S2C, S2D
	Fig. S3
	Fig. S4 (data analysis)
	Fig. S5, with support of Peter Bode
	Fig. S6
	Fig. S7
	Tab. S3, with support of Laura Lopez
	Preparation of manuscript
Laura Lopez:	Mass spectrometry
Regina Hecker:	Figs. 1A, 1B, S1
David Herrero:	Figs. 1D, 1E, S2A
Dominik Laubscher:	Figs. 4A, 4B
Maria Gierisch:	Fig. 4F

6.1 Abstract

Pediatric tumors harbor very low numbers of somatic mutations and therefore offer few targets to improve therapeutic management with targeted drugs. In particular, outcomes remain dismal for patients with metastatic alveolar rhabdomyosarcoma (aRMS), where the chimeric transcription factor PAX3/7-FOXO1 has been implicated but problematic to target. In this report, we addressed this challenge by developing a two-armed screen for druggable upstream regulatory kinases in the PAX3/7-FOXO1 pathway. Screening libraries of kinome siRNA and small molecules, we defined PLK1 as an upstream-acting regulator. Mechanistically, PLK1 interacted with and phosphorylated PAX3-FOXO1 at the novel site S503 leading to protein stabilization. Notably, PLK1 inhibition led to elevated ubiquitination and rapid proteasomal degradation of the PAX3-FOXO1 chimeric oncoprotein. On this basis, we embarked on a preclinical validation of PLK1 as target in a xenograft mouse model of aRMS, where the PLK1 inhibitor BI 2536 reduced PAX3-FOXO1-mediated gene expression and elicited tumor regression. Clinically, analysis of human aRMS tumor biopsies documented high PLK1 expression to offer prognostic significance for both event-free and overall survival. Taken together, these preclinical studies validate the PLK1 - PAX3-FOXO1 axis as a rational target to treat alveolar rhabdomyosarcoma.

6.2 Introduction

Rhabdomyosarcoma is the most common pediatric soft tissue sarcoma and can be divided into two main subgroups with different outcomes reflecting distinct genetic backgrounds. Alveolar rhabdomyosarcoma (aRMS) is more aggressive than embryonal rhabdomyosarcoma (eRMS) and often displays resistance to conventional chemo- and radiotherapy resulting in a 5-year survival rate of only 30% (Breneman et al., 2003). Until now, there are no alternative therapeutic strategies to these conventional treatments. Searching for appropriate molecular targets, large proteomic screening and sequencing approaches have been undertaken showing that pediatric tumors harbor far fewer somatic mutations than adult tumors (Vogelstein et al., 2013). In contrast to eRMS, analyzing genetic landscapes of alveolar rhabdomyosarcoma even further minimized the number of potential targets and excluded enrichment of any mutated oncogenic canonical pathway in the majority of patients (Chen et al., 2013; Shern et al., 2014). These findings indicate that aRMS is

driven by very few individual oncogenes and consequently reinforce the focus on the role of the tumor specific chimeric transcription factor PAX3/7-FOXO1.

The fusion protein is expressed in about 80% of aRMS tumors suggesting a dominant role as oncogenic driver (Shern et al., 2014; Sorensen et al., 2002). Its transforming capacity (Linardic, 2008; Olanich and Barr, 2013) is underlined by the ability to affect multiple oncogenic downstream pathways (Cao et al., 2010; Davicioni et al., 2006; Ebauer et al., 2007; Khan et al., 1998; Lae et al., 2007; Wachtel et al., 2004). Furthermore, aRMS is addicted to expression of the fusion protein as its continuous activity is essential for maintaining tumor cell survival (Ayyanathan et al., 2000; Bernasconi et al., 1996). Finally, its presence has also important prognostic significance (Missiaglia et al., 2012; Stegmaier et al., 2011). PAX3-FOXO1 is, in conclusion, a highly relevant potential target and offers the opportunity for development of novel directed therapies. However, directly antagonizing transcription factors remains a pharmaceutical challenge and alternative indirect strategies interfering with the regulatory network of the fusion protein need to be developed.

PAX3-FOXO1 is characterized by high expression, exclusive nuclear subcellular localization, enhanced protein stability, and increased transcriptional activity compared to wild type PAX3 or FOXO1 (Bennicelli et al., 1999; Bennicelli et al., 1996; Davis and Barr, 1997; del Peso et al., 1999; Miller and Hollenbach, 2007). Currently, we aim at mechanistically understanding these different levels of regulation required for the oncogenic function. We, as well as others, were able to demonstrate that the transcriptional activity of PAX3-FOXO1 depends on its phosphorylation state providing novel therapeutic opportunities (Amstutz et al., 2008; Jothi et al., 2013; Liu et al., 2013a).

Polo-like kinase 1 (PLK1) is known as key regulator of mitosis with critical roles in mitotic entry, centrosome maturation, cohesin release, bipolar spindle formation, mitotic exit, and cytokinesis. Overexpression of PLK1 is linked to poor prognosis in a variety of different cancers (Holtrich et al., 1994; Strebhardt and Ullrich, 2006). In contrast to healthy cells, it localizes to the nucleus already before G2/M in cancer cells and can be detected during the entire interphase (Cholewa et al., 2013). Therefore, cancer-cell specific functions in G1/S transition and DNA replication are suggested beyond its role in regulation of mitosis. Interestingly, PLK1 is associated with PI3K and MAPK pathways, both of which are thought to play important roles in aRMS (Guenther et al., 2013; Renshaw et al., 2013). Hence, PLK1 overexpression might not just be a consequence of enhanced proliferation, but it is likely that PLK1 actively

contributes to early carcinogenesis. However, a specific role for PLK1 in aRMS has not yet been described.

Here, we utilized a two-armed screening strategy to identify PLK1 as upstream regulator of PAX3-FOXO1, whereby PLK1 phosphorylated and subsequently stabilized the fusion protein. Since we observed objective regression of xenograft tumors upon PLK1 inhibition and found that PLK1 expression in patient biopsies has significant prognostic value, we propose the PLK1 - PAX3-FOXO1 axis to be a very promising novel target for aRMS therapy.

6.3 Material and methods

Cell lines

The aRMS cell lines Rh4, Rh41 (Peter Houghton, St. Jude Children's Hospital, Memphis, TN, USA), RMS13 (Roland Kappler, Ludwig–Maximilian University Munich, Germany), Rh3, Rh5, Rh10 (Susan Ragsdale, St. Jude Children's Hospital, Memphis, TN, USA), CW9019 (Soledad Gallego, Hospital Universitari Vall d'Hebron, Barcelona, Spain) and Rh30 as well as HEK293T cells (American Type Culture Collection ATCC, LGC Promochem, Molsheim Cedex, France) were cultured in Dulbecco's modified Eagle's medium (Sigma-Aldrich, Buchs, Switzerland), supplemented with 100 U/ml penicillin/streptomycin, 2 mM L-glutamine and 10% FBS (Life Technologies, Zug, Switzerland) in 5% CO_2 at 37°C. RD and Rh36 eRMS cells were kindly provided by Peter Houghton (St. Jude Children's Hospital, Memphis, TN, USA). Ruch2 and Ruch3 cell lines were established in our laboratory (Scholl et al., 2000).

aRMS and eRMS cell lines were tested and authenticated by cell line typing analysis (STR profiling) in 2011/2014 and positively matched (Hinson et al., 2013).

Plasmids and transfection methods

Rh4 cells were stably transfected with reporter plasmids containing the luciferase gene downstream of the AP2β promoter (pGl4.19, Promega, Dübendorf, Switzerland) and selected with 1 mg/ml G-418 sulfate (Promega, Dübendorf, Switzerland) to generate Rh4-AP2β-LF cells. Rh4luc and RMS13luc were generated by retroviral infection with the plasmid pLIB-LN (Takara Bio Europe/Clontech, Saint-Germain-en-Laye, France) and selection using 1 mg/ml G-418 sulfate.

FLAG-tagged PAX3-FOXO1 and FLAG-tagged GFP were generated by insertion of cDNA into pCMV-SC-NF (N-terminal FLAG, Stratagene, Agilent Technologies, Basel, Switzerland). PAX3-FOXO1 was cloned into pMSCV-IRES-GFP (Addgene, no. 33336, Cambridge, MA, USA) to perform site directed mutagenesis using QuikChange recommendations (Stratagene, Agilent Technologies, Basel, Switzerland). Parental DNA template was digested with DpnI (Thermo Scientific, Reinach, Switzerland).

Rh4 and RD cells were transfected using JetPrime™ (Polyplus-Transfections, Illkirch, France), HEK293T cells by $CaPO_4$.

siRNA kinome library screens and data analysis

A kinome siRNA library targeting 719 kinases was used (Ambion Silencer® V3 Kinase siRNA Library, Life Technologies, Zug, Switzerland) together with a sub-library targeting 47 kinases (Ambion Silencer® Select Costum siRNA Library, Life Technologies) with 3 unique siRNA sequences per gene. Ambion non-targeting siRNA served as negative control, whereas PAX3-FOXO1 break-point specific siRNA (Kikuchi et al., 2008), luciferase specific siRNA (pGL4, Custom Select) and KIF11 siRNA (AM4639; all Ambion, Life Technologies) were used as positive controls. Reverse transfection was carried out with $1x10^4$ cells per 96-well at a final concentration of 50 nM using N-TER nanoparticle transfection reagent (Sigma-Aldrich). Luciferase activity was determined by the Luciferase Assay System E1501 (Promega, Dübendorf, Switzerland) 48h post transfection and values normalized to viable cell numbers determined by WST-1 assay (Roche Diagnostics, Rotkreuz, Switzerland). Measurements were normalized using the per-plate median normalization method (excluding controls). Triplicate median-normalized luciferase values were averaged for each kinase before calculating the ratio to the averaged WST-1 absorbance (normalized luciferase activity). Cell viability of Rh4 and RMS13 cells was measured 72h post transfection using WST-1. Both screens were performed in triplicates and non-targeting, PAX3-FOXO1, pGL4 and KIF11 siRNAs were included in duplicates on each plate.

Small-molecule compounds screen and dose response studies

A small-molecule compound library (Supplementary Tab. S2) covering 161 different inhibitors was used to treat $5x10^3$ Rh4-AP2-LF cells per 96-well 24h after plating at a final concentration of 500 nM for 24h. Luciferase activity/cell viability ratio was

determined as described above. For dose response curves, this ratio was plotted against the logarithm of drug concentrations and IC_{50} values were calculated by non-linear regression curve fitting using GraphPad Prism software (GraphPad Software Inc., San Diego, CA, USA).

PLK1 silencing and small-molecule inhibition

Knockdowns of PLK1 and PLK4 were achieved by reverse transfection of 1.9-3.8x10^5 cells in 6-well plates using scrambled (4390846) or PLK1 and PLK4 directed siRNAs (25 nM 1341, 8 nM S449, 25 nM S21083; all Ambion, Life Technologies) with INTERFERin™ according to the manufacturer's protocol (Polyplus-Transfections, Illkirch, France). Cells were lysed 48h post transfection.

2x10^5 cells per 6-well were treated 24h after seeding using 15 nM BI 2536 (Axon Medchem, Groningen, NL) or 20 nM BI 6727 (Selleck Chemicals, Houston TX, USA). Cells were lysed for RNA or protein extraction after 48h. For proteasomal degradation studies, 10 nM - 50 nM Bortezomib (Cilag, Schaffhausen, Switzerland) was simultaneously added and cells were lysed after 20h.

Caspase 3/7 activity assay

For caspase 3/7 activity assays cells were seeded and treated in white 96-well plates with clear bottom (Greiner Bio one, Frickenhausen, Germany). Caspase activity was determined by Caspase-Glo® 3/7 Assay (Promega, Dübendorf, Switzerland) according to the manufacturer's instructions. Luminescence was measured using the multi-detection micro-plate reader Synergy HT (Bio-Tek Instrument, Winooski, USA).

Cell cycle analysis

Cells were treated in 6-well plates, detached by trypsin (0.05% Trypsin, w/ EDTA, Life Technologies), washed in PBS, fixed in 70% ice-cold ethanol and incubated at -20°C for at least 2h. Before flow cytometry analysis (Beckman Coulter Cytomics FC500; Hialeah, FL, USA), cells were washed by PBS and resuspended in 500 µl PI solution (20 µg/ml PI and 200 µg/ml RNase in PBS with 0.1% Triton X-100). Data were processed by FlowJo software (Treestar, Ashland, OR, USA).

qRT- PCR

Total RNA was extracted using the Qiagen RNeasy Kit (Qiagen, Basel, Switzerland) and reverse-transcribed using oligo (dT) primers and Omniscript reverse transcriptase (Qiagen). qRT-PCR was performed for PLK1 (Hs00153444_m1), PLK4 (Hs00179514_m1), PAX3-FOXO1 (Hs03024825_ft), AP2β (Hs00231468_m1), FGFR4 (Hs01106908_m1), CDH3 (Hs00999918_m1), PIPOX (Hs04188864_m1) and MYL1 (Hs00984899_m1) using TaqMan gene expression master mix (all Life Technologies). Cycle threshold (C_T) values were normalized to GAPDH (Hs02758991_g1). Relative expression levels were calculated using the $\Delta\Delta C_T$ method based on experiments performed in triplicates. Geometric mean values and the 95% confidence interval were calculated based on four to six biological replicates.

Immunoblotting

Total cell extracts were separated using 4-12% Bis-Tris SDS-PAGE gels (Life Technologies) and transferred to nitrocellulose membranes (PROTAN, Schleicher & Schuell, Kassel, Germany). After blocking with 5% milk powder in TBS/0.1% Tween, membranes were incubated with primary antibodies overnight at 4°C. After washing in TBS/0.1% Tween, membranes were incubated with IgG HRP-linked antibody for 1h at room temperature. Proteins were detected using ECL detection reagent (Fisher Scientific, Wohlen, Switzerland) after washing in TBS/0.1% Tween.

Antibodies

Western blot membranes were incubated with anti-FOXO1 (H-128; 1:1000; Santa Cruz Biotechnology, Heidelberg, Germany), anti-PLK1 (clone 35-206, 05-844; 1:1000; Millipore, Zug, Switzerland), anti-FOXO1A phospho S322 + S325 (phospho S503 + S506 in PAX3-FOXO1; ab60945; 1:500 Abcam, Cambridge, UK), anti-HA (05-904; 1:1000; Millipore, Zug, Switzerland), anti-PLK4 (clone 6H5, MABC544 1:250; Millipore, Zug, Switzerland), NMYC (9405; 1:1000; Cell Signaling, Bioconcept, Allschwil, Switzerland) or anti-PARP (9542; 1:1000; Cell Signaling) antibodies. Anti-β-Tubulin I mouse mAb (1:40,000; Sigma-Aldrich), anti-β-Actin (13E5) rabbit mAb (4970; 1:1000; Cell Signaling) and anti-GAPDH (D16H11) XP™ rabbit mAb (5174; 1:1000; Cell Signaling) were used as loading controls. Membranes were incubated with the secondary antibodies anti-mouse IgG HRP-linked antibody (7076; 1:2000;

Cell Signaling) or anti-rabbit IgG HRP-linked antibody (7074; 1:2000; Cell Signaling) for 1h at room temperature.

IP experiments were performed using anti-FOXO1 (H-128; Santa Cruz Biotechnology), anti-PAX3/7 (N-19, Santa Cruz Biotechnology) or monoclonal ANTI-FLAG® M2 antibody (F1804, Sigma-Aldrich).

For immunohistochemistry, mouse anti-Myf4 monoclonal antibody (1:20; Novocastra Laboratories Ltd.), AP2β (1:40; Santa Cruz Biotechnology) and rabbit p-cadherin antibody (1:100; Santa Cruz Biotechnology) were used.

Co-immunoprecipitation

Cells from one confluent 10 cm dish were lysed in 1 ml lysis buffer and incubated for 10 min at 4°C with Dynabeads® Protein G (Novex by Life Technologies) coupled to indicated antibodies. Beads were washed three times with lysis buffer, proteins eluted in 1x NuPage LDS sample buffer (Life Technologies) at 70°C and analyzed by Western blotting.

Stability assay

$2x10^5$ RD cells were seeded per 6-well the day before transfection with 1 µg pMSCV-PAX3-FOXO1-IRES-GFP or pMSCV-PAX3-FOXO1-S503A-IRES-GFP. Cells were treated with 35 µM cycloheximide (Sigma-Aldrich) or DMSO for 6h before lysis and protein extraction. Protein levels were analyzed by Western blotting.

Purification of FLAG-PAX3-FOXO1

Rh4, RMS13 or HEK293T cells were transfected with pCMV-FLAG-PAX3-FOXO1 in 15 cm plates, lysed 40h post transfection and FLAG-PAX3-FOXO1 was immunoprecipitated using 75 µl Dynabeads® per plate coupled to 8 µg monoclonal ANTI-FLAG® M2 antibody. After washing, bead-bound FLAG-PAX3-FOXO1 was either used for *in vitro* kinase assays or the protein was eluted by 1x NuPage LDS buffer and directly subjected to mass spectrometry.

In vitro kinase assay

Bead-bound protein was dephosphorylated using 300 units CIAP enzyme (alkaline phosphatase, calf intestinal HC, Promega, Dübendorf, Switzerland) for 90 min at 37°C (50 mM Tris HCl pH 7.5, 1 mM $MgCl_2$, 0.1 mM $ZnCl_2$). FLAG-PAX3-FOXO1 was phosphorylated after washing using 500 ng or 2.5 µg of recombinant PLK1 (Life Technologies) for 30 min at 30°C (250 mM HEPES pH 7.5, 50 mM $MgCl_2$, 12.5 mM DTT, 0.05% Triton X-100, 200 µM ATP). 4x NuPage LDS buffer was added for elution and proteins were separated by gel electrophoresis. After staining with colloidal coomassie (Instant blue, Expedeon, Harston, UK), the band corresponding to FLAG-PAX3-FOXO1 was excised and prepared for mass spectrometry.

Mass spectrometry

4x NuPage LDS buffer (Life Technologies) was added to *in vitro* kinase assay reactions for elution and proteins were separated by gel electrophoresis. After staining gels with colloidal coomassie (Instant blue, Expedeon, Harston, UK), the band corresponding to PAX3-FOXO1 was excised, washed 3x with 50% ACN and dried in a speed vacuum centrifuge. Reduction of disulphide bridges was achieved by adding 10 mM DTT in 50 mM AmBic (pH8) for 45 min at 56°C. DTT was removed and 50 mM IAM was added for alkylation of cysteines. After 1h of incubation at room temperature, the gel pieces were again washed 3x and dried. Digestion was performed with 50 ng of trypsin or chymotrypsin (V511C, V1061, Promega, Dübendorf, Switzerland) overnight at 37°C. Peptides were extracted using 50% ACN/5% TFA, dried, resuspended in 3% ACN/0.1% TFA, and purified using ZipTip C18 column tips. Finally, peptides were dried in a speed vacuum centrifuge, resuspended in 3% ACN, 0.2% formic acid and 10 mM citric acid solution and injected into the mass spectrometer (LTQ OrbitrapXL; Thermo Fischer Scientific, Bremen, Germany) coupled to an Eksigent-Nano-HPLC system (Eksigent Technologies, Dublin, CA, USA). Solvent composition was 0.1% formic acid for channel A, and 0.1% formic acid and 99.9% acetonitrile for channel B. Peptides were loaded on a self-made tip-column (75 µm × 80 mm) packed with Magic RP C18 AQ, 200A, 3 µm beads (Bischoff GmbH, Leonberg, Germany), and eluted at a flow rate of 200 nL/min by a gradient of 5-30% ACN in 55 min, 30-50% in 5 min, 50-95% in 5 min. Full-scan MS spectra (300−2.000 m/z) were acquired at a resolution of 60.000 at 400 m/z after reaching an accumulation value of 500.000. Collision-induced dissociation (CID) fragmentation was performed on the five most intense signals per cycle. CID spectra were acquired using a normalized collision energy of 35 and a

maximum injection time of 50 ms. Charge state screening was enabled, and unassigned and singly charged states were rejected. Precursor masses previously selected for MS/MS were excluded from further selection for 45 s, and the exclusion window was set to 20 ppm. The size of the exclusion list was set to a maximum of 500 entries. The samples were acquired using internal lock mass calibration on m/z 429.088735 and 445.120025.

Database search and protein identification

The MS raw files were converted into Mascot generic files (mgf) with Mascot Distiller software 2.4.3.3 (Matrix Science Ltd., London, UK) and peak lists searched using Mascot Server 2.3.02 against the forward UniProtKB/Swiss-Prot database for human, concatenated to a reversed decoyed FASTA database consisting of a total of 135,183 proteins and 260 common protein contaminants (NCBI taxonomy ID 9606, release date 2012-04-12). The protein sequence of PAX3-FOXO1 (gi|431254|gb|AAC50053.1|) was included in the database as in (Shapiro et al., 1993). The parameters for precursor tolerance and fragment ion tolerance were set to ± 5 ppm and ± 0.8 Da, respectively. Carbamidomethylation of cysteine was set as fixed modification, while phosphorylation (S, T, Y) and oxidation (M) were set as variable. Peptides having an expectation value higher as 0.05 and/or a Mascot score lower as 20 were excluded. All the spectra of phosphorylated peptides were manually validated.

Ubiquitination studies

Rh4 cells were transfected with pCMV-FLAG-PAX3-FOXO1 plasmid and pCDNA3-HA-ubiquitin at a ratio of 1:2 for 48h. Cells were treated with 200 nM PLK1 inhibitors for 21h prior to addition of 10 μM MG-132 (Calbiochem, Millipore, Zug, Switzerland) for 5h. After lysis (2% SDS, 150 mM NaCl, 10 mM Tris/HCl, 2 mM Na_3VO_4, 50 mM NaF), samples were boiled for 10 min, sonicated, diluted with 9 volumes of dilution buffer (150 mM NaCl, 10 mM Tris/HCl, 2 mM EDTA, 1% TritonX) and incubated for 30 min at 4°C. IP was performed using Dynabeads® coupled to ANTI-FLAG® M2 antibody for 1h at 4°C. Beads were washed three times with lysis buffer, proteins eluted with 3x FLAG peptide (Sigma-Aldrich) and analyzed by Western blotting.

Xenograft studies

$5x10^6$ Rh4, Rh4luc or RMS13luc cells were engrafted subcutaneously in 6 weeks old NOD/Scid il2rg$^{-/-}$ mice (male and female, 20-25 g, Charles River, Sulzfeld, Germany). Mice bearing established tumors with volumes of 65 - 470 mm^3 were treated intravenously with either sterile 0.9% NaCl or BI 2536 at 40 mg/kg on two consecutive days weekly for three cycles. BI 2536 was formulated in hydrochloric acid (0.1 N) diluted with 0.9% NaCl (Steegmaier et al., 2007). Total tumor volumes were determined either by measuring two diameters (d1, d2) in right angles using a digital caliper ($V= (4/3) \pi r^3$; r= (d1+d2)/4) or by *in vivo* imaging. D-luciferin (Caliper Life Sciences, Oftringen, Switzerland) was injected intraperitoneally (10 µl/g body weight), and tumors were monitored by the IVIS Lumina XR imaging system (Caliper Life Sciences). Control mice were euthanized when reaching a tumor volume of 1000 mm^3.

Immunohistochemistry

Three-micron thick sections of formalin-fixed, paraffin-embedded tissue were mounted on glass slides (SuperFrost Plus; Menzel, Braunschweig, Germany), deparaffinized, rehydrated and stained with hematoxylin and eosin (H&E). Immunohistochemical stainings were performed using the Ventana Benchmark system (Ventana Medical Systems, Tucson, AZ) and Ventana UltraView DAB reagents.

Tissue arrays

Tissue arrays have been previously described (Grass et al., 2009; Wachtel et al., 2006). Immunohistochemistry was performed on Leica BondMax instruments using Refine HRP-Kits (Leica DS9800, Leica Microsystems Newcastle, Ltd.). Paraffin-slides were dewaxed, followed by pretreatment (Epitop Retrieval Buffer 2, 45 min, 100°C) and incubated with anti-PLK1 antibody (1:600). Tumors showing at least 1-5% of cells with a very high staining intensity were assigned to the high expression group. In contrast, tumors with low expression showed homogenous overall staining of reduced intensity. Anti-Ki-67 rabbit monoclonal antibody (MIB1; 30-9; Ventana Medical Systems) was used as proliferation marker (< 50% = low; > 50% = high). TMAs were analyzed double-blinded.

6.4 Results

Kinome-wide siRNA screen identifies PAX3-FOXO1 regulators

To identify kinases regulating the activity of the oncogenic transcription factor PAX3-FOXO1, we established a stable reporter cell line to monitor fusion protein activity (Fig. 1A). Rh4 aRMS cells with a transcriptome very similar to tumor biopsies (Wachtel et al., 2004) were stably transfected with a PAX3-FOXO1-responsive luciferase reporter employing a well-characterized endogenous AP2β promoter fragment (Ebauer et al., 2007) to generate Rh4-AP2β-LF cells. Depletion of PAX3-FOXO1 by siRNA (Kikuchi et al., 2008) or silencing of luciferase itself resulted in a more than 70% decrease in luciferase activity (Supplementary Fig. S1A). Therefore, this reporter assay constitutes a valid tool for functional screening of PAX3-FOXO1 upstream regulators.

First, we performed a kinome-wide siRNA screen (Fig. 1A). Rh4-AP2β-LF cells were transfected with three unique siRNA sequences targeting each of the 719 kinases (Fig. 1B and Supplementary Fig. S1B). PAX3-FOXO1, KIF11 (mitotic motor protein) and luciferase control siRNAs were included on each plate and the ratio of luciferase activity to cell viability from averaged triplicate values was determined for each siRNA. Only siRNAs that reduced this ratio by at least 1.5 SDs from the mean of the luciferase control were considered as potential candidates. Applying this criterion for at least two independent siRNAs, we identified 47 candidates that potentially contribute to the activity of PAX3-FOXO1 (Supplementary Tab. S1). Importantly, these kinases are all expressed in Rh4 cells and primary aRMS tumors, at least at the mRNA level (Davicioni et al., 2006; Wachtel et al., 2004).

To narrow down the list of candidates, we applied a secondary viability screen using an siRNA library containing three additional targeting sequences per kinase (sequence panels A, B and C). We determined mean relative cell viability after individual silencing for 72 hours in Rh4 and RMS13 cells. Next to two positive controls (PAX3-FOXO1 and KIF11) included on each screening plate, we found that knockdown of PLK1 clearly had the strongest impact on cell viability in both cell lines (up to 61% reduction), whereas the per-plate means reached only 7% to 22% (Fig. 1C). These results suggest that PLK1 expression might be important for aRMS cell survival.

Small-molecule inhibitor screen reveals PLK1 as potential PAX3-FOXO1 regulator

In parallel to the siRNA screen, we conducted a small-molecule, mainly kinase-directed drug screen, to further examine the regulation of PAX3-FOXO1 activity (Fig. 1A). This approach is able to directly identify available pharmaceutical inhibitory compounds. We treated Rh4-AP2β-LF cells with 161 inhibitors (Supplementary Tab. S2) at a final concentration of 500 nM and measured cell viability as well as luciferase activity after 24 hours. Ranking compound activity according to ratio of luciferase activity over cell viability, 10 out of 161 inhibitors reduced normalized luciferase activity by at least 44% compared to untreated Rh4-AP2β-LF cells (Fig. 1D). With a normalized luciferase reduction by 76% (relative ratio 0.24), the top candidate was the PLK1 inhibitor BI 2536 (Steegmaier et al., 2007).

To further validate BI 2536, Rh4-AP2β-LF cells were treated with increasing concentrations for 24 hours. This resulted in a dose dependent reduction of normalized luciferase activity with an IC_{50} of 17.40 nM (Fig 1E; $IC_{50/48h}$ =15.75 nM; $IC_{50/72h}$ =10.20 nM, Supplementary Fig. S1C). Interestingly, the median IC_{50} value of aRMS cell lines was 15.03 nM versus a median IC_{50} of 31.86 nM in eRMS cell lines (Supplementary Fig. S2A). PLK1 inhibition by BI 2536 induced apoptosis in Rh4 cells as shown by PARP cleavage (Supplementary Fig. S2B) as well as by relative increase in caspase 3/7 activity (Supplementary Fig. S2C). To demonstrate the potential relevance of PLK1 in aRMS, we analyzed the expression of PLK1 protein across a panel of eight different aRMS cell lines by immunoblotting. All of the cell lines expressed the kinase with Rh4, Rh41 and RMS13 cells displaying the highest protein levels (Fig. 1F).

In conclusion, we identified PLK1 as the most promising candidate kinase by both siRNA and small-molecule compound screen, which therefore represents a potential target for treatment of aRMS.

PLK1 inhibition reduces PAX3-FOXO1 activity

To confirm PLK1 as regulator of the fusion protein, we analyzed a panel of PAX3-FOXO1 target genes. We measured relative mRNA expression of the activated target genes AP2β, FGFR4, CDH3 and PIPOX (Cao et al., 2010; Davicioni et al., 2006; Lae et al., 2007; Marshall et al., 2012; Thuault et al., 2013; Wachtel et al., 2004; Wachtel et al., 2006) and the repressed differentiation marker MYL1 (De Pitta et al., 2006) by qRT-PCR after 48 hours of either PLK1 silencing (si1341 and siS449) or small-molecule

inhibition (BI 2536 and BI 6727). In RMS13 cells, knockdown of PLK1 achieved 80% (si1341) and 82% (siS449) of silencing without affecting PAX3-FOXO1 mRNA expression. However, expression of all target genes was significantly modulated (Fig. 2A). In Rh4 cells, knockdown efficiencies by si1341 reached 86% with similar modulation of target gene expression, whereas silencing by siS449 reached 81% without significant effects on target genes (Fig. 2B). Nevertheless, treatment with both inhibitors, BI 2536 and BI 6727, significantly affected target gene expression in both cell lines.

In summary, PLK1 inhibition, either by genetic or pharmacological means, significantly altered transcription of PAX3-FOXO1 downstream targets suggesting a specific link between the kinase and the fusion protein.

PLK1 binds to and phosphorylates PAX3-FOXO1

We assessed direct interaction of PLK1 and PAX3-FOXO1 by co-immunoprecipitation of the endogenous proteins in Rh4 cells. PAX3-FOXO1 was pulled down using either anti-PAX3 or anti-FOXO1 antibody. In both cases, PLK1 was co-immunoprecipitated with the fusion protein but not with the negative control as shown by Western blot analysis (Fig. 3A). In a reciprocal approach, the kinase was pulled down by anti-PLK1 antibody and PAX3-FOXO1 was found to co-immunoprecipitate as well (Fig. 3B). These findings indicate that PLK1 and PAX3-FOXO1 can directly interact in aRMS cells.

Furthermore, we interrogated this interaction under drug treatment conditions. Rh4 cells were transfected with FLAG-tagged PAX3-FOXO1 or FLAG-tagged GFP, which was then immunoprecipitated after DMSO or BI 2536 treatment for 16 hours using an anti-FLAG antibody. Again, we found PLK1 to interact with the fusion protein, but not with GFP (Fig. 3C). Surprisingly, interaction even increased after treatment with BI 2536, which arrested cells in G2/M (Supplementary Fig. S2D and (Lenart et al., 2007; Steegmaier et al., 2007)). This indicates that PLK1 might control PAX3-FOXO1 mainly at the transition to mitosis.

PLK1 substrates contain the consensus motifs [D/E/N]Xp[S/T] or p[S/T]F (Kettenbach et al., 2012) and several of these can also be found in PAX3-FOXO1 suggesting that it might be a direct target of PLK1. *In silico* analysis using GPS-Polo 1.0 (Liu et al., 2013b) predicted S503 and S457 as potential phosphorylation sites with a high cut-off threshold (Fig. 3D). To directly analyze whether one of these consensus sites is phosphorylated in the fusion protein, FLAG-tagged PAX3-FOXO1 was purified

from aRMS cells. Using mass spectrometry, we identified the peptide TSSNASTISGR containing S503 as one out of eleven phospho-peptides (Supplementary Tab. S3). Furthermore, applying a phospho-specific antibody to exactly localize the phosphorylated residue, we detected phosphorylation at S503+S506 (corresponding to phospho-S322+S325 in FOXO1 against which the antibody is directed) directly demonstrating that the predicted site is phosphorylated in aRMS cells (Fig. 3E).

To assess whether PLK1 can phosphorylate S503, we purified FLAG-PAX3-FOXO1 from HEK293T cells, dephosphorylated the protein by calf intestine alkaline phosphatase (CIAP) and subsequently performed *in vitro* kinase assays using recombinant PLK1. Mass spectrometry confirmed that PLK1 phosphorylated the peptide TSSNASTISGR. In total, this peptide contains six serine or threonine sites, but the data indicated that only S503 or T504 could be considered as potential phosphorylation sites (Supplementary Fig. S3). To distinguish these two possibilities, we used the phospho-specific antibody recognizing phospho-S503+S506. Western blot analysis indeed revealed specific phosphorylation at these positions indicating that S503 is the site being phosphorylated by PLK1 (Fig. 3F).

These data suggest that PLK1 and PAX3-FOXO1 are direct interaction partners and that PLK1 can phosphorylate the fusion protein at S503.

PLK1 stabilizes PAX3-FOXO1 protein

To further explore the biological functions of this phosphorylation site, we transfected RD eRMS cells lacking endogenous PAX3-FOXO1 with plasmids expressing either PAX3-FOXO1 wild type or mutated PAX3-FOXO1-S503A. Cells were then treated with cycloheximide for 6 hours to assess protein turnover by immunoblotting and densitometric quantification. Interestingly, the mutant protein was significantly less stable than the wild type protein (protein amount reduced by 47%) (Figs. 4A and 4B).

Next, the stability of endogenous PAX3-FOXO1 upon PLK1 depletion was examined in two aRMS cell lines. Treatment with siRNA 1341 for 48 hours reduced PLK1 protein by 43% in RMS13 cells, respectively by 53% in Rh4 cells and induced a slight degradation of PAX3-FOXO1 (23% and 11%, calculated from representative blots shown in Fig. 4C). After silencing with the more efficient siRNA S449 (reduction of PLK1 by 94% (RMS13) and 83% (Rh4)), we observed degradation of the fusion protein by 48% and 41% compared to scrambled control treatment (Fig. 4D). These results suggest that stability of PAX3-FOXO1 is modulated by phosphorylation at S503.

Indeed, inhibition of PLK1 activity by BI 2536 (15 nM) and BI 6727 (20 nM) led to similar reduction of PAX3-FOXO1 protein levels (53% and 64% in RMS13, 44% and 49% in Rh4 cells) (Fig. 4E). In addition, increased ubiquitination of PAX3-FOXO1 upon PLK1 inhibition confirmed its proteasomal degradation (Fig. 4F), which moreover, could be rescued by adding low concentrations of the proteasomal inhibitor bortezomib (Adams et al., 1999) in a dose dependent manner (Fig. 4G).

In conclusion, these experiments imply that PLK1-mediated phosphorylation at S503 protects PAX3-FOXO1 from ubiquitination and consequent proteasomal degradation and thus maintains the transcriptional activity of the fusion protein.

PLK1 inhibition causes tumor regression in xenografts

Based on our *in vitro* results, we further validated PLK1 as an *in vivo* target using xenograft mouse models. Immunocompromised NOD/Scid il2rg$^{-/-}$ (NSG) mice were engrafted subcutaneously with Rh4, Rh4luc and RMS13luc cells expressing luciferase for *in vivo* imaging. Mice with established tumors of varying sizes (65 mm^3 - 470 mm^3) were treated intravenously with vehicle or BI 2536 at a dose of 40 mg/kg for three weeks on two consecutive days per week (Steegmaier et al., 2007). Every treatment group of three to five mice included two mice with large tumors of at least 300 mm^3. Absolute tumor volumes measured by caliper in mice bearing Rh4 tumors revealed a complete tumor regression upon BI 2536 treatment in all mice, even when the starting volume was as high as 370 mm^3 (Fig. 5A). Similarly, luciferase activity was reduced in both cell lines by close to 100% (Figs. 5A and 5B). Tumors of additional mice were treated for two cycles only, isolated after a two-week recovery phase, paraffin-embedded, and immunohistochemically stained. Vehicle treated tumors showed highly cellular histology with strong expression of myogenin and AP2β consistent with aRMS. In contrast, treated xenografts displayed a high degree of necrotic areas and fibrosis. Importantly, expression of PAX3-FOXO1 target genes AP2β and p-cadherin (CDH3) was significantly lower compared to untreated xenografts.

These data impressively illustrate that PLK1 activity plays a major role in aRMS tumor cell survival corroborating our *in vitro* results. Therefore, PLK1 inhibitors such as BI 2536 might represent very potent novel treatment options for aRMS.

PLK1 is overexpressed in human tumor biopsies and correlates with PAX3-FOXO1 activity and survival

To ensure that our findings are not restricted to aRMS cell lines, PLK1 expression was analyzed in patient tumor biopsies. We utilized PLK mRNA expression data of PAX3-FOXO1 positive aRMS tumors from two independent data sets (Davicioni et al., 2006; Wachtel et al., 2004) and compared them to PLK expression in normal muscle tissue (Bakay et al., 2006). We found that mRNA levels of PLK1 and PLK4, but not PLK2 and PLK3, were significantly higher in tumor samples than in normal muscle biopsies (Fig. 6A and Supplementary Fig. S4).

To validate PLK1 as a clinically relevant therapeutic target, we immuno-histochemically stained a tissue microarray including tumor biopsies of 49 aRMS patients. Tumors were divided into high and low expressing subgroups as described in the material and methods section (Fig. 6B). To correlate PAX3-FOXO1 activity with PLK1 expression *in vivo*, we assessed in parallel expression of the PAX3-FOXO1 target gene AP2β. In a majority of tumors (34 out of 45), AP2β staining from the same tumor significantly correlated with expression of PLK1 (Pearson correlation p-value: 0.0004, Fig. 6C). This was not the case for co-staining with the proliferation marker MIB1 (Supplementary Fig. S5). These results support our previous findings and a mechanism whereby activity of PAX3-FOXO1 is modulated by PLK1.

Importantly, outcome as measured for event-free (EFS) and overall survival (OS) by Kaplan-Meier analysis was significantly worse for patients with high PLK1 expression (Fig. 6D). Five-year survival rates for patients in the PLK1 high expression cohort were only 15.4% (EFS) and 20.2% (OS). Therefore, the hazard ratio for events was 2.3 times higher (Wald test: $p = 0.019$) and for death even 3.16 times higher (Wald test: $p = 0.004$) for patients with high PLK1 expression. Moreover, multivariate analysis including the factors age, sex and tumor localization identified PLK1 status as the only significant risk associated variable (Tab. 1). The very dismal survival rates for the high expression cohort emphasize the importance of PLK1 expression and suggest that PLK1 is a prognostic risk factor for fusion positive RMS.

In summary, our results imply that PLK1 is a highly attractive target for the treatment of aggressive aRMS, which warrants further investigations in clinical studies.

6.5 Discussion

This study describes a novel PLK1 - PAX3-FOXO1 oncogenic axis in aRMS. We show modulation of PAX3-FOXO1 activity by PLK1 based on direct protein-protein interaction and phosphorylation at S503 leading to stabilization of the fusion protein. In addition, *in vivo* treatment with PLK1 inhibitor demonstrated tumor regression and immunohistochemical analysis of PLK1 protein expression in human biopsies revealed its novel prognostic impact.

To improve previous screenings for targets in aRMS, which concentrated mainly on cell viability (Hu et al., 2009), we focused on transcriptional activity of PAX3-FOXO1 by employing aRMS (Rh4) cells stably expressing an AP2β-promoter reporter construct. Using the ratio of reporter activity versus cell viability, we were able to exclude generally cytotoxic drugs. Strikingly, a kinome-wide siRNA as well as a small-molecule library screen identified PLK1 as top hit. KEGG pathway analysis (string-db.org) showed that several additional candidates are associated with MAPK or phosphatidylinositol signaling, both of which have been previously reported in RMS (Guenther et al., 2013; Renshaw et al., 2013)

To confirm PLK1 as an upstream modulator of PAX3-FOXO1 activity, we assessed expression of known endogenous PAX3-FOXO1 target genes (AP2β, FGFR4, CDH3, PIPOX and MYL1) upon inhibition by two drugs as well as by two different siRNAs in two aRMS cell lines. We observed significant target gene modulation, with the exception of one siRNA in Rh4 cells. It is likely that the lack of effect might be due to compensatory effects by other members of the PLK family since BI 2536 and BI 6727 are known to affect the activities of PLK2, PLK3, and potentially PLK4 (Rudolph et al., 2009; Steegmaier et al., 2007). Indeed, next to PLK1 also PLK4 is overexpressed in aRMS biopsies compared to normal muscle and, although not identified in the primary screen, its depletion reduced target gene expression in Rh4 cells suggesting overlapping functions of PLK1 and PLK4 (Supplementary Fig. S6). Nevertheless, our findings support the conclusion that PLK1 regulates PAX3-FOXO1 activity.

To further sustain this notion, we demonstrated direct protein-protein interaction of the endogenous proteins by co-immunoprecipitations in aRMS cells. Also, recombinant PLK1 phosphorylated the fusion protein at S503 in *in vitro* kinase assays. This residue is located within a very conserved domain in the FOXO1 part of the fusion protein and the corresponding serine in wild type FOXO1 (S322) is a site known to be phosphorylated by recombinant CK1 (Rena et al., 2002). A recent study demonstrated

that wild type FOXO1 interacts with and is phosphorylated also by PLK1 during G2/M (Yuan et al., 2014). Similarly, we observed enhanced interaction in this cell cycle phase. However, phosphorylation of wild type FOXO1 triggers nuclear export (Rena et al., 2002; Yuan et al., 2014), whereas PAX3-FOXO1 is located exclusively in the nucleus (del Peso et al., 1999; and own observations). Hence, phosphorylation of S503 by PLK1 must have different consequences. In fact, we observed faster degradation of PAX3-FOXO1-S503A compared to wild type after cycloheximide block due to enhanced ubiquitination upon PLK1 inhibition. It has previously also been shown that PAX3-FOXO1 has increased posttranslational stability compared to wild type proteins (Miller and Hollenbach, 2007). Our results are furthermore in line with studies demonstrating PLK1 to mediate stabilization of transcription factors such as the oncogene MYC (Tan et al., 2013). Interestingly, we found the fusion target gene NMYC to be degraded upon PLK1 inhibition, either by a direct or indirect mechanism (Supplementary Fig. S7), which might further sensitize aRMS as well as other NMYC expressing tumors to PLK1 inhibitors. In accordance with the proposed function of PAX3-FOXO1 in checkpoint adaptation (Kikuchi et al., 2014), PLK1 might prevent premature degradation of PAX3-FOXO1 during the transition phase. In summary, this suggests a model whereby PLK1 phosphorylation can stabilize PAX3-FOXO1, mainly during G2/M transition, whereas at the same time it would inhibit the wild type tumor suppressor FOXO1 to ensure cell cycle progression and survival.

We observed an almost complete tumor regression *in vivo* upon treatment with BI 2536 in two different aRMS cell lines. This is in agreement with an objective response demonstrated for the Rh30r aRMS xenograft by the Pediatric Preclinical Testing Program (Gorlick et al., 2014). This particular xenograft was derived from a patient that had failed prior therapies suggesting that PLK1 expression might be of prognostic relevance. Indeed, expression of PLK1 in 49 aRMS tumor biopsies significantly predicted poor prognosis for event-free and overall survival. To our knowledge, PLK1 expression is therefore one of the first predictive markers next to EPHB4 that is able to stratify patients within the group of fusion-positive tumors (Aslam et al., 2014).

Summarizing, our data suggest that PLK1 is a highly relevant clinical target in aRMS with several PLK1 inhibitors already in clinical development. Since it has been shown that mice can tolerate higher systemic exposure to PLK1 inhibitors than humans (Gorlick et al., 2014), it is likely that combination therapies need to be developed to overcome this obstacle. Nevertheless, this study reveals an important new role for PLK1 in aRMS biology apart from its known function in cell cycle that might explain

increased sensitivity. Hence, our results should be directly translatable to clinical studies.

6.6 Figure legends

Fig. 1. siRNA and drug screening identify PLK1 as regulator of PAX3-FOXO1

(A) Schematic representation of screening strategy. PAX3-FOXO1 is phosphorylated, transcriptionally active and induces expression of the luciferase gene, which is under the control of the PAX3-FOXO1-responsive AP2β promoter. Kinase silencing and small- molecule inhibition reduce PAX3-FOXO1 transcriptional activity and result in a decreased expression of the luciferase gene.

(B) Results of kinome-wide siRNA screen. RNA silencing was carried out for 48h using 50 nM siRNA. The luciferase readout was normalized to cell viability measured by WST-1 assay. siRNAs targeting luciferase (pGL4) and PAX3-FOXO1 served as positive controls for reduced activity/cell viability ratio (LF/V) and siKIF11 for reduced cell viability. Reduced LF/V ratio upon PLK1 silencing is marked in black. *Data points*, mean of three independent experiments performed in triplicates; *threshold*, 1.5 SDs of mean of luciferase knockdown.

(C) Sub-screen of candidate kinases. RNA silencing was carried out in Rh4 and RMS13 cells for 72h using 50 nM siRNA. Cell viability was measured by WST-1 assay and set relative to scrambled knockdown. *Data points*, mean of three independent experiments performed in triplicates; Student's t-test for PLK1 knockdown *** $p < 0.001$, ** $p < 0.01$.

(D) Illustration of the ten most effective drugs. Rh4-AP2β-LF cells were treated with a small-molecule compound library at a final concentration of 500 nM for 24h and luciferase activity (LF) and cell viability (V) were measured. Relative values compared to untreated cells as well as the resulting LF/V ratios are shown. *Columns*, mean of technical triplicates; *bars,* SD.

(E) Drug response curve of BI 2536 based on LF/V ratio. Rh4-AP2β-LF cells were treated with increasing concentrations of BI 2536 for 24h. LF/V values were measured relative to untreated cells. *Data points,* mean of technical triplicates; non-linear regression curve fitting using Prism GraphPad.

(F) PLK1 expression in aRMS cell lines shown by Western blot analysis.

Fig. 2. PLK1 silencing and inhibition reduce PAX3-FOXO1 activity

Relative mRNA expression of PAX3-FOXO1 and its target genes upon PLK1 knockdown and inhibition. C_T values relative to scrambled knockdown or DMSO treatment were measured by qRT-PCR and normalized to GAPDH expression.

(A and B) PLK1 was silenced for 48h using two different sequences (25 nM si1341 and 8 nM siS449) in RMS13 and Rh4 cells.

(C and D) RMS13 and Rh4 cells were treated with 15 nM BI 2536 or 20 nM BI 6727 for 48h.

Columns, geometric mean of at least 4 independent experiments performed in triplicates; *bars,* 95% confidence interval; * significant according to 95% CI.

Fig. 3. PLK1 phosphorylates PAX3-FOXO1

(A) Western blot analysis showing endogenous Co-IP of PLK1 after PAX3-FOXO1 immunoprecipitation in Rh4 cells. Beads-only were used as negative control.

(B) Western blot analysis showing endogenous Co-IP of PAX3-FOXO1 after PLK1 immunoprecipitation in Rh4 cells. Beads-only were used as negative control.

(C) Western blot analysis of PLK1 after FLAG immunoprecipitation from Rh4 cells expressing FLAG-PAX3-FOXO1. Cells were treated with DMSO or 15 nM BI 2536 for 16h. FLAG-GFP was used as negative control.

(D) *In silico* analysis using the phospho-site prediction software GPS-Polo 1.0 for phosphorylation of PAX3-FOXO1 by PLK.

(E) Western blot analysis of FLAG-PAX3-FOXO1 purified from Rh4 cells using anti phospho-S503+S506 antibody.

(F) PLK1 *in vitro* kinase assay. HEK293T cells were transfected by FLAG-PAX3-FOXO1 expressing plasmid, purified, dephosphorylated by CIAP, and re-phosphorylated by recombinant PLK1. Phospho-peptide identified by mass spectrometric analysis and Western blot analysis using anti phospho-S503+S506 antibody are shown.

Fig. 4. PLK1 stabilizes PAX3-FOXO1

(A) Western blot analysis of exogenous, wild type or phospho-mutant PAX3-FOXO1 degradation. RD cells were transfected with PAX3-FOXO1 wild type or PAX3-FOXO1-

S503A expressing constructs and treated for 6h with DMSO or 35 μM cycloheximide (CHX).

(B) Quantification of exogenous PAX3-FOXO1 degradation by densitometry. Levels were normalized to GAPDH. *Columns,* mean of three independent experiments; *bars,* SD; Student's t-test ** p= 0.0052.

(C and D) Western blot analysis of endogenous PAX3-FOXO1 degradation upon PLK1 silencing. RMS13 and Rh4 cells were transfected with 25 nM si1341 or 8 nM siS449 for 48h.

(E) Western blot analysis of endogenous PAX3-FOXO1 degradation upon PLK1 inhibition. RMS13 and Rh4 cells were treated with DMSO, 15 nM BI 2536 or 20 nM BI 6727 for 48h.

(F) Ubiquitination studies. Western blot analysis after FLAG immunoprecipitation from Rh4 cells expressing FLAG-PAX3-FOXO1 and HA-ubiquitin. Cells were treated with DMSO, 200 nM BI2536 or 200 nM BI6727 for 21h prior to addition of 10 μM MG-132 for 5h.

(G) Western blot analysis showing rescue of endogenous PAX3-FOXO1 degradation by the proteasomal inhibitor bortezomib. Rh4 cells were treated with 15 nM BI 2536 for 20h. Bortezomib was simultaneously titrated to the cells. Densitometric quantification normalized to β-tubulin is indicated.

Fig. 5. PLK1 inhibition causes tumor regression *in vivo*

In vivo drug treatment of NOD/Scid il2rg$^{-/-}$ mice engrafted with Rh4 (n=10), Rh4luc (n=6) and RMS13luc (n=6) (luc = luciferase expressing). Mice bearing established tumors were treated intravenously for three cycles with either vehicle control or BI 2536 at a dose of 40 mg/kg twice weekly on two consecutive days (indicated by triangles).

(A) Absolute and relative tumor volumes upon treatment. Absolute tumor volume was measured by caliper (upper two panels). *In vivo* imaging was performed for luciferase expressing tumors. Relative bioluminescence (photons/second) is depicted (lower four panels).

(B) Illustration of tumor regression by picture series during treatment phase of two representative mice.

(C) Immunohistochemistry of a control and a BI 2536 treated tumor. Rh4luc tumors were treated for two cycles with either vehicle control or BI 2536 at a dose of 40 mg/kg. Tumors were excised two weeks after the end of treatment and immunohistochemically stained.

Fig. 6. PLK1 is an overexpressed, prognostic marker that correlates with PAX3-FOXO1 activity in tumor biopsies

(A) PLK1 gene expression in normal human muscle (n=121) and in PAX3-FOXO1 positive aRMS patient-derived biopsies (n=46) measured by microarray (Affymetrix HG-U133A). *Box plot,* minimum to maximum; Student's t-test $p < 0.0001$.

(B) Patient-derived tissue microarray immunohistochemically stained for PLK1 (n=49) and AP2β (n=45) expression. Patients were grouped according to high (n=26) and low (n=23) PLK1 expression and high (n=28) and low AP2β (n=17) expression. Representative tumor of PLK1 high expression cohort and a tumor with very low expression are shown next to AP2β staining of the same tumor.

(C) Pearson correlation of PLK1 and AP2β expression based on tissue microarray (n=45); $p= 0.0004$.

(D) Kaplan-Maier survival curves of PLK1 low and high expression cohorts based on tissue microarray. Log-rank test.

6.7 Supplementary figure legends

Fig. S1. Establishment of screening approach

Establishment and validation of the screening approach using a stable endogenous reporter cell system. aRMS cells were transfected with the AP2β luciferase reporter construct.

(A) siRNA mediated knockdown was carried out for 48h at a concentration of 50 nM targeting luciferase and PAX3-FOXO1. Luciferase activity was normalized to cell viability measured by WST-1. PAX3-FOXO1 knockdown efficiency was assessed using Western blotting (inlay). *Columns*, mean of four independent experiments performed in triplicates; *bars*, SD; Student's t-test *** $p < 0.0001$.

(B) Methodology of the functional kinome-wide siRNA screen.

(C) Drug response curve of BI 2536 based on LF/V ratio. Rh4-AP2β-LF cells were treated with increasing concentrations of BI 2536 for 48h (upper panel) and 72h (lower panel). LF/V values were measured relative to untreated cells. *Data points,* mean of technical triplicates; non-linear regression curve fitting using Prism GraphPad.

Fig. S2. BI 2536 causes apoptosis and cell cycle arrest

(A) IC_{50} values for BI 2536 were calculated for different aRMS and eRMS cell lines after 72h.

(B) Rh4 cells were treated with 15 nM BI 2536 for 24h. PARP cleavage is presented by Western blot analysis.

(C) Rh4 cells were treated with increasing concentrations of BI 2536 for 24h and 48h. Relative caspase 3/7 activity is displayed.

(D) Rh4 cells were treated with 15 nM BI 2536 for 24h. Cell cycle distribution was measured by FACS analysis after PI-staining.

Fig. S3. PLK1 phosphorylates PAX3-FOXO1 *in vitro*

Representative MS spectra for identification of the phospho-peptide TSSNASTISGR.

(A) Dephosphorylated peptide showing the ion at 620 m/z representative of unmodified S503.

(B) Peptide after PLK1 *in vitro* kinase assay showing a shift of the ion to 700 m/z indicating phosphorylation of S503 or T504.

Fig. S4. PLK4 is overexpressed in tumor biopsies

PLK2, PLK3 and PLK4 gene expression in normal human muscle (n=121) and in PAX3-FOXO1 positive aRMS patient-derived biopsies (n=46) measured by microarray (Affymetrix HG-U133A). *Box plot,* minimum to maximum; Student's t-test *** $p < 0.0001$.

Fig. S5. PLK1 staining does not correlate with MIB1 staining in tumor biopsies

Pearson correlation of PLK1 and MIB1 staining based on tissue microarray (n=42); p= 0.1137.

Fig. S6. PLK4 silencing reduces PAX3-FOXO1 activity

Relative mRNA expression of PAX3-FOXO1 and its target genes upon PLK1, PLK4 and PLK1+PLK4 knockdowns. C_T values relative to scrambled knockdown were measured by qRT-PCR and normalized to GAPDH expression. Silencing was performed for 48h using 8 nM siPLK1 (s449) and 25 nM siPLK4 in Rh4 cells. Western blot analysis is showing PLK4 knockdown efficiency. *Columns,* geometric mean of 4 independent experiments performed in triplicates; *bars,* 95% confidence interval; * significant according to 95% CI.

Fig. S7. PLK1 inhibition causes NMYC degradation

Western blot analysis of endogenous NMYC degradation upon PLK1 inhibition. RMS13 and Rh4 cells were treated with DMSO, 15 nM BI 2536 or 20 nM BI 6727 for 48h.

6.8 Figures and tables

Fig. 1

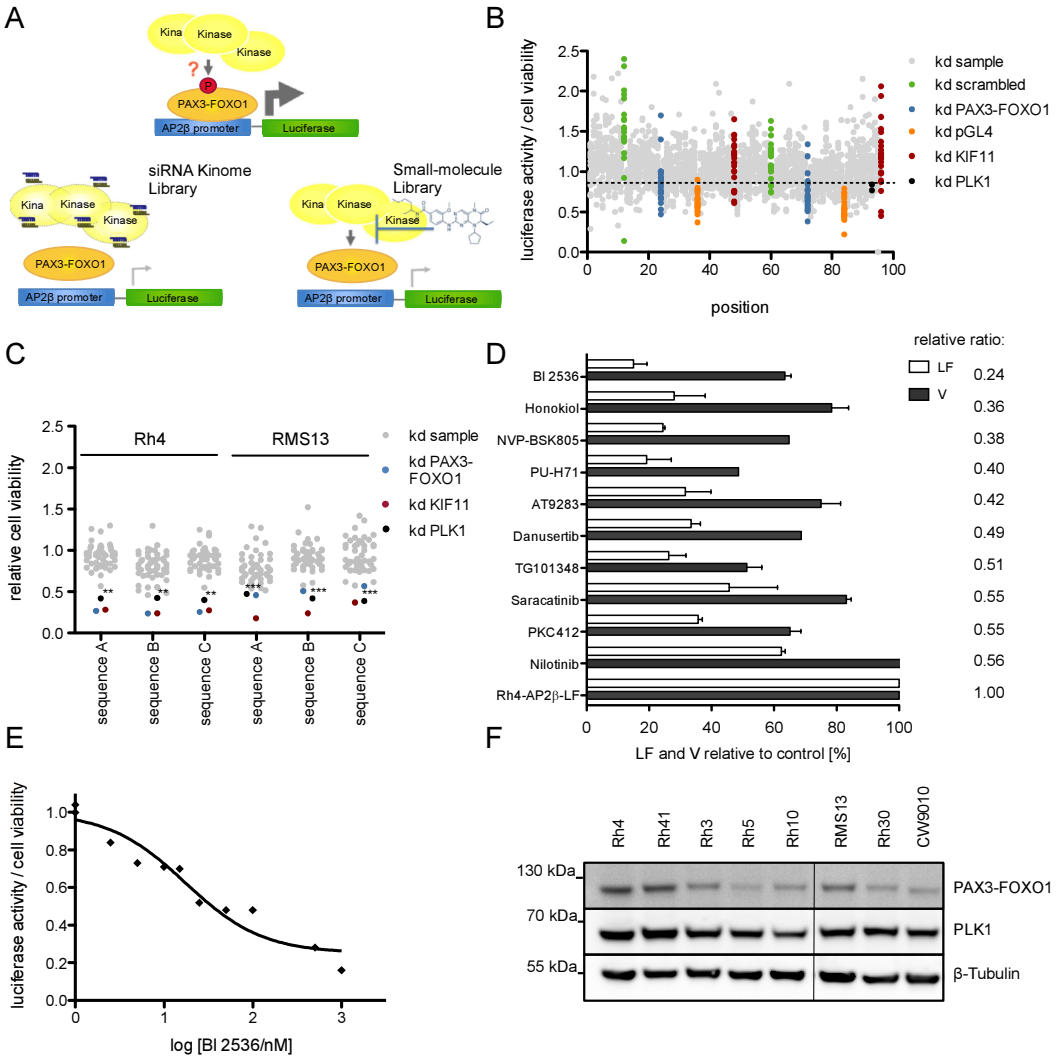

Fig. 2

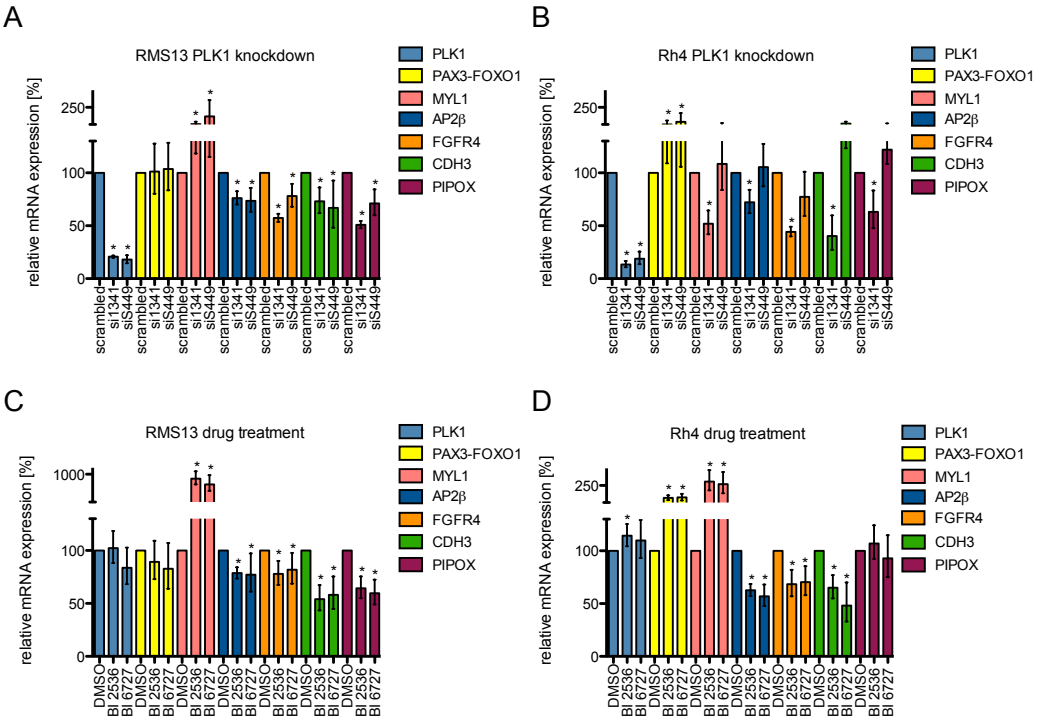
A
RMS13 PLK1 knockdown
relative mRNA expression [%]
PLK1
PAX3-FOXO1
MYL1
AP2β
FGFR4
CDH3
PIPOX
scrambled
si1341
siS449
B
Rh4 PLK1 knockdown
C
RMS13 drug treatment
DMSO
BI 2536
BI 6727
D
Rh4 drug treatment

Fig. 3

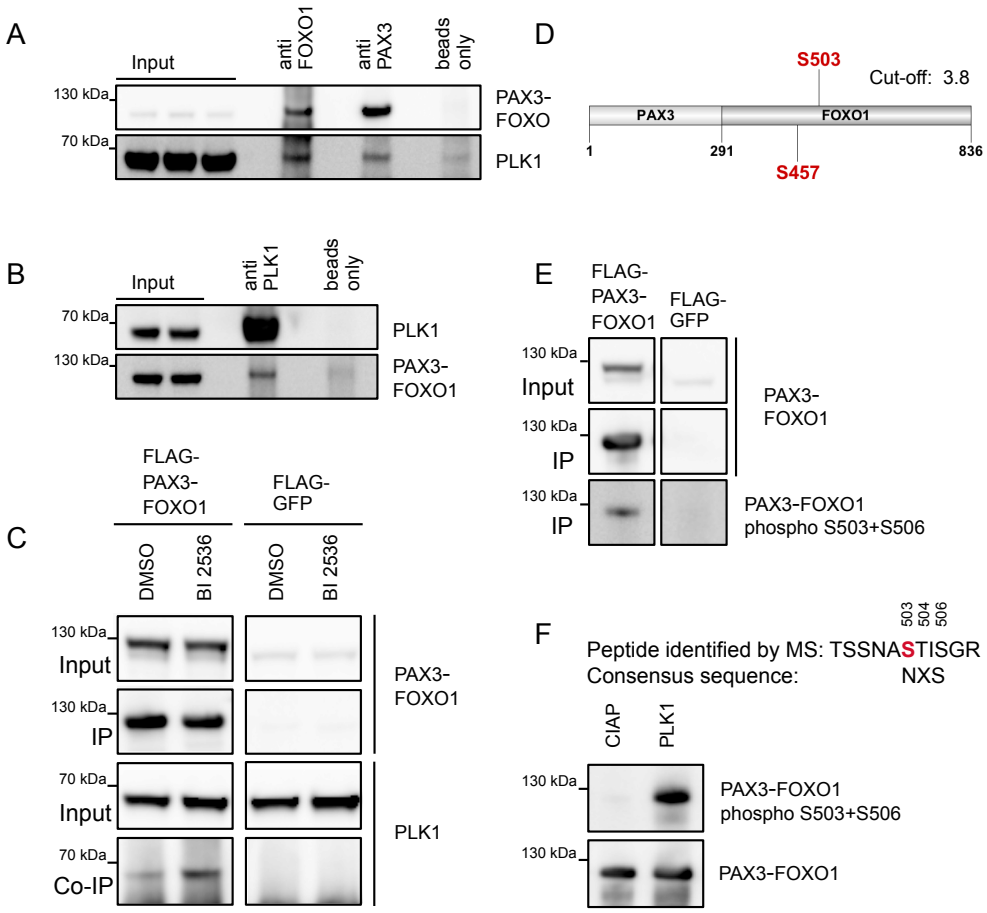
A
Input
anti FOXO1
anti PAX3
beads only
130 kDa
70 kDa
PAX3-FOXO
PLK1
B
Input
anti PLK1
beads only
70 kDa
130 kDa
PLK1
PAX3-FOXO1
C
FLAG-PAX3-FOXO1
FLAG-GFP
DMSO
BI 2536
DMSO
BI 2536
130 kDa
Input
130 kDa
IP
70 kDa
Input
70 kDa
Co-IP
PAX3-FOXO1
PLK1
D
S503
Cut-off: 3.8
PAX3
FOXO1
1
291
836
S457
E
FLAG-PAX3-FOXO1
FLAG-GFP
130 kDa
Input
130 kDa
IP
130 kDa
IP
PAX3-FOXO1
PAX3-FOXO1 phospho S503+S506
F
503 504 506
Peptide identified by MS: TSSNASTISGR
Consensus sequence: NXS
CIAP
PLK1
130 kDa
130 kDa
PAX3-FOXO1 phospho S503+S506
PAX3-FOXO1

Fig. 4

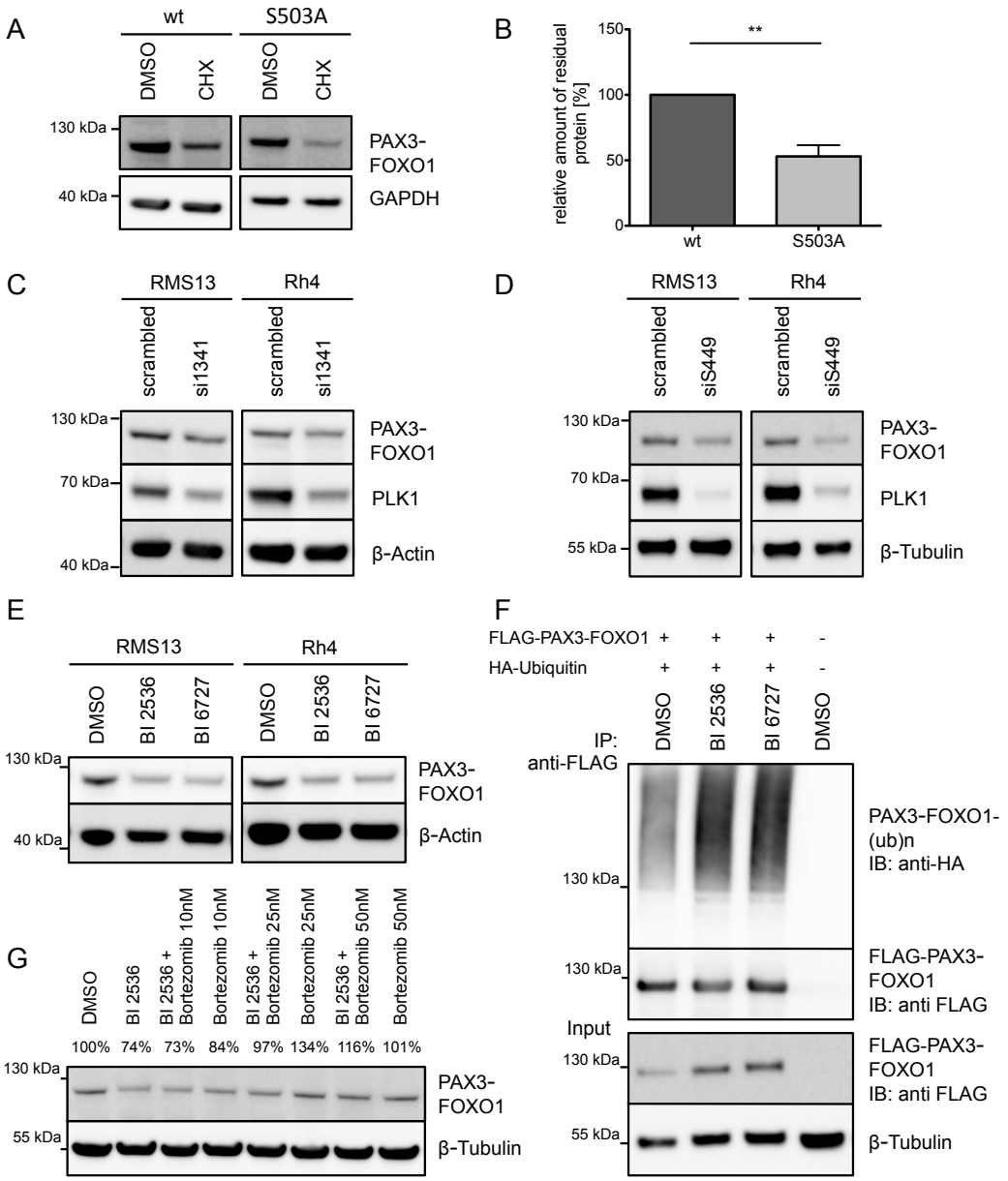
A
wt
S503A
DMSO
CHX
DMSO
CHX
130 kDa
40 kDa
PAX3-FOXO1
GAPDH
B
relative amount of residual protein [%]
150
100
50
0
**
wt
S503A
C
RMS13
Rh4
scrambled
si1341
scrambled
si1341
130 kDa
70 kDa
40 kDa
PAX3-FOXO1
PLK1
β-Actin
D
RMS13
Rh4
scrambled
siS449
scrambled
siS449
130 kDa
70 kDa
55 kDa
PAX3-FOXO1
PLK1
β-Tubulin
E
RMS13
Rh4
DMSO
BI 2536
BI 6727
DMSO
BI 2536
BI 6727
130 kDa
40 kDa
PAX3-FOXO1
β-Actin
F
FLAG-PAX3-FOXO1 + + + -
HA-Ubiquitin + + + -
DMSO
BI 2536
BI 6727
DMSO
IP: anti-FLAG
130 kDa
PAX3-FOXO1-(ub)n
IB: anti-HA
130 kDa
FLAG-PAX3-FOXO1
IB: anti FLAG
Input
130 kDa
FLAG-PAX3-FOXO1
IB: anti FLAG
55 kDa
β-Tubulin
G
DMSO
BI 2536
BI 2536 + Bortezomib 10nM
Bortezomib 10nM
BI 2536 + Bortezomib 25nM
Bortezomib 25nM
BI 2536 + Bortezomib 50nM
Bortezomib 50nM
100% 74% 73% 84% 97% 134% 116% 101%
130 kDa
55 kDa
PAX3-FOXO1
β-Tubulin

Fig. 5

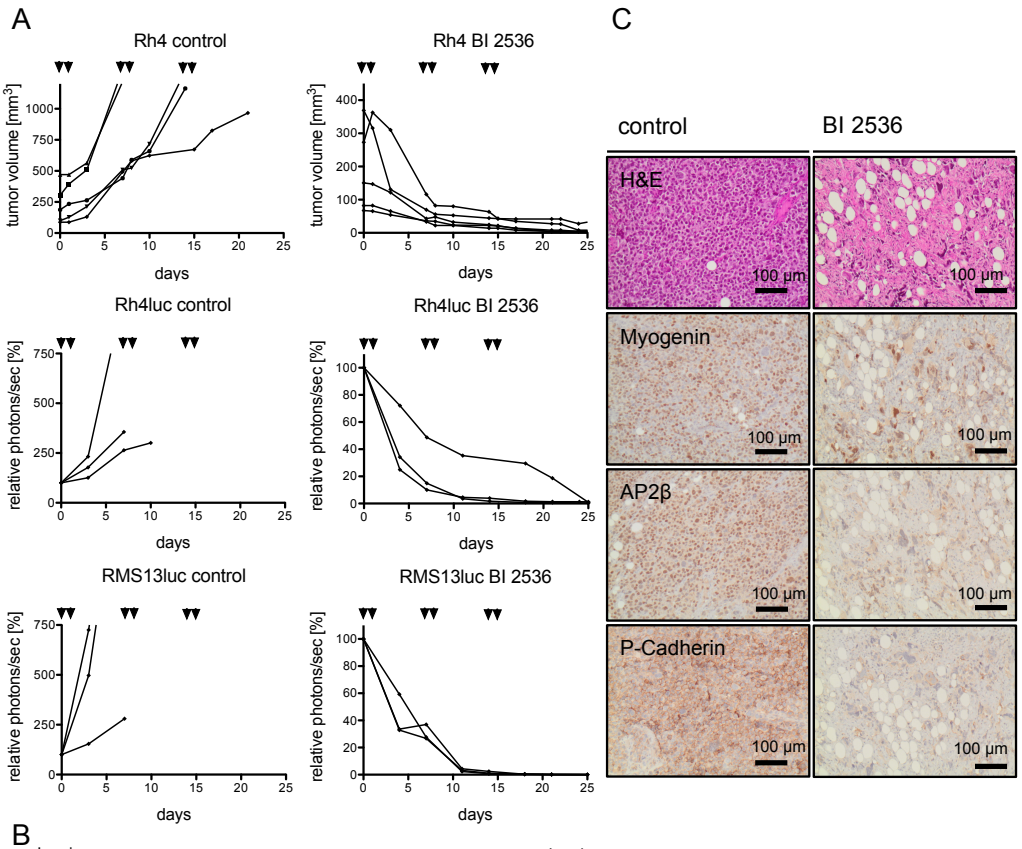
A
Rh4 control
Rh4 BI 2536
tumor volume [mm3]
days
Rh4luc control
Rh4luc BI 2536
relative photons/sec [%]
RMS13luc control
RMS13luc BI 2536
C
control
BI 2536
H&E
Myogenin
AP2β
P-Cadherin
100 µm

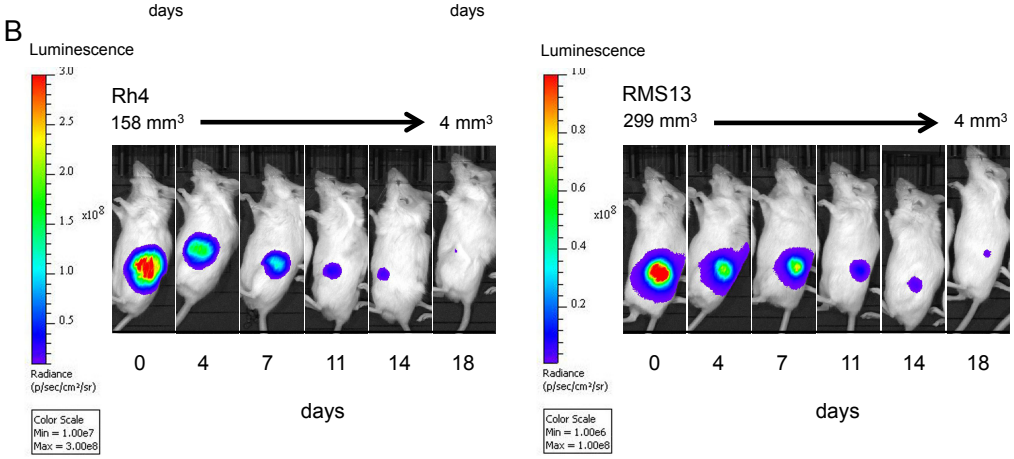
B
Luminescence
Rh4
158 mm3
4 mm3
RMS13
299 mm3
4 mm3
x10^8
Radiance (p/sec/cm²/sr)
Color Scale
Min = 1.00e7
Max = 3.00e8
Min = 1.00e6
Max = 1.00e8
0 4 7 11 14 18
days

Fig. 6

A

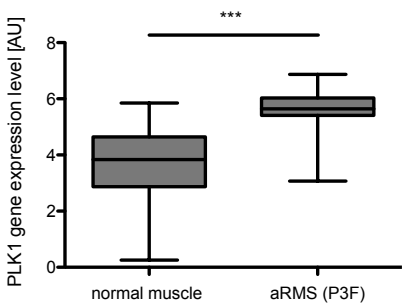

B

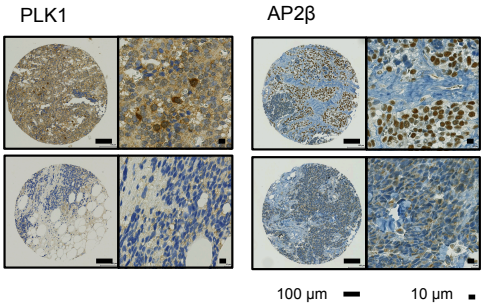

C

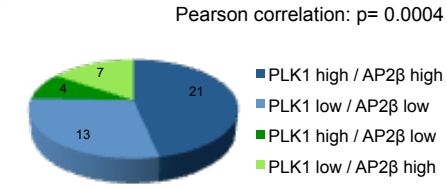

D

PLK1	5yr EFS	95% CI	5yr OS	95% CI
low n=23	42.4%	26.1-68.8%	59.7%	42.4-84.0%
high n=26	15.4%	6.2-37.9 %	20.2%	8.6-47.2%

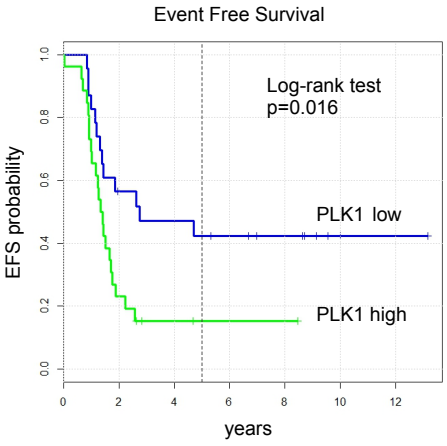

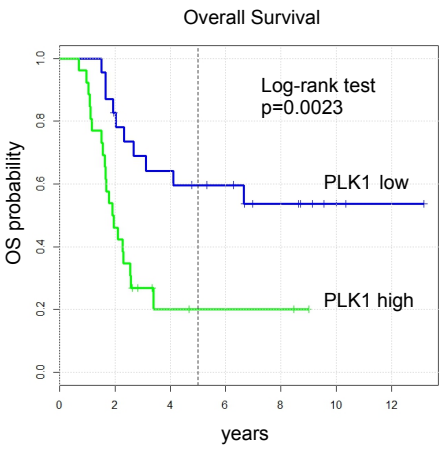

Tab. 1

	relative risk	p-value
Event Free Survival		
Age	0.996	0.892
Sex (male vs. female)	0.709	0.367
Localization (unfavorable vs. favorable)	0.704	0.577
PLK1 (high vs. low)	2.340	0.028
Overall Survival		
Age	1.016	0.571
Sex (male vs. female)	0.701	0.392
Localization (unfavorable vs. favorable)	1.230	0.797
PLK1 (high vs. low)	2.560	0.020

Tab. 1. Multivariate analysis

6.9 Supplementary figures and tables

Fig. S1

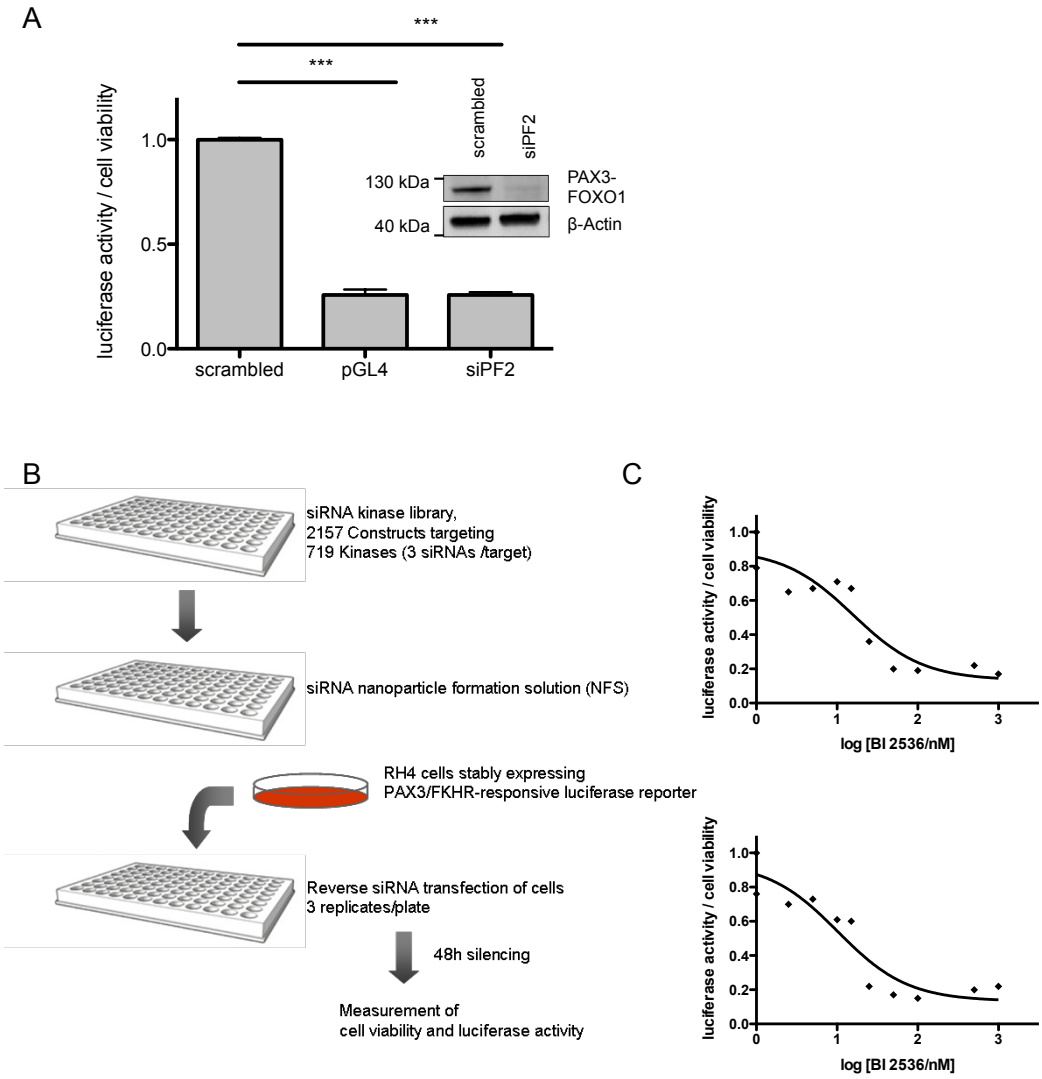

Fig. S2

A

Cell line	BI 2536 IC_{50}	Type
Rh4	14.58 nM	alveolar
Rh30	15.48 nM	alveolar
RMS13	14.18 nM	alveolar
Rh41	16.70 nM	alveolar
RD	33.04 nM	embryonal
Rh36	30.67 nM	embryonal
Ruch2	44.74 nM	embryonal
Ruch3	14.70 nM	embryonal

B

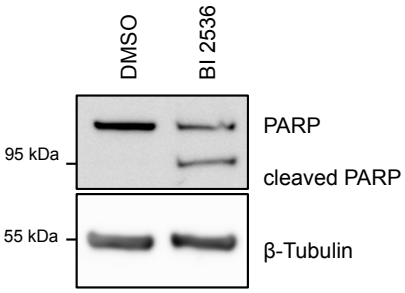

C

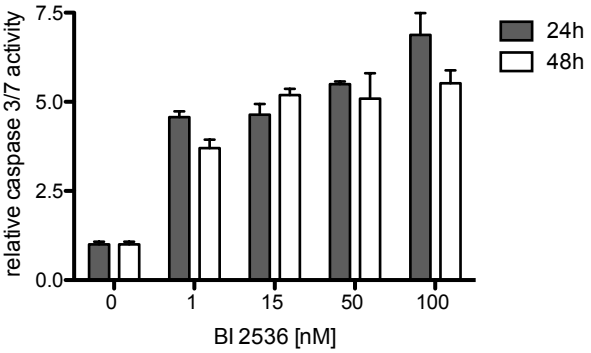

D

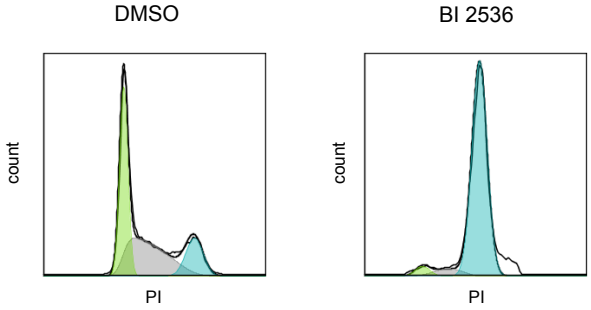

Fig. S3

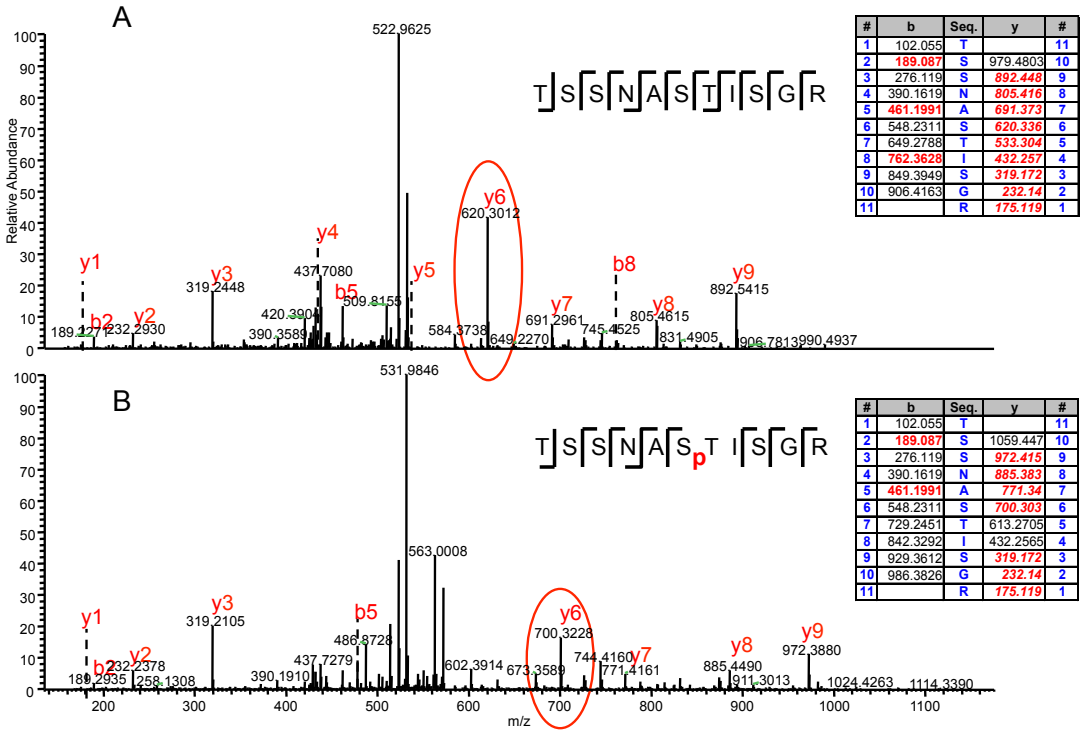

#	b	Seq.	y	#
1	102.055	T		11
2	189.087	S	979.4803	10
3	276.119	S	892.448	9
4	390.1619	N	805.416	8
5	461.1991	A	691.373	7
6	548.2311	S	620.336	6
7	649.2788	T	533.304	5
8	762.3628	I	432.257	4
9	849.3949	S	319.172	3
10	906.4163	G	232.14	2
11		R	175.119	1

#	b	Seq.	y	#
1	102.055	T		11
2	189.087	S	1059.447	10
3	276.119	S	972.415	9
4	390.1619	N	885.383	8
5	461.1991	A	771.34	7
6	548.2311	S	700.303	6
7	729.2451	T	613.2705	5
8	842.3292	I	432.2565	4
9	929.3612	S	319.172	3
10	986.3826	G	232.14	2
11		R	175.119	1

Fig. S4

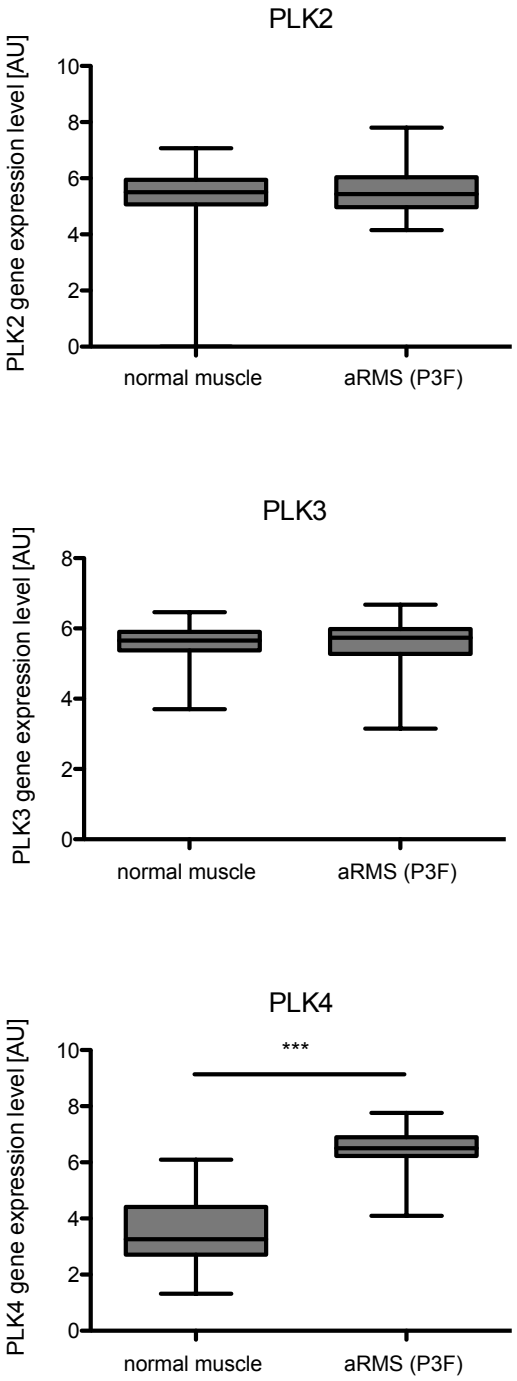
PLK2
PLK2 gene expression level [AU]
10
8
6
4
2
0
normal muscle
aRMS (P3F)
PLK3
PLK3 gene expression level [AU]
8
6
4
2
0
normal muscle
aRMS (P3F)
PLK4
***
PLK4 gene expression level [AU]
10
8
6
4
2
0
normal muscle
aRMS (P3F)

Fig. S5

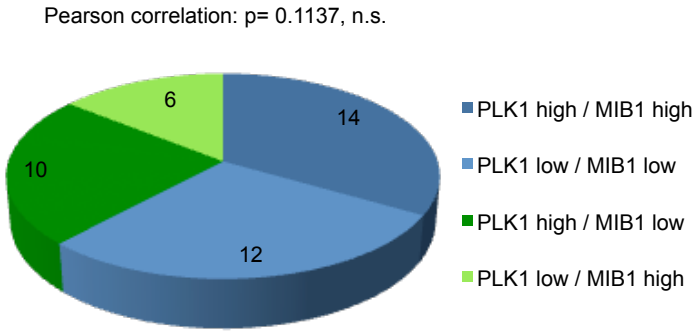
Pearson correlation: p= 0.1137, n.s.
14
12
10
6
PLK1 high / MIB1 high
PLK1 low / MIB1 low
PLK1 high / MIB1 low
PLK1 low / MIB1 high

Fig. S6

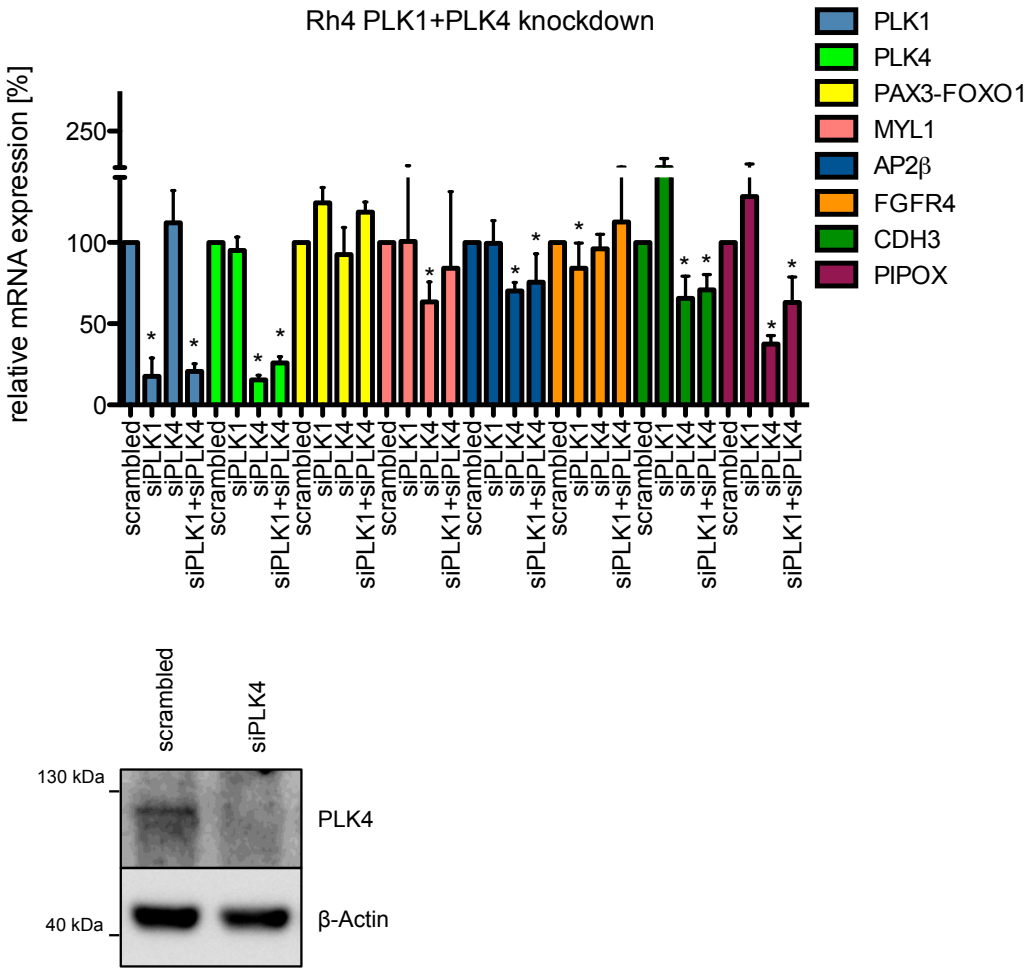
Rh4 PLK1+PLK4 knockdown
relative mRNA expression [%]
250
100
50
0
PLK1
PLK4
PAX3-FOXO1
MYL1
AP2β
FGFR4
CDH3
PIPOX
scrambled
siPLK1
siPLK4
siPLK1+siPLK4
scrambled
siPLK1
siPLK4
siPLK1+siPLK4
scrambled
siPLK1
siPLK4
siPLK1+siPLK4
scrambled
siPLK1
siPLK4
siPLK1+siPLK4
scrambled
siPLK1
siPLK4
siPLK1+siPLK4
scrambled
siPLK1
siPLK4
siPLK1+siPLK4
scrambled
siPLK1
siPLK4
siPLK1+siPLK4
scrambled
siPLK1
siPLK4
siPLK1+siPLK4
scrambled
siPLK1
siPLK4
siPLK1+siPLK4

scrambled
siPLK4
130 kDa
40 kDa
PLK4
β-Actin

Fig. S7

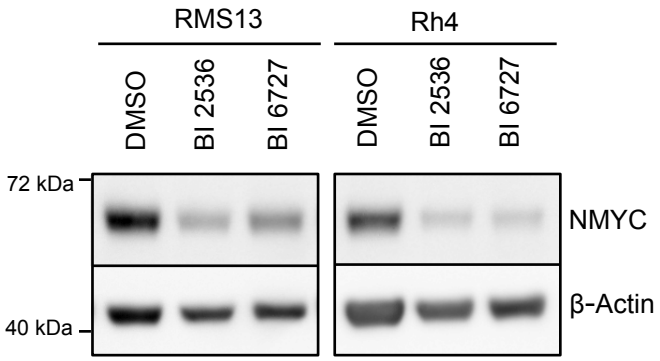
RMS13
Rh4
DMSO
BI 2536
BI 6727
DMSO
BI 2536
BI 6727
72 kDa
40 kDa
NMYC
β-Actin

Tab. S1

Gene Symbol	Entrez Gene Name	MAPK signaling	Phosphatidyl-inositol signaling	Cell cycle regulation
AGK	acyl glycerol kinase			
ALPK3	alpha-kinase 3			
AKT3	v-akt murine thymoma viral oncogene homolog 3 (protein kinase B, gamma)	+		
BUB1B	budding uninhibited by benzimidazoles 1 homolog beta (yeast)			+
CAMK2N1	calcium/calmodulin-dependent protein kinase II inhibitor 1			
CDC2L5	cell division cycle 2-like 5 (cholinesterase-related cell division controller)			+
CSNK1A1	casein kinase 1, alpha 1			
DDR1	discoidin domain receptor tyrosine kinase 1			
EPHA2	EPH receptor A2			
GLYCTK	glycerate kinase			
GUK1	guanylate kinase 1			
ITGB1BP3	integrin beta 1 binding protein 3			
KCNE1	potassium voltage-gated channel, Isk-related family, member 1			
MAP3K7CL	MAP3K7 C-terminal-like protein/TAK1-like protein			
MAPKSP1	MAPK scaffold protein 1	+		
MAST2	microtubule associated serine/threonine kinase 2			
MKNK1	MAP kinase-interacting serine/threonine kinase 1	+		
MUSK	muscle, skeletal, receptor tyrosine kinase			
MYLK4	myosin light chain kinase family, member 4			
NEK2	NIMA (never in mitosis gene a)-related kinase 2			+
NMRK1	nicotinamide riboside kinase 1			
PFKL	phosphofructokinase, liver			
PI4KA	phosphatidylinositol 4-kinase, catalytic, alpha		+	
PI4K2B	phosphatidylinositol 4-kinase type 2 beta		+	
PIK3C2A	phosphoinositide-3-kinase, class 2, alpha		+	
PIK3R3	phosphoinositide-3-kinase, regulatory subunit, 3 (gamma)		+	
PIM1	pim-1 oncogene			+
PIM3	pim-3 oncogene		+	+
PIP4K2A	phosphatidylinositol-4-phosphate 5-kinase, type II, alpha		+	
PIP4K2B	phosphatidylinositol-4-phosphate 5-kinase, type II, beta			
PLK1	polo-like kinase 1			+
PRKCA	protein kinase C, alpha	+	+	+
PRKD1	protein kinase D1			
RFK	riboflavin kinase			
RPS6KA5	ribosomal protein S6 kinase, 90kD, polypeptide 5	+		
ROCK2	Rho-associated, coiled-coil containing protein kinase 2			+
SH3BP4	SH3-domain binding protein 4			
SIK3	SIK family kinase 3			
SKP2	S-phase kinase-associated protein 2 (p45)			+
SLK	STE20-like kinase			
TEX14	testis expressed 14			+
TRIB2	tribbles homolog 2 (Drosophila)			
TRIB3	tribbles homolog 3 (Drosophila)			
TTK	TTK protein kinase			+
UCK1	uridine-cytidine kinase 1			
YES1	v-yes-1 Yamaguchi sarcoma viral oncogene homolog 1			
ZMYND8	zinc finger, MYND-type containing 8			

Tab. S2

Compound name	Company	Target
ABT-737	Abbott, Baar/Zug, Switzerland	BCL-2, BCL-xl inhibitor
OSI-027	Active Biochem, Maplewood, NJ, USA	mTORC1/2 inhibitor
PP242	Active Biochem, Maplewood, NJ, USA	mTORC1/2 inhibitor
IGC-001	AdooQ Bioscience, Irvine, CA, USA	Beta-catenin inhibitor
A 769662	Axon Medchem, Groningen, NL	AMPK activator
ABT-102	Axon Medchem, Groningen, NL	TRVP1 antagonist
AEG 3482	Axon Medchem, Groningen, NL	JNK inhibitor
AG 013736 - Axitinib	Axon Medchem, Groningen, NL	VEGFR inhibitor
AMN 107 (Nilotinib)	Axon Medchem, Groningen, NL	BCR-ABL inhibitor
Apratastat	Axon Medchem, Groningen, NL	TACE/MMP inhibitor
AS 252424	Axon Medchem, Groningen, NL	PI3K p110 gamma inhibitor
Atazanivir	Axon Medchem, Groningen, NL	Protease inhibitor
AZD 2281 - Olaparib	Axon Medchem, Groningen, NL	PARP inhibitor
AZD 7762	Axon Medchem, Groningen, NL	CHK inhibitor
BACE 1 inhibitor	Axon Medchem, Groningen, NL	Beta secretase inhibitor
BI 2536	Axon Medchem, Groningen, NL	PLK-1 inhibitor
BMS 189961	Axon Medchem, Groningen, NL	RAR gamma agonist
BMS 270394	Axon Medchem, Groningen, NL	RAR gamma agonist
Bosutinib (SKI 606)	Axon Medchem, Groningen, NL	BCR-ABL/SRC inhibitor
Butabindide	Axon Medchem, Groningen, NL	TPPII inhibitor
BX 795	Axon Medchem, Groningen, NL	PDK1/TBK1 inhibitor
BX 912	Axon Medchem, Groningen, NL	PDK1 inhibitor
BZ - Gamma Secretase inhibitor	Axon Medchem, Groningen, NL	Gamma secretase inhibitor
Cediranib	Axon Medchem, Groningen, NL	VEGFR inhibitor
CH 55	Axon Medchem, Groningen, NL	RARα/β agonist
Chir98014	Axon Medchem, Groningen, NL	GSK-3 inhibitor
CI-1033 - Canertinib	Axon Medchem, Groningen, NL	EGFR inhibitor
Combretastatin-A4 (CA-4)	Axon Medchem, Groningen, NL	Inhibitor of tubulin polymerization
CP 690550	Axon Medchem, Groningen, NL	JAK-3 inhibitor
CT 99021 - CHIR 99021	Axon Medchem, Groningen, NL	GSK-3 inhibitor
DAPT	Axon Medchem, Groningen, NL	Gamma secretase inhibitor
Dasatinib	Axon Medchem, Groningen, NL	BCR-ABL/SRC inhibitor
DBZ	Axon Medchem, Groningen, NL	Gamma secretase inhibitor
Deguelin	Axon Medchem, Groningen, NL	Anti-cancer agent
DM 3189	Axon Medchem, Groningen, NL	BMP inhibitor
Doramapimod	Axon Medchem, Groningen, NL	p38 MAPK inhibitor
DR 2313	Axon Medchem, Groningen, NL	PARP inhibitor
FK 866	Axon Medchem, Groningen, NL	NAPRT1 inhibitor, anti-cancer agent
GDC 0879	Axon Medchem, Groningen, NL	B-Raf inhibitor
GDC 0941	Axon Medchem, Groningen, NL	PI3K inhibitor
GSK 269962A	Axon Medchem, Groningen, NL	ROCK1 inhibitor
GW 441756	Axon Medchem, Groningen, NL	TrkA inhibitor
GW 786034	Axon Medchem, Groningen, NL	VEGFR/KIT/PDGFR inhibitor
GW 843682X	Axon Medchem, Groningen, NL	PLK inhibitor
HU-308	Axon Medchem, Groningen, NL	CB2 agonist
Imatinib	Axon Medchem, Groningen, NL	Bcr-Abl inhibitor
Iressa (Gefitinib)	Axon Medchem, Groningen, NL	EGFR inhibitor
JWH 018	Axon Medchem, Groningen, NL	CB2 agonist
JWH 073	Axon Medchem, Groningen, NL	CB1/2 agonist
JWH 133	Axon Medchem, Groningen, NL	CB2 agonist
Ko 143	Axon Medchem, Groningen, NL	BCRP inhibitor

Lamotrigine	Axon Medchem, Groningen, NL	Glutamate antagonist
Lapatinib	Axon Medchem, Groningen, NL	EGFR/ErbB-2 inhibitor
LE-135	Axon Medchem, Groningen, NL	RAR antagonist
LY 2157299	Axon Medchem, Groningen, NL	TGF beta inhibitor
LY 294002	Axon Medchem, Groningen, NL	PI3K inhibitor
Masitinib mesylate	Axon Medchem, Groningen, NL	KIT/PDGFR inhibitor
MK 1775	Axon Medchem, Groningen, NL	Wee1 inhibitor
Myoseverin	Axon Medchem, Groningen, NL	Microtubule inhibitor
NSC 348884	Axon Medchem, Groningen, NL	Nucleophosmin inhibitor
NSC 625987	Axon Medchem, Groningen, NL	CDK4 inhibitor
NU 1025	Axon Medchem, Groningen, NL	PARP inhibitor
NU 7441	Axon Medchem, Groningen, NL	DNA-PK inhibitor
NVP-BAG956	Axon Medchem, Groningen, NL	PI3K/PDK1 inhibitor
NVP-BEZ235	Axon Medchem, Groningen, NL	PI3K/mTOR inhibitor
NVP-TAE684	Axon Medchem, Groningen, NL	ALK inhibitor
OSI 774 - Erlotininb	Axon Medchem, Groningen, NL	EGFR inhibitor
Palmitoylethanolamide	Axon Medchem, Groningen, NL	Endocannabinoid
PD 0325901	Axon Medchem, Groningen, NL	MEK inhibitor
PD 166793	Axon Medchem, Groningen, NL	MMP inhibitor
PD 169316	Axon Medchem, Groningen, NL	p38 MAPK inhibitor
PD 180970	Axon Medchem, Groningen, NL	Src kinase inhibitor
PD 184352	Axon Medchem, Groningen, NL	MEK 1 inhibitor
PD 98059	Axon Medchem, Groningen, NL	MEK inhibitor
PF-00356231	Axon Medchem, Groningen, NL	MMP-12 inhibitor
PI 103	Axon Medchem, Groningen, NL	Class I PI3K inhibitor
PIK 75	Axon Medchem, Groningen, NL	PI3K p110 alpha inhibitor
PIK 90	Axon Medchem, Groningen, NL	PI3K p110 alpha inhibitor
PLX 4720	Axon Medchem, Groningen, NL	B-Raf inhibitor
Ruboxistaurin (LY333531)	Axon Medchem, Groningen, NL	PKC beta inhibitor
Saracatinib	Axon Medchem, Groningen, NL	Src and Abl inhibitor
SB 202190	Axon Medchem, Groningen, NL	p38 MAPK inhibitor
SB 203580	Axon Medchem, Groningen, NL	p38 MAPK inhibitor
SB 216763	Axon Medchem, Groningen, NL	GSK-3 inhibitor
SD 169	Axon Medchem, Groningen, NL	p38 alpha MAPK inhibitor
SD 208	Axon Medchem, Groningen, NL	TGF-betaR1 inhibitor
SL 327	Axon Medchem, Groningen, NL	MEK inhibitor
Sorafenib (BAY 43-9006)	Axon Medchem, Groningen, NL	Raf/Mek/Erk inhibitor
Stobadine	Axon Medchem, Groningen, NL	Antioxidant
SU 6656	Axon Medchem, Groningen, NL	Src kinase inhibitor
Sunitinib - SU 11248	Axon Medchem, Groningen, NL	Multiple RTK inhibitor
Tandutinib	Axon Medchem, Groningen, NL	FLT3 inhibitor
TGX 221	Axon Medchem, Groningen, NL	PI3K p110 beta inhibitor
Tiplaxtinin	Axon Medchem, Groningen, NL	PAI-1 inhibitor
Tyrphostin AG 490	Axon Medchem, Groningen, NL	JAK2 inhibitor
U 73122	Axon Medchem, Groningen, NL	Phospholipase C inhibitor
ZD 6474 (Vandetanib)	Axon Medchem, Groningen, NL	VEGFR/EGFR inhibitor
481407 NF-kB Inhibitor	Calbiochem, Zug, Switzerland	NF-kB Inhibitor
Compound C	Calbiochem, Zug, Switzerland	AMPK inhibitor
JAK inhibitor I	Calbiochem, Zug, Switzerland	JAKs inhibitor
PD150606	Calbiochem, Zug, Switzerland	Calpain inhibitor
Mifepristone	Cayman, Ann Arbor, MI, USA	Progesterone and glucocorticoid receptor (GR) antagonist
Piceatannol	Cayman, Ann Arbor, MI, USA	Syk inhibitor
Vorinostat/SAHA	Cayman, Ann Arbor, MI, USA	HDAC inhibitor
Bortezomib(Velcade)	Cilag, Schaffhausen, Switzerland	Proteasome inhibitor
Cyclopamine	Enzo Life Sciences, Lausen, Switzerland	Hedgehog Pathway Inhibitor
L-aminoadipic acid	Enzo Life Sciences, Lausen, Switzerland	Glutamine synthase inhibitor
Tacrolimus	Enzo Life Sciences, Lausen, Switzerland	Calcineurin inhibitor
XL228	Exelixis, San Francisco, CA, USA	Multiple Tyr-kinase inhibitor (IGF1-R, Bcr-Abl)

Obatoclax	GeminX, Montreal, Canada	Bcl-2 inhibitor
2-Deoxy-D-glucose	Invitrogen, Basel, Switzerland	Glycolysis inhibitor
NVP-AEW541	Novartis, Basel, Switzerland	IGF-1R inhibitor
NVP-BGJ398	Novartis, Basel, Switzerland	FGF-R inhibitor
NVP-BKM120	Novartis, Basel, Switzerland	PI3K inhibitor
NVP-BSK805	Novartis, Basel, Switzerland	JAK2 inhibitor
NVP-TKI258	Novartis, Basel, Switzerland	FGF-R inhibitor
PKC412 (midostaurin)	Novartis, Basel, Switzerland	Multi-targeted kinase inhibitor
[Ala92]-p16 (84-103)	Selleck Chemicals, Houston, TX, USA	Cdk inhibitor
AT9283	Selleck Chemicals, Houston, TX, USA	Aurora kinases, JAK2, Flt3, and Abl inhibitor
AZD1152-HQPA	Selleck Chemicals, Houston, TX, USA	Aurora B inhibitor
Bax inhibitor peptide P5	Selleck Chemicals, Houston, TX, USA	Bcl-2 protein family inhibitor
Bax inhibitor peptide V5	Selleck Chemicals, Houston, TX, USA	Bcl-2 protein family inhibitor
CP-690550	Selleck Chemicals, Houston, TX, USA	JAK3 Inhibitor
GDC-0449	Selleck Chemicals, Houston, TX, USA	Hedgehog Pathway Inhibitor
Gefitinib	Selleck Chemicals, Houston, TX, USA	EGFR kinase inhibitor
JIP-1 (153-163)	Selleck Chemicals, Houston, TX, USA	JNK inhibitor
KU-55933	Selleck Chemicals, Houston, TX, USA	ATM inhibitor
MK-2206	Selleck Chemicals, Houston, TX, USA	Akt inhibitor
MLN8237	Selleck Chemicals, Houston, TX, USA	Aurora kinase inhibitor
NVP-AUY922	Selleck Chemicals, Houston, TX, USA	HSP90 inhibitor
PHA-739358(Danusertib)	Selleck Chemicals, Houston, TX, USA	Aurora kinases, Bcr-Abl and FGFR inhibitor
Pimecrolimus	Selleck Chemicals, Houston, TX, USA	Calcineurin inhibitor
S31-201	Selleck Chemicals, Houston, TX, USA	Stat Inhibitor
SNS-314	Selleck Chemicals, Houston, TX, USA	Aurora kinases A, B, and C inhibitor
SU11274	Selleck Chemicals, Houston, TX, USA	c-Met inhibitor
TG101348/SAR302503	Selleck Chemicals, Houston, TX, USA	JAK2 (Flt3) inhibitor
TW-37	Selleck Chemicals, Houston, TX, USA	Bcl-2 protein family inhibitor
Vandetanib	Selleck Chemicals, Houston, TX, USA	VEGFR, EGFR Inhibitor
xav-939	Selleck Chemicals, Houston, TX, USA	Wnt/b-catenin signal transduction pathway inhibitor
Y-27632	Selleck Chemicals, Houston, TX, USA	p160 ROCK inhibitor
3-Bromopyruvate	Sigma Aldrich, Buchs, Switzerland	Alkylating agent and a potent inhibitor of glycolysis
3-MA	Sigma Aldrich, Buchs, Switzerland	Vps34 inhibitor (class III PI3K)
6-aminonicotinamide	Sigma Aldrich, Buchs, Switzerland	Pentose phosphate pathway inhibitor
AMD3100	Sigma Aldrich, Buchs, Switzerland	CXCR4 inhibitor
BAY 61-3606	Sigma Aldrich, Buchs, Switzerland	Syk inhibitor
BMS-345541	Sigma Aldrich, Buchs, Switzerland	IκB inhibitor
Cycloheximide	Sigma Aldrich, Buchs, Switzerland	Protein synthesis inhibitor
Cyclosporine	Sigma Aldrich, Buchs, Switzerland	Immunosupressant
Etomoxir	Sigma Aldrich, Buchs, Switzerland	Inhibitor of fatty acid oxidation
Honokiol	Sigma Aldrich, Buchs, Switzerland	pAkt, scr, p44/42 MAPK
L-685,485	Sigma Aldrich, Buchs, Switzerland	Gamma secretase inhibitor
L-methionine sulfoximide	Sigma Aldrich, Buchs, Switzerland	Gamma-glutamylcysteine synthetase and glutamine synthetase
Lonidamine	Sigma Aldrich, Buchs, Switzerland	Mitochondrial hexokinase inhibitor
NEC-1	Sigma Aldrich, Buchs, Switzerland	Necroptosis/RIPK inhibitor
Nocodazole	Sigma Aldrich, Buchs, Switzerland	Cell cycle G2/M inhibitor
PP2	Sigma Aldrich, Buchs, Switzerland	Src inhibitor
PU-H71	Sigma Aldrich, Buchs, Switzerland	HSP90 inhibitor
Ranolazine	Sigma Aldrich, Buchs, Switzerland	Partial inhibitor of fatty acid oxidation
Roscovitine/Celiciblib	Sigma Aldrich, Buchs, Switzerland	Cdk inhibitor
Thapsigargin	Sigma Aldrich, Buchs, Switzerland	Inhibitor of SERCA and EGFR down-regulator
VPA	Sigma Aldrich, Buchs, Switzerland	HDAC inhibitor

Tab. S3

Identified phospho-peptides *	Rh4	RMS13	Known phospho-sites in PAX3-FOXO1
ASAPQSDEGSDIDSEPDLPLKR	+	+	Octapeptide: S197, S201, S205, S209; Amstutz et al. 2008 S201, S205; Dietz et al. 2009 and 2011
HGFSSYTDSFVPPSGPSNPMNPTIGNGLSPQNSIR	+	+	
ASLQSGQEGAGDSPGSQFSK	+	+	
WPASPGSHSNDDFDNWSTFRPR	+	+	
TSSNASTISGR		+	
TSSNASTISGRLSPIMTEQDDLGEGDVHSMVYPPSAAK	+	+	
LSPIMTEQDDLGEGDVHSMVYPPSAAK	+		
YTYGQSSMSPLPQMPIQTLQDNK	+	+	
SSYGGMSQYNCAPGLLKELLTSDSPPHNDIMTPVDPGVAQPNSR		+	
ELLTSDSPPHNDIMTPVDPGVAQPNSR	+	+	
NDLMDGDTLDFNFDNVLPNQSFPHSVK	+	+	

* coverage after trypsin digestion up to 71%;
S430 (Liu et al. 2013) not covered

7 Extended results

7.1 Material and methods

Material and methods are mainly described Manuscript I.

Drugs and antibodies

Rh4 cells have been treated with BI 2536 (Axon Medchem, Groningen, NL), BI 6727 (Selleck Chemicals, Houston TX, USA), KaryoMAX® COLCEMID® Solution (GIBCO, Invitrogen, Basel, Switzerland), Vincristin-Teva® (Teva Pharma, Basel, Switzerland), hesperadin (Selleck Chemicals, Houston, TX, USA), Z-VAD-FMK (Selleck Chemicals, Houston, TX, USA), and AEW 541 (Novartis, Basel, Switzerland).

Western blot membranes were incubated with anti-FOXO1 (H-128; 1:1000; Santa Cruz Biotechnology, Heidelberg, Germany), anti-FOXO1A phospho S322 + S325 (phospho S503 + S506 in PAX3-FOXO1; ab60945; 1:500 Abcam, Cambridge, UK), anti-FOXO1 phospho S329 (phospho S510 in PAX3-FOXO1; ab58519; 1:500 Abcam), anti-phospho-(Ser) CDKs substrate (P-S2-100) rabbit mAb (9477; 1:1000; Cell Signaling, Bioconcept, Allschwil, Switzerland), anti-phospho-PLK binding motif (ST*P) (D73F6) rabbit mAb (5243; 1:1000; Cell Signaling), anti-PARP (9542; 1:1000; Cell Signaling), and anti-cyclin B1 (4138; 1:1000; Cell Signaling) antibodies. Anti-β-actin (13E5) rabbit mAb (4970; 1:1000; Cell Signaling) and anti-GAPDH (D16H11) XP™ rabbit mAb (5174; 1:1000; Cell Signaling) were used as loading controls.

Immunofluorescence

Rh4 cells were grown on chamber slides. Cells were fixed with 4% paraformaldehyde (Carl Roth, Amsterdam, Netherlands) in PBS for 15 min, quenched in 0.1 M glycine in PBS for 5 min, and permeabilized with 0.5% Triton X-100 in PBS for 15 min. Upon blocking in 3% BSA, cells were incubated with mouse anti-α-tubulin antibody (1:5000; clone B-5-1-2, Sigma-Aldrich, Buchs, Switzerland) for 1h at room temperature. Alexa Fluor® 488 goat anti-mouse IgG (1:500; Invitrogen, Basel, Switzerland) was used as secondary antibody. VECTASHIELD® mounting media (Vector Labs, USA) supplemented with DAPI was applied. Cells were analyzed using a Nikon Eclipse TE2000-U microscope (Nikon, Egg, Switzerland).

7.2 Results

PLK1 phosphorylates PAX3-FOXO1 at multiple sites *in vitro*

In total, PAX3-FOXO1 contains 23 PLK1 recognition motifs with the consensus sequences [D/E/N]Xp[S/T] or p[S/T]F, as they have been reported by Kettenbach et al. (2012). Furthermore, GPS-Polo 1.0 *in silico* analysis predicted 11 sites with different scores to be phosphorylated by members of the PLK family (Liu et al., 2013b) (Figs. 1A and 1B). We previously investigated the role of S503 in PAX3-FOXO1 stabilization (Manuscript I). However, remaining sites should be considered for validation in future studies as at least some of them might also contribute to fusion protein regulation. To experimentally demonstrate their direct *in vitro* phosphorylation by PLK1, we transfected HEK293T cells with FLAG-PAX3-FOXO1 encoding plasmid and dephosphorylated the purified protein by calf intestine alkaline phosphatase (CIAP) before performing *in vitro* kinase assays with different concentrations of recombinant PLK1. Results are schematically summarized in Fig. 1C for comparison to *in silico* predicted residues. Two of the depicted phospho-sites, S503/S506 and S510, were identified using phospho-specific antibodies for detection by Western blotting (Fig. 1D). In addition, samples were subjected to mass spectrometry for identification of phospho-peptides and phosphorylation sites were mapped by MASCOT analysis. A summary of five experiments is illustrated, and experiment details and MASCOT scores are listed in Figs. 1C and 1E. We applied two different PLK1 concentrations supposing higher specificity of phosphorylation events mediated by lower kinase concentrations, which was the case for phosphorylation at S30, S389/S393, S399, S503, and S510. Nevertheless, all assays and all identified phospho-sites should be considered at this moment due to limiting factors for technical implementation of the procedure. Varying protein coverage and CIAP dephosphorylation efficiency were difficult to standardize, leading to exclusion of false-negative peptides in individual experiments. Still, software-based prediction, consensus sequence comparison, detected phosphorylation in aRMS cells, and *in vitro* kinase assay results were overall concordant implying that repetition of the assay generated reliable data for validation in future studies. In summary, our findings suggest that PLK1 phosphorylates PAX3-FOXO1 at multiple sites *in vitro,* indicating high regulatory impact on PAX3-FOXO1 activity beyond the previously investigated function in protein stabilization.

CDK1 phosphorylates PAX3-FOXO1 at priming sites for PLK binding *in vitro*

Binding of PLK1 depends on priming events, either by self-priming or by CDK1 phosphorylation of PLK1 substrates (Reinhardt and Yaffe, 2013). Potential PLK binding sites in PAX3-FOXO1 were predicted using GPS-Polo 1.0 (Liu et al., 2013b). Interestingly, all of the identified sites are located within CDK1 consensus sequences as shown by phospho-prediction using GPS 2.1 (Xue et al., 2008) (Fig. 2A), proposing CDK1 as initiator of PLK1 - PAX3-FOXO1 axis activation. To confirm CDK1 as upstream kinase of the fusion protein, we used a CDK substrate specific antibody for detection of phosphorylation mediated by CDK1 in *in vitro* kinase assays (Fig. 2B). To further demonstrate that CDK1 phosphorylation initiates PLK1 recruitment, we applied an antibody detecting phosphorylated PLK binding motifs (ST*P) in PAX3-FOXO1 (Fig. 2C). In fact, Western blot analysis showed CDK1 phosphorylation of PAX3-FOXO1 *in vitro* within PLK binding motifs. Subsequently, we performed immunoprecipitation of FLAG-tagged PAX3-FOXO1 expressed in Rh4 cells to demonstrate that this mechanism also exists in aRMS cells. Applying antibody recognizing phosphorylated PLK binding motifs, we observed priming of PAX3-FOXO1 and increased interaction of PLK1 and the fusion protein under conditions of PLK1 inhibition (Fig. 2D). These observations indicate involvement of CDK1 phosphorylation rather than PLK1 self-priming. To show that CDK1 is in fact active under these conditions, we applied BI 2536 and BI 6727 and investigated CDK1 activity using CDK1 substrate antibody on Western blots of whole cell extracts. We observed enhanced expression of CDK1 co-activator cyclin B1 and increased CDK1 substrate phosphorylation, respectively CDK1 activity, as well as phosphorylation of PLK binding motifs. Applying the CDK1 inhibitor RO-3306, CDK1 phosphorylation activity as well as phosphorylation of PLK binding motifs decreased (Figs. 2E and 2F). In summary, these findings demonstrate that CDK1 might contribute to phosphorylation and regulation of the fusion protein. We suggest that PLK1 binding depends on CDK1 activity and thus, CDK1 might be responsible for recruiting PLK1 to PAX3-FOXO1.

PLK1 inhibition causes cell cycle arrest and activates the mitotic spindle assembly checkpoint

PLK1 plays a major role in cell cycle regulation. To investigate the effect of PLK1 inhibition on cell cycle progression in aRMS, we stained Rh4 cells with propidium iodide and subjected them to FACS analysis. We observed a strong G2/M arrest after PLK1 silencing and after treatment with PLK1 directed inhibitors (Fig. 3A). Additional

investigation of the induced cell cycle arrest by Western blot analysis revealed activation of the spindle assembly checkpoint in prometaphase as cyclin B1 was accumulated in PLK1 depleted cells (Fig. 3B). To verify checkpoint activation, we treated aRMS cells with PLK1 inhibitors showing increased cyclin B1 levels, while simultaneous use of hesperadin, a drug previously reported to override mitotic arrest (Lenart et al., 2007), prevented this accumulation, indicating checkpoint rescue (Fig. 3C). Furthermore, we confirmed our observations at single cell level by immunofluorescence microscopy. Untreated mitotic cells showed normal metaphases whereas BI 2536 treated cells demonstrated a phenotype of aberrant mono-polar spindles circled by chromosomes (Fig. 3D). Thus, our data imply that PLK1 inhibition in aRMS cells induces polo-arrest leading to spindle assembly checkpoint activation.

Mitotic arrest leads to degradation of PAX3-FOXO1

To test whether cell cycle arrest directly affects PAX3-FOXO1, we applied the mitotic inhibitors vincristine and colcemid. Both inhibitors cause G2/M arrest as demonstrated by FACS analysis after propidium iodide staining in Rh4 cells (Fig. 4A). Analyzing the fusion protein by Western blotting, we observed lower levels of PAX3-FOXO1 not only after BI 2536 and BI 6727 treatment, but also after vincristine and colcemid induced G2/M cell cycle arrest (Fig. 4B). This suggests either a mechanism that is regulating PAX3-FOXO1 in a cell cycle dependent manner or specific degradation of PAX3-FOXO1 during mitotic checkpoint activation.

Importantly, this degradation was not caused by apoptosis as the apoptotic inhibitor Z-VAD-FMK that completely inhibited caspase 3/7 activity (Fig. 4C) was not sufficient to rescue PAX3-FOXO1 degradation (Fig. 4B). To confirm that the degradation is not a consequence of apoptotic mechanisms, we investigated PAX3-FOXO1 protein levels after treatment with the IGF1R inhibitor AEW 541. Like PLK1 inhibitors, vincristine, and colcemid, this inhibitor induced apoptosis of aRMS cells as demonstrated by caspase 3/7 activity assays and PARP cleavage (Figs. 4D and 4F). However, in contrast to mitotic inhibitors, AEW 541 did neither cause G2/M arrest (Fig. 4E) nor did it induce PAX3-FOXO1 degradation (Fig. 4F). Taken together, these data suggest that PAX3-FOXO1 degradation is rather the consequence of mitotic arrest than the result of apoptotic mechanisms.

aRMS tumors relapse after BI 2536 withdrawal and develop resistance to PLK1 inhibition

In order to investigate PLK1 inhibition *in vivo*, we treated established aRMS tumors for three cycles and achieved nearly complete tumor regression irrespective of starting volumes (Fig. 5). Nevertheless, we decided to further follow tumor regrowth in five mice after discontinuation of treatment. Tumors suddenly relapsed around day 30 about two weeks after the last injection in four out of five mice and on day 50 in one of the cases. We started retreatment of two relapsed tumors and were able to achieve a second response to the drug. However, despite a reduction in tumor volume after the first week of treatment, tumors started to regrow after the second week during treatment phases. In a third round, relapse was already observed after week 1, indicating increasing resistance to PLK1 inhibition. These preliminary observations in only few mice urgently need further investigations as they might have major implications on therapy outcome. Furthermore, careful examination of escape mechanisms potentially supports prevention of resistance development.

7.3 Figure legends

Fig. 1. PLK1 phosphorylates PAX3-FOXO1 at multiple predicted sites *in vitro*

(A and B) *In silico* analysis of PAX3-FOXO1 phosphorylation by PLK using the phospho-site prediction software GPS-Polo 1.0.

(C-E) PLK1 *in vitro* kinase assays. HEK293T cells were transfected with FLAG-tagged PAX3-FOXO1 expressing plasmid, purified, dephosphorylated by CIAP, and re-phosphorylated by recombinant PLK1.

(C) Summary of *in vitro* results depicted as graphic illustration for comparison to *in silico* results.

(D) Western blot analysis using phospho-S503+S506 and phospho-S510 antibodies.

(E) Phospho-peptides identified by mass spectrometry and phospho-site mapping by MASCOT analysis of five independent experiments.

Fig. 2. CDK1 phosphorylates PAX3-FOXO1 *in vitro* and potentially primes for PLK1 binding

(A) *In silico* analysis of PAX3-FOXO1 phosphorylation using GPS-Polo 1.0 for prediction of phosphorylated polo-box binding motifs and GPS 2.1 for phosphorylation by CDK1. Prediction scores are listed.

(B and C) CDK1 *in vitro* kinase assays. HEK293T cells were transfected with FLAG-tagged PAX3-FOXO1 expressing plasmid, purified, dephosphorylated by CIAP, and re-phosphorylated by recombinant CDK1.

(B) Western blot analysis using CDK substrate antibody.

(C) Western blot analysis using PLK binding motif antibody.

(D) Western blot analysis of PLK1 and of phosphorylation at PLK binding motifs after FLAG immunoprecipitation from Rh4 cells expressing FLAG-tagged PAX3-FOXO1. Cells were treated with DMSO or 15 nM BI 2536 for 16h. FLAG-tagged GFP was used as negative control.

(E and F) Rh4 cells were treated with 15 nM BI 2536 or 20 nM BI 6727 for 24h. CDK1 was inhibited by 5-10 µM RO-3306.

(E) Western blot analysis of phosphorylation at PLK binding motifs.

(F) Western blot analysis of CDK1 activity (CDK1 substrate antibody).

Fig. 3. PLK1 inhibition induces G2/M arrest and activation of the spindle assembly checkpoint

(A) Rh4 cells were treated with 25 nM PLK1 directed siRNA (S449) and with 15 nM BI 2536 or 20 nM BI 6727 for 48h. Cell cycle distribution was measured by FACS analysis after PI-staining.

(B) Western blot analysis after silencing of PLK1 in Rh4 cells for 48h using 25 nM siRNA (S449).

(C) Western blot analysis after treatment of Rh4 cells with 15 nM BI 2536 +/- 100 nM hesperadin and 20 nM BI 6727+/- 100 nM hesperadin for 24h.

(D) Immunofluorescence microscopy of Rh4 cells treated with DMSO or 15 nM BI 2536 for 2h. DAPI (blue) and α-tubulin (green) staining.

Fig. 4. Mitotic arrest induces degradation of PAX3-FOXO1

(A) Rh4 cells were treated with 10 nM vincristine and 135 nM colcemid for 48h. Cell cycle distribution was measured by FACS analysis after PI-staining.

(B) Western blot analysis of Rh4 cells treated with 15 nM BI 2536, 20 nM BI 6727, 10 nM vincristine, and 135 nM colcemid +/- 50 µM Z-VAD-FMK for 48h.

(C) Relative caspase 3/7 activity of Rh4 cells treated with 15 nM BI 2536, 20 nM BI 6727, 10 nM vincristine, and 135 nM colcemid +/- 50 µM Z-VAD-FMK for 48h; *Columns,* mean of technical replicates; *bars*, SD; *** $p \leq 0.0005$, ** $p = 0.0017$.

(D) Relative caspase 3/7 activity of Rh4 cells treated with increasing concentrations of BI 2536 and 1 µM AEW 541 for 24h and 48h. *Columns,* mean of technical replicates; *bars*, SD; *** $p < 0.0001$, ** $p = 0.0025$.

(E) Rh4 cells were treated with 1 µM AEW 541 for 48h. Cell cycle distribution was measured by FACS analysis after PI-staining.

(F) Western blot analysis of Rh4 cells treated with 1 µM AEW 541 for 24h and 48h.

Fig. 5. aRMS tumors relapse after BI 2536 withdrawal and develop resistance to PLK1 inhibition

In vivo drug treatment of NOD/Scid il2rg$^{-/-}$ mice engrafted with Rh4 (n=5). Mice bearing established tumors were treated intravenously with either vehicle control or BI 2536 at a dose of 40 mg/kg twice weekly on two consecutive days (indicated by triangles). Absolute tumor volume was measured by caliper.

7.4 Figures

Fig. 1

A

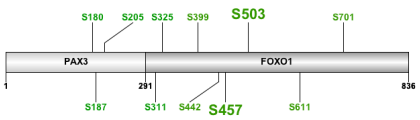

B

PLK phosphorylation	Peptide	Score	Cutoff
180	ERKEAEESEKKAKHS	3.243	2.590
187	SEKKAKHSIDGILSE	3.091	2.590
205	APQSDEGSDIDSEPD	3.312	2.590
311	TYQLSETSYQPTSIP	3.112	2.590
325	PQAVSDPSSTVHRPQ	2.855	2.590
399	NSIRHNLSLHSKFIR	2.764	2.590
442	AASMDNNSKFAKSRS	3.069	2.590
457	RAAKKKASLQSGQEG	3.942	2.590
503	PRTSSNASTISGRLS	3.844	2.590
611	KYTYGQSSMSPLPQM	2.707	2.590
701	HNKMMNPSSHTHPGH	2.826	2.590

C

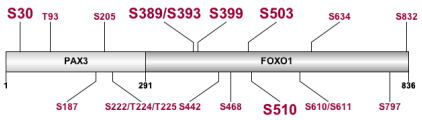

D

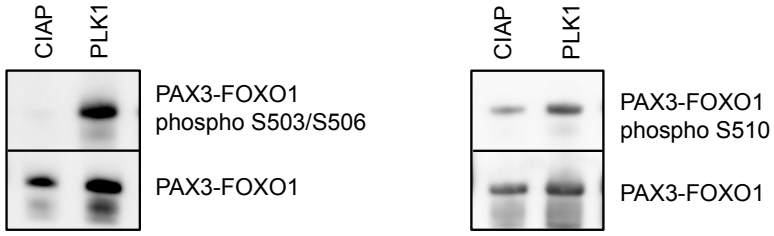

E

Peptide	In vitro kinase assay 2500ng (2x)	In vitro kinase assay 500ng (3x)	Probability relative to other possible residues within the relevant phospho-peptide (MASCOT analysis) 2500 ng	2500 ng	500 ng	Phospho-antibody	Residue in PAX3-FOXO1	Site prediction	Consensus Sequence	Detected in aRMS cells
SGFPLEVSTPLGQGR	2x	1x	S8 no score	S8 42.90%; T9 57.08%	S8 67.89%		**S30**		yes	
YQETGSIRPGAIGGSKPK	1x		T4 90.80%				T93			
AKHSIDGILSER	1x			S4 100%			S187			
ASAPQSDEGSDIDSEPDLPLKR	2x		S10 91.36%	S10 95.12%			S205	yes	yes	yes
TTFTAEQLEELER	1x			T1,T2 49.54%			S222/T224/T225		yes	
SRTTFTAEQLEELER	2x		S1,T3,T4 33.29%	S1 46.60; T3,T4 17.80%						
HGFSSYTDSFVPPSGPSNPMNPTIGNGLSPQNSIR		1x			S29,S33 38.83%		**S389/S393**			yes
HNLSLHSK	2x	1x	S4 99.69%	S4 99.49%	S4 80.72%		**S399**	yes	yes	
AASMDNNSKFAK	2x		S8 98.85%	S8 98.86%			S442	yes	yes	
ASLQSGQEGAGDSPGSQFSK	1x		S13 99.58%				S468			yes
TSSNASTISGR	1x	2x *		S6, T7 49.14%	S6,T7 39.92% S6 95.73%*	yes	**S503**	yes	yes	yes
Ser 510						yes	**S510**			yes
YTYGQSSMSPLPQMPIQTLQDNK	1x		S6, S7 48.88%				S610/S611	yes		yes
SSYGGMSQYNCAPGLLK	2x		S7 77.55%	S7 73.87%			S634		yes	
LDCDMESIIR	2x		S7 100%	S7 100%			S797			
TTTHSWVSG	1x		S5 67.97%				S832			

* First identification: phospho-peptide only found after PLK1 assay
Second identification (independent assay): phospho-peptide found before and after PLK1 assay, but phosphorylation detected at distinct sites (based on MASCOT analysis)

Fig. 2

A

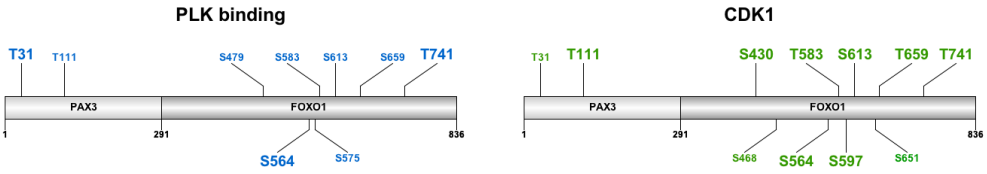

* Cutoff: 3.9

CDK1 phosphorylation	Peptide	Score	Cutoff	PLK binding	Score	Cutoff
31	GFPLEVSTPLGQGRV	4.043	2.300	PLK-binding	10.268	5.268
104	RPGAIGGSKPKQVTT	2.367	2.300			
111	SKPKQVTTPDVEKKI	5.892	2.300	PLK-binding	6.196	5.268
326	QAVSDPSSTVHRPQP	2.921	2.300			
327	AVSDPSSTVHRPQPL	2.583	2.300			
389	PTIGNGLSPQNSIRH	3.388	2.300			
430	EGGKSGKSPRRRAAS	6.410	2.300			
468	GQEGAGDSPGSQFSK	3.986	2.300			
479	QFSKWPASPGSHSND	2.396	2.300	PLK-binding	5.500	5.268
510	STISGRLSPIMTEQD	3.295	2.300			
564	DNLNLLSSPTSLTVS	5.986	2.300	PLK-binding	8.232	5.268
575	LTVSTQSSPGTMMQQ	3.360	2.300	PLK-binding	6.500	5.268
583	PGTMMQQTPCYSFAP	6.158	2.300	PLK-binding	6.661	5.268
597	PPNTSLNSPSPNYQK	4.187	2.300			
599	NTSLNSPSPNYQKYT	3.439	2.300			
613	TYGQSSMSPLPQMPI	4.396	2.300	PLK-binding	5.714	5.268
651	KELLTSDSPPHNDIM	4.014	2.300			
659	PPHNDIMTPVDPGVA	5.655	2.300	PLK-binding	6.232	5.268
737	TSGMNRLTQVKTPVQ	2.741	2.300			
741	NRLTQVKTPVQVPLP	7.899	2.300	PLK-binding	7.679	5.268

B

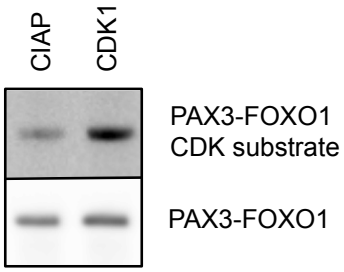

C

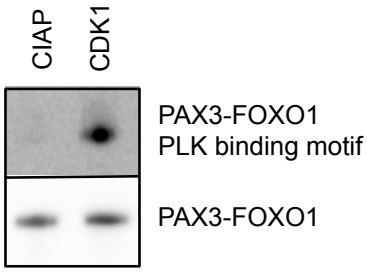

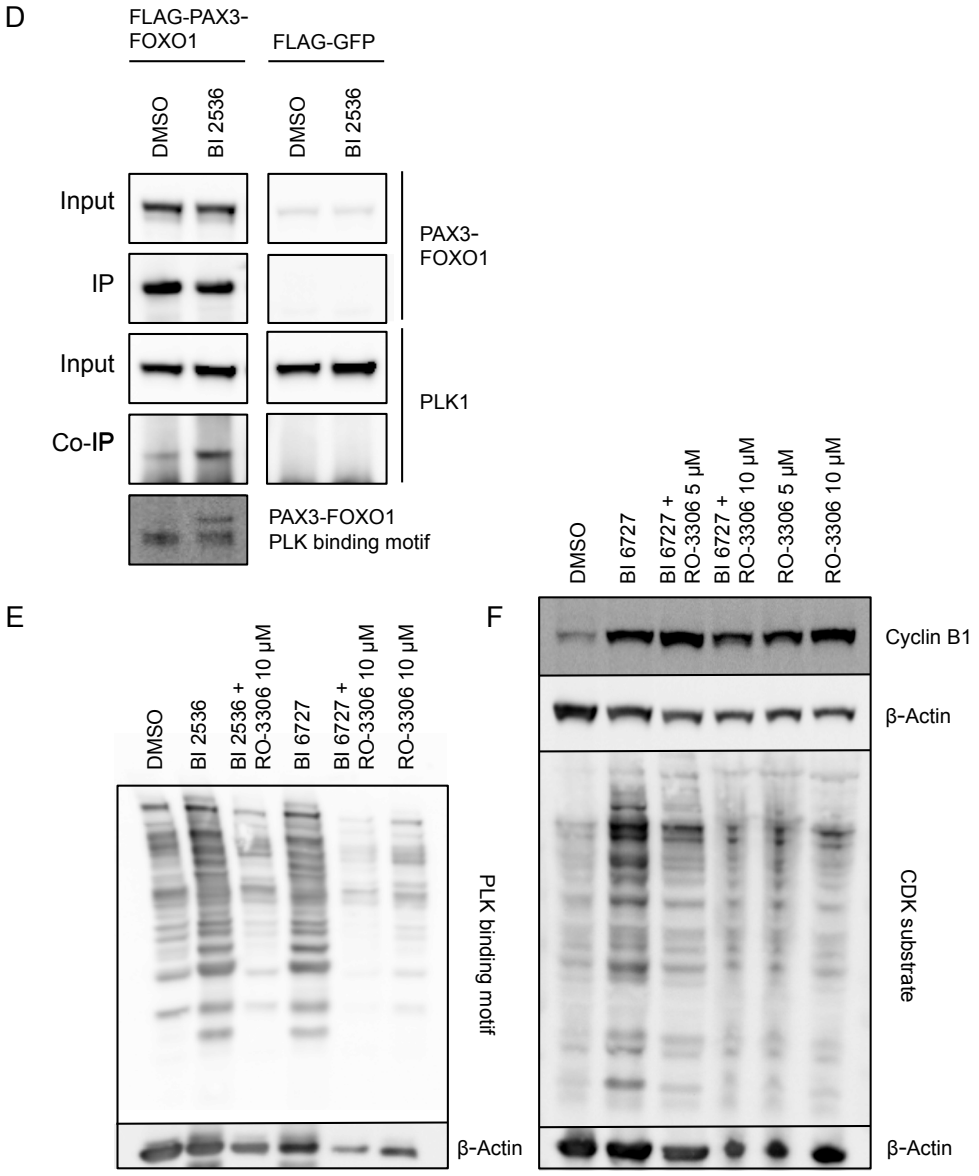
D
FLAG-PAX3-FOXO1
FLAG-GFP
DMSO
BI 2536
DMSO
BI 2536
Input
IP
Input
Co-IP
PAX3-FOXO1
PLK1
PAX3-FOXO1
PLK binding motif
E
DMSO
BI 2536
BI 2536 + RO-3306 10 µM
BI 6727
BI 6727 + RO-3306 10 µM
RO-3306 10 µM
PLK binding motif
β-Actin
F
DMSO
BI 6727
BI 6727 + RO-3306 5 µM
BI 6727 + RO-3306 10 µM
RO-3306 5 µM
RO-3306 10 µM
Cyclin B1
β-Actin
CDK substrate
β-Actin

Fig. 3

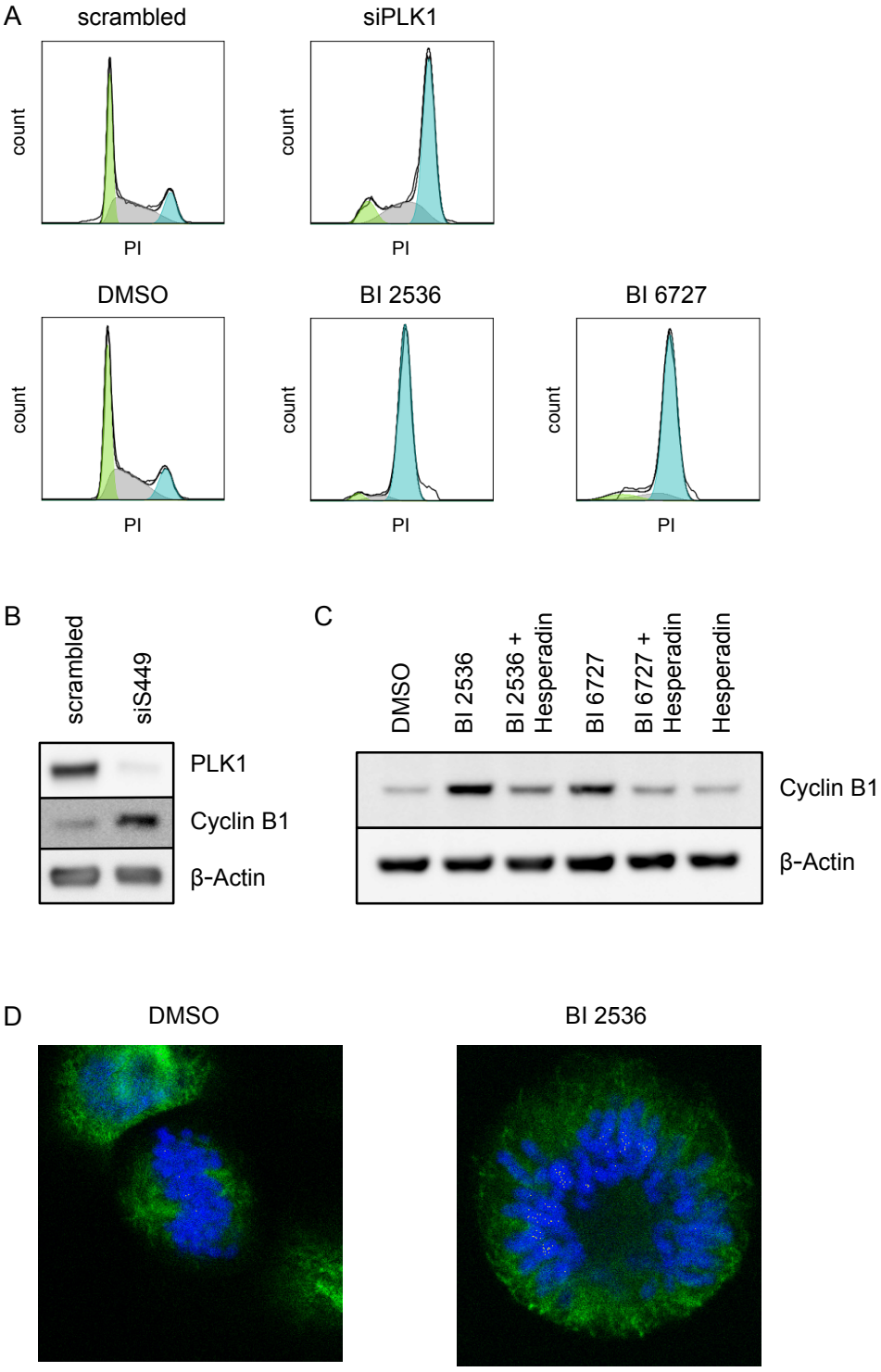
A
scrambled
siPLK1
count
PI
DMSO
BI 2536
BI 6727
B
scrambled
siS449
PLK1
Cyclin B1
β-Actin
C
DMSO
BI 2536
BI 2536 + Hesperadin
BI 6727
BI 6727 + Hesperadin
Hesperadin
Cyclin B1
β-Actin
D
DMSO
BI 2536

Fig. 4

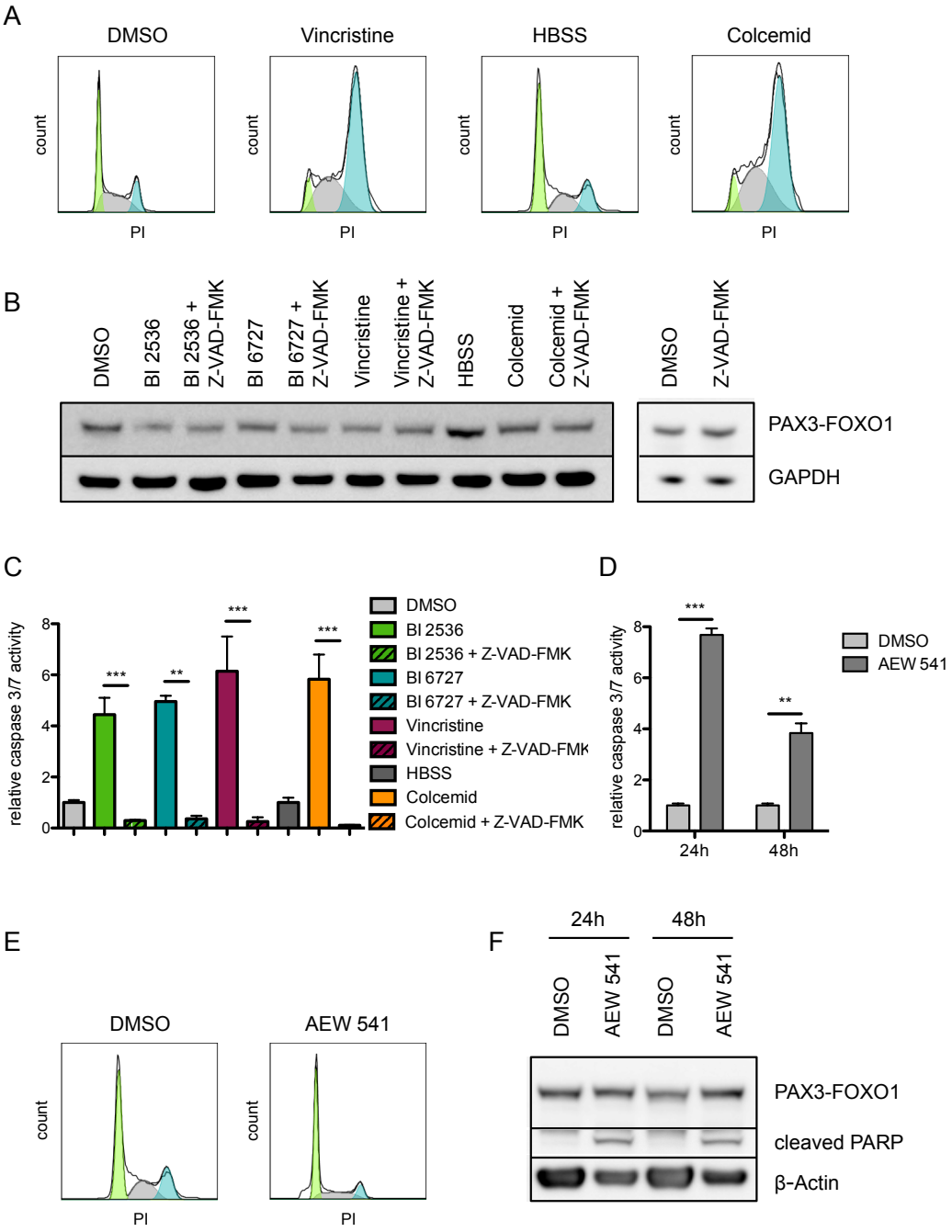
A
DMSO
Vincristine
HBSS
Colcemid
count
PI
B
DMSO
BI 2536
BI 2536 + Z-VAD-FMK
BI 6727
BI 6727 + Z-VAD-FMK
Vincristine
Vincristine + Z-VAD-FMK
HBSS
Colcemid
Colcemid + Z-VAD-FMK
DMSO
Z-VAD-FMK
PAX3-FOXO1
GAPDH
C
relative caspase 3/7 activity
DMSO
BI 2536
BI 2536 + Z-VAD-FMK
BI 6727
BI 6727 + Z-VAD-FMK
Vincristine
Vincristine + Z-VAD-FMK
HBSS
Colcemid
Colcemid + Z-VAD-FMK
D
relative caspase 3/7 activity
DMSO
AEW 541
24h
48h
E
DMSO
AEW 541
count
PI
F
24h
48h
DMSO
AEW 541
DMSO
AEW 541
PAX3-FOXO1
cleaved PARP
β-Actin

Fig. 5

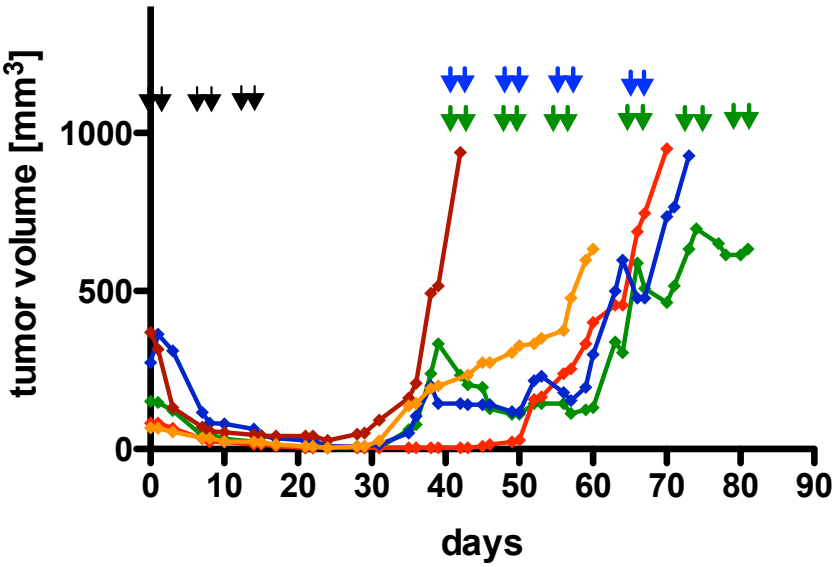

8 Manuscript 2: CK1α cooperates with PLK1 in regulating PAX3-FOXO1 activity

In preparation

Verena Thalhammer[1], Laura A. Lopez-Garcia[1], Dominik Laubscher[1], Regina Hecker[1], and Beat W. Schäfer[1]

[1]Department of Oncology and Children's Research Center, University Children's Hospital Zurich, Zurich, Switzerland

Contributions

Verena Thalhammer:	Fig. 1, with support of Laura Lopez
	Fig. 3, with support of Laura Lopez
	Figs. 4B, 4C
	Fig. 5C
	Fig. 6
	Fig. 7 (data analysis)
	Preparation of manuscript
Laura Lopez:	Mass spectrometry
Regina Hecker:	Fig. 2
Dominik Laubscher:	Figs. 4A, 5A, 5B

8.1 Abstract

The oncogenic transcription factor PAX3-FOXO1 is the major driver of alveolar rhabdomyosarcoma. Therefore, targeting PAX3-FOXO1 function might improve treatment of this highly aggressive tumor. The oncogenic potential of PAX3-FOXO1 is the results of a chromosomal translocation that is further activated by posttranslational modifications.

In the present study, we identified specific phospho-sites by mass spectrometric analysis showing that the fusion protein is highly phosphorylated. Combining these data with the results of a kinome-wide siRNA reporter activity screen, we were able to match specific serine residues with kinases that mediate their phosphorylation. This approach highlighted CK1α and PLK1 as potential upstream regulators of PAX3-FOXO1. Having described the role of PLK1 in fusion protein regulation in a previous study, we aimed at focusing on CK1α and interestingly then discovered overlapping functions with PLK1. We demonstrated *in vitro* phosphorylation of the fusion protein at different residues within its octapeptide domain as well as at the position S503/S506. By site-specific mutagenesis of PAX3-FOXO1 and its heterologous expression as well as by CK1α silencing in aRMS cells, we investigated two different mechanisms leading to enhanced PAX3-FOXO1 activity. On the one hand, phosphorylation stabilized the fusion protein through its FOXO1 part, and on the other hand, it enhanced its transcriptional activity through the octapeptide in its PAX3 part. These new insights in PAX3-FOXO1 regulation might help to improve PAX3-FOXO1 targeting by rationally designed combination therapy, taking advantage of the complementary functions of CK1α and PLK1.

8.2 Introduction

Transcription factors play a major role in tumorigenesis, as well as in tumor maintenance. However, direct targeting of oncogenic transcription factors is difficult as they are characterized by nuclear expression and by large surface areas rather than by deep binding pockets, which both limits the accessibility for small molecules (Yeh et al., 2013). Activities of oncogenic transcription factors can be modulated by multiple mechanisms including epigenetic regulation, protein synthesis, protein stability, posttranslational modifications, protein-protein interactions, and DNA binding restricted by chromatin configuration.

Alveolar rhabdomyosarcoma represents an ideal model for studying oncogenic transcription factors, as expression of the chimeric transcription factor PAX3-FOXO1 is the only major recurrent genomic alteration that could be detected in this tumor by whole-genome sequencing (Chen et al., 2013; Shern et al., 2014). Moreover, we were able to show in the preceding study that PAX3-FOXO1 stability and its transcriptional activity depend on phosphorylation events. Its stability is regulated by PLK1 phosphorylation within the FOXO1 part of the protein (Manuscript I), whereas phosphorylation of the octapeptide located in between the paired domain and the homeodomain of PAX3 regulates its DNA binding ability (Amstutz et al., 2008).

The human casein kinase 1 (CK1) family consists of seven serine/threonine protein kinases harboring a highly conserved kinase domain with redundant and also distinct functions. Next to its role in circadian rhythm, CK1 is implicated in cancer by regulation of cell growth and survival (Cheong and Virshup, 2011). CK1α was shown to form a complex with MDM2, which impedes p53 while it positively regulates E2F1 (Huart et al., 2009). Furthermore, CK1 is an important regulator of the Wnt/β-catenin signaling pathway. CK1γ, CK1δ and CK1ε activate the pathway, whereas CK1α contributes to the degradation of β-catenin. In addition, CK1δ and CK1ε were demonstrated to suppress apoptosis and regulate mitotic function causing progression of colon, pancreatic and breast cancer (Cheong and Virshup, 2011). However, a specific function of CK1 in aRMS has not been described so far.

Applying a kinome-wide siRNA library, we identified PLK1 and CK1α to regulate PAX3-FOXO1 activity with the strongest effects on cell viability compared to 45 further candidate kinases. Here we show that, besides PLK1, CK1α was the only candidate predicted to directly phosphorylate the fusion protein. Thus, we demonstrate regulation of PAX3-FOXO1 activity by phosphorylation involving two complementary functions of CK1α and PLK1. These activities suggest an actionable, rational treatment combination for this rare pediatric sarcoma.

8.3 Material and methods

Cell lines, plasmids and transfection methods

Rh4 aRMS cells, RD eRMS cells (kindly provided by Peter Houghton, St. Jude Children's Hospital, Memphis, TN, USA), HEK293T cells (American Type Culture Collection ATCC, LGC Promochem, Molsheim Cedex, France) and 293 GPG cells (kindly provided by Richard C. Mulligan, Children's Hospital, Boston, MA, USA) were cultured in Dulbecco's

modified Eagle's medium (Sigma-Aldrich, Buchs, Switzerland), supplemented with 100 U/ml penicillin/streptomycin, 2 mM L-glutamine and 10% FBS (Life Technologies, Zug, Switzerland) in 5% CO_2 at 37°C. Culture medium for 293 GPG cells was additionally supplemented with 1 µg/ml tetracycline, except for periods of virus production.

PAX3-FOXO1 was cloned into a pCMV-SC-NF vector (N-terminal FLAG, Stratagene, Agilent Technologies, Basel, Switzerland) and into a pMSCV-IRES-GFP vector (Addgene, no. 33336, Cambridge, MA, USA).

Site-directed mutagenesis was performed using QuikChange recommendations (Stratagene, Agilent Technologies, Basel, Switzerland). Parental DNA template was digested with DpnI (Thermo Scientific, Reinach, Switzerland).

Rh4, RD and 293 GPG cells were transfected using JetPrime™ (Polyplus-Transfections, Illkirch, France), HEK293T cells by $CaPO_4$.

Purification of FLAG-PAX3-FOXO1 from Rh4 and HEK293T cells

Rh4 or HEK293T cells were transfected with pCMV-FLAG-PAX3-FOXO1 in 15 cm plates, lysed 40 hours post transfection and FLAG-PAX3-FOXO1 was immunoprecipitated using 75 µl Dynabeads (Novex by Life Technologies, Zug, Switzerland) per plate coupled to 8 µg monoclonal ANTI-FLAG® M2 antibody (F1804, Sigma-Aldrich, Buchs, Switzerland). After washing, bead-bound FLAG-PAX3-FOXO1 was either used for *in vitro* kinase assays or the protein was eluted by 1x NuPage LDS buffer (Life Technologies, Zug, Switzerland) and directly subjected to mass spectrometry.

In vitro kinase assay

Bead-bound protein was dephosphorylated using 300 units CIAP enzyme (alkaline phosphatase, calf intestinal HC, Promega, Dübendorf, Switzerland) for 90 min at 37°C (50 mM Tris HCl pH 7.5, 1 mM $MgCl_2$, 0.1 mM $ZnCl_2$). FLAG-PAX3-FOXO1 was phosphorylated after washing using 2.5 µg of recombinant CK1α or PLK1 (PV3850 and PV3501; Life Technologies, Zug, Switzerland) for 30 min at 30°C (250 mM HEPES pH 7.5, 50 mM $MgCl_2$, 12.5 mM DTT, 0.05% Triton X-100, 200 µM ATP). 4x NuPage LDS buffer (Life Technologies, Zug, Switzerland) was added for elution and proteins were separated by gel electrophoresis. After staining with colloidal coomassie (Instant

blue, Expedeon, Harston, UK), the band corresponding to PAX3-FOXO1 was excised and prepared for mass spectrometry.

Mass spectrometry

Sample preparation and mass spectrometry procedures are described in Manuscript I.

siRNA kinome library screen and data analysis

siRNA kinome screen and data analysis are described in Manuscript I.

Silencing

Knockdown of CK1α was achieved by reverse transfection of $1.9x10^5$ cells in 6-well plates using 8 nM scrambled (scrambled #2 Silencer® Select siRNA, 4390846) or 8 nM CK1α-directed siRNAs (Silencer® Select siRNA S3625, S3626 and S3624, Ambion, Life Technologies, Zug, Switzerland) with INTERFERin™ according to the manufacturer's protocol (Polyplus-Transfections, Illkirch, France). Cells were lysed 48h post transfection.

Immunoblotting

Total cell extracts were separated using 4-12% Bis-Tris SDS-PAGE gels (Life Technologies, Zug, Switzerland) and transferred to nitrocellulose membranes (PROTAN, Schleicher & Schuell, Kassel, Germany). After blocking with 5% milk powder in TBS/0.1% Tween, the membrane was incubated with the primary antibodies anti-FOXO1 (H-128; 1:1000; Santa Cruz Biotechnology, Heidelberg, Germany), anti-phospho-FOXO1A (phospho S322 + S325 = phospho S503 + S506 in PAX3-FOXO1; ab60945; 1:500; Abcam, Cambridge, UK) overnight at 4°C. Anti-β-actin (13E5) rabbit mAb (4970; 1:1000; Cell Signaling, Bioconcept, Allschwil, Switzerland) and anti-GAPDH (D16H11) XP™ rabbit mAb (5174; 1:1000; Cell Signaling) were used as loading controls. The membrane was washed three times in TBS/0.1% Tween and incubated with anti-rabbit IgG HRP-linked antibody (7074; 1:2000; Cell Signaling) for 1h at room temperature. Proteins were detected using ECL detection reagent (Fisher Scientific, Wohlen, Switzerland) after three washings in TBS/0.1% Tween.

Stability assay

$2x10^5$ RD cells were seeded per 6-well the day before transfection with 1 µg pMSCV-PAX3-FOXO1-IRES-GFP or pMSCV-PAX3-FOXO1-S503A-IRES-GFP. Cells were treated with 35 µM cycloheximide (Sigma-Aldrich, Buchs, Switzerland) or DMSO for 6h before cell lysis and protein extraction. Protein levels were analyzed by Western blotting.

qRT-PCR

Total RNA was extracted using the Qiagen RNeasy Kit (Qiagen, Basel, Switzerland) and reverse-transcribed using oligo (dT) primers and Omniscript reverse transcriptase (Qiagen, Basel, Switzerland). qRT-PCR was performed for PLK1 (Hs00153444_m1), PAX3-FOXO1 (Hs03024825_ft), AP2β (Hs00231468_m1), FGFR4 (Hs01106908_m1), CDH3 (Hs00999918_m1), PIPOX (Hs04188864_m1), MYL1 (Hs00984899_m1), MYCN (Hs02330075_m1), MYOD1 (Hs02330075_g1), PRKAR2B (Hs00176966_m1) and POU4F1 (Hs00366711_m1) using TaqMan gene expression master mix (Life Technologies, Zug, Switzerland). Cycle threshold (C_T) values were normalized to GAPDH (Hs02758991_g1). Relative expression levels were calculated using the $\Delta\Delta C_T$ method.

Cell viability assay

Reverse transfection was carried out using $1x10^4$ cells per 96-well. Cell viability of Rh4 and RMS13 cells was measured by WST-1 assay (Roche Diagnostics, Rotkreuz, Switzerland) 72h post transfection of 50 nM CK1α-directed siRNAs (Silencer® Select siRNA S3625, S3626 and S3624, Ambion, Life Technologies, Zug, Switzerland) and PLK1-directed siRNAs (Silencer® Select siRNA S450, S448 and S449, Ambion, Life Technologies, Zug, Switzerland) with N-TER nanoparticle transfection reagent (Sigma-Aldrich, Buchs, Switzerland). Values were calculated relative to scrambled knockdown based on three biological replicates of technical triplicates.

Retroviral infections

293 GPG cells have been stably transfected with packaging plasmids containing the Gag and Pol genes of moloney murine leukemia virus and the VSV-G gene of vesicular stomatitis virus. Cells were cultured in DMEM containing 1 µg/ml tetracycline, except for periods of virus production to repress expression of VSV-G coat protein regulated by a TET repressor. $2.5x10^6$ cells were seeded per 10 cm dish without tetracycline. Medium was changed after 24h and cells were transfected with retroviral plasmids containing wild type or mutant PAX3-FOXO1 using JetPrime™ (Polyplus-Transfections, Illkirch, France). The virus supernatant was collected 72h post transfection, centrifuged for 4 min at 1200 rpm, and filtered using a 0.45 nm cellulose acetate membrane filter tip. $1.5x10^5$ RD cells were plated per 6-well 24h before infection with virus supernatant. Polybrene was added to a final concentration of 10 µg/ml. Infection rates were increased by centrifugation for 1h at 800 x g and 32°C. Virus supernatant was removed and cells were washed by PBS. Cells were harvested 120h post infection.

8.4 Results

Phosphorylation of PAX3-FOXO1 in aRMS cells

In order to investigate the phosphorylation status of PAX3-FOXO1 in aRMS, we transfected plasmids encoding FLAG-tagged PAX3-FOXO1 into Rh4 cells. After purification using anti-FLAG antibody, we digested the protein by trypsin or chymotrypsin and performed mass spectrometry for identification of phospho-peptides. Achieving 92% protein coverage, we were able to interrogate 90% of all potential serine, threonine and tyrosine phosphorylation sites (Fig. 1A). Peptides found to be phosphorylated by mass spectrometric analysis are indicated in Fig. 1B. Furthermore, we carried out MASCOT analysis to narrow our search down to residues with the highest probability relative to other possible sites within the relevant phospho-peptides. Like this, we found 10 phosphorylated residues and one additional phospho-peptide (TSSNASTISGR) in which the modified site could not be located precisely by MASCOT analysis (Fig. 1C). In addition, all the phospho-peptides were also identified when PAX3-FOXO1 was purified from RMS13 cells (Manuscript I). These results demonstrate that PAX3-FOXO1 is heavily phosphorylated and indicate that the transcription factor is regulated by posttranslational modifications.

siRNA screen identifies CK1α and PLK1 as potential upstream kinases of PAX3-FOXO1

To identify potential upstream kinases responsible for phosphorylation of the identified sites, we first performed a kinome-wide siRNA screen. For the screen, we employed a reporter cell line expressing luciferase under the control of the PAX3-FOXO1 responsive AP2β promoter. To measure significant reduction of PAX3-FOXO1 activity, the ratio of luciferase activity to cell viability from averaged triplicate values was determined for each targeting sequence. We thereby identified CK1α (CSNK1A1) and PLK1 among 47 candidates that contributed to transcriptional activity of PAX3-FOXO1 (Fig. 2 and Manuscript I) suggesting modulation of fusion protein activity by direct phosphorylation.

CK1α and PLK1 are predicted to phosphorylate PAX3-FOXO1 at identified sites

In a second step we combined the phosphorylation data with the results of our whole-kinome siRNA screen (Manuscript I) to scan for putative direct upstream kinases. Towards this end, *in silico* analysis was conducted using the phospho-site prediction software GPS 2.1 (Xue et al., 2008). Five out of the 47 candidate kinases were predicted to phosphorylate PAX3-FOXO1 (CSNK1A1, PLK1, NEK2, PKCA, and YES1). Interestingly, the predicted sites for CSNK1A1 (CK1α) and PLK1 overlapped with the phospho-residues found in PAX3-FOXO1 purified from Rh4 cells. However, it is important to realize that the prediction tool includes only 408 kinases for analysis. Predicted sites for PLK (all isoforms) according to the PLK specific tool GPS-Polo 1.0 (Liu et al., 2013b), and for CK1α are depicted in Fig. 3A including a list of individual scores. In conclusion, four of the phospho-residues mapped in Fig. 1 (S201, S205, S503 and S506) could be categorized as potential CK1α or PLK1 substrates implying that these two kinases might play a major role in the regulation of the oncogenic fusion protein. Subsequently, *in vitro* phosphorylations of PAX3-FOXO1 by CK1α and PLK1 were performed.

CK1α and PLK1 phosphorylate PAX3-FOXO1 *in vitro* at S503/S506 and at multiple sites within the octapeptide

To demonstrate direct phosphorylation of PAX3-FOXO1 by CK1α and PLK1, we transfected HEK293T cells with FLAG-PAX3-FOXO1 expressing plasmids, dephosphorylated the purified proteins by calf intestine alkaline phosphatase (CIAP),

and subsequently carried out *in vitro* kinase assays. Having identified phospho-peptides by comparing mass spectrometric data of dephosphorylated PAX3-FOXO1 to CK1α-, respectively PLK1-treated PAX3-FOXO1, we exactly mapped localizations of phospho-sites by MASCOT analysis. Within the octapeptide, three serines (S197, S205 and S209) have been phosphorylated by CK1α and two serines (S187 and S205) by PLK1 (Fig. 3B). As predicted, additional Western blot analysis revealed further phosphorylation at S503/S506 (Fig. 3C). Interestingly, S205 as well as S503 can be phosphorylated by either of the two enzymes. Polo-like kinases and casein kinases in fact both belong to the rare group of acidophilic kinases (Cheong and Virshup, 2011; Salvi et al., 2012), suggesting homologous substrate sequences. The result is also in agreement with *in silico* predicted sites as well as with consensus recognition motifs for CK1 (D/E-X-X-S/T) and for PLK1 (D/E/N-X-S/T) (Cheong and Virshup, 2011; Kettenbach et al., 2012). Importantly, these sites were also phosphorylated in aRMS cells (Fig. 3D). Thus, both, CK1α and PLK1 are supposed to be able to phosphorylate the fusion protein at multiple sites within the octapeptide and at S503/S506 indicating complementary roles in the regulation of PAX3-FOXO1.

CK1α and PLK1 stabilize PAX3-FOXO1 by phosphorylation of S503

In a next step, we assessed the biological function of individual phospho-sites. We previously demonstrated by site-specific mutagenesis and cycloheximide treatment studies in RD cells that phosphorylation of S503 mediates enhanced fusion protein stability (Fig. 4A and Manuscript I). Verifying these finding, we investigated PAX3-FOXO1 protein levels after CK1α silencing in Rh4 cells. As expected, we observed degradation of the fusion protein by Western blot analysis using three different siRNA sequences (Fig. 4B). However, knockdown efficiencies remain to be tested. Furthermore, densitometric quantification revealed a mean significant reduction of protein amount by 50% relative to scrambled knockdown suggesting that CK1α stabilizes the fusion protein by phosphorylation at S503 as it has previously also been shown for PLK1 (Fig. 4C and Manuscript I).

CK1α and PLK1 activate PAX3-FOXO1 by multiple phosphorylation events in the octapeptide region

The impact of phosphorylation of the octapeptide on DNA binding and transcriptional activation of PAX3-FOXO1 has previously been demonstrated in transactivation assays

using a 6xCD19 reporter plasmid in HEK293T cells (Amstutz et al., 2008). In order to test PAX3-FOXO1 mutants, we developed a read-out system in the embryonal rhabdomyosarcoma cell line RD. We chose the PAX3-FOXO1 target genes MYCN, PIPOX, MYOD1, PRKAR2B and POU4F1, which were upregulated after retroviral infection of the fusion protein (Davicioni et al., 2006). Relative transactivation of these genes was measured by qRT-PCR comparing wild type to mutant PAX3-FOXO1. Relative basal expression in RD cells is indicated by transduction of GFP expressing retroviral plasmids. In addition, we used DNA binding mutants PAX3-FOXO1-G48S and PAX3-FOXO1-N269A as positive controls. In order to assess the role of octapeptide phosphorylation, we transduced PAX3-FOXO1 with loss of function mutations at all six octapeptide serines, including the four identified CK1α and PLK1 sites. In preliminary experiments, we found reduced transactivation by the octapeptide mutant for all tested target genes after 120 hours. As expression of wild type PAX3-FOXO1 and PAX3-FOXO1-6xA was almost identical, phosphorylation of the octapeptide might indeed impact PAX3-FOXO1 activity in rhabdomyosarcoma cells (Figs. 5A and 5B).

To further investigate the biological function of CK1α in aRMS cells and to validate it as upstream regulator of PAX3-FOXO1, we silenced the kinase and again measured PAX3-FOXO1 target gene expression. Endogenous mRNA levels of the target genes AP2β, FGFR4 and CDH3 (Cao et al., 2010; Davicioni et al., 2006; Khan et al., 2001; Lae et al., 2007; Marshall et al., 2012; Taylor et al., 2009; Thuault et al., 2013; Wachtel et al., 2004; Wachtel et al., 2006) were analyzed by qRT-PCR after 48 hours of silencing. In addition, transcription of MYL1, a muscle differentiation marker that is normally repressed by PAX3-FOXO1 (De Pitta et al., 2006) was assessed. Three different CK1α targeting siRNAs individually resulted in reduction of FGFR4 and CDH3 expression with minor effects on AP2β, while MYL1 mRNA was upregulated except for one of three targeting sequences (Fig. 5C). PAX3-FOXO1 mRNA levels were not decreased by CK1α silencing, implying regulation of PAX3-FOXO1 by posttranslational modifications.

Taken together, silencing of CK1α modulated PAX3-FOXO1 transcriptional activity similar to PLK1 knockdown (Manuscript I). This suggests an essential contribution of CK1α and PLK1 to fusion protein regulation.

CK1α and PLK1 depletion reduce cell viability of aRMS cells

We furthermore tested whether CK1α could be an appropriate therapeutic target in aRMS cells like it has been previously proposed for PLK1. Therefore, we determined cell viability upon CK1α and PLK1 depletion relative to scrambled treatment of the two aRMS cell lines Rh4 and RMS13. We applied three different sequences per kinase target for 72 hours and observed significant reduction of cell viability for both targets in both cell lines. The maximum reduction of Rh4 cell viability was 42% upon CK1α knockdown and 61% upon PLK1 knockdown (Fig. 6A). In RMS13 cells, CK1α depletion resulted in a maximum reduction of cell viability by 51% and PLK1 silencing by 60% (Fig. 6B). If double knockdowns can induce synergism in cytotoxicity remains to be investigated. Nevertheless, these data demonstrate that CK1α and PLK1 are both essential for the survival of aRMS tumors, likely based on their capability to phosphorylate PAX3-FOXO1.

CK1α expression negatively correlates with the expression of PLK1 in aRMS tumor biopsies

To finally show that CK1α expression is also relevant in patient-derived tumor biopsies, we conducted microarray expression analysis of translocation positive aRMS tumors (Davicioni et al., 2006) and found relevant expression across all these tumors. Interestingly, we also observed a significant negative correlation of CK1α and PLK1 expression in these tumor samples, indicating that both kinases might not just complement, but also compensate for each other (Fig. 7).

8.5 Discussion

In this study, we show that CK1α regulates PAX3-FOXO1, as it has been predicted in our kinome-wide siRNA screen. Its impact on fusion protein activity is verified by the identification of five *in vitro* phospho-sites of which at least two (S205 and S503/S506) also exist *in vivo* with demonstrated effects on PAX3-FOXO1 function. Moreover, we reveal complementary biological functions of CK1α and PLK1 in phosphorylation of these sites.

First, we showed phosphorylation of S503/S506. Previous studies already reported phosphorylation of S322 and S325 by CK1 in wild type FOXO1, which are corresponding to S503 and S506 in the fusion protein (Rena et al., 2002).

Interestingly, phosphorylation of S503 can be mediated either by CK1α or by PLK1 resulting in stabilization of the fusion protein as already discussed in Manuscript I. However, the role of phosphorylated S506 as well as double phosphorylation needs to be examined in future studies.

Second, CK1α phosphorylated the octapeptide region of PAX3-FOXO1 *in vitro* at three different serines (S197, S205 and S209), and PLK1 phosphorylated it at two different serines (S187 and S205). Interestingly, several studies have described the relevance of this domain and we previously found that this region is phosphorylated at least at four out of six different residues (S187, S193, S197, S201, S205, and S209) regulating DNA binding and thus transcriptional activity of the fusion protein in HEK293T cells (Amstutz et al., 2008). Here, we detected phosphorylation at S201 and S205 but not at S209 in PAX3-FOXO1 purified from Rh4 cells, which is line with the observations of Dietz et al. (2011). However, Amstutz et al. (2008) found that single loss of function mutation at S205 did not affect transactivation, whereas double mutation of S205 and S209 did reduce fusion protein activity, which even further decreased when also S197 and S187 were mutated indicating that also phosphorylation at S187, S197 and S209 might be relevant for PAX3-FOXO1 activation.

We established a system to investigate the function of the octapeptide, utilizing fusion negative embryonal RMS cells to express mutant PAX3-FOXO1. Mutation of all six serines within the octapeptide resulted in reduction of fusion protein activity. Single site mutations as well as different combinations remain to be tested.

Dietz et al. (2011) demonstrated that phosphorylation of S201 in Pax3 is mediated by Gsk3β, whereas both S205 in Pax3 and PAX3-FOXO1 as well as S209 in Pax3, were proposed to be phosphorylated by casein kinase 2 (Ck2) (Dietz et al., 2009; Iyengar et al., 2012). Of notice, all the *in vitro* kinase assays in these studies were performed with cell extracts from mouse myoblasts but not with cell extracts from aRMS cells. Identification was performed based on the kinase's ability to utilize GTP as substrate instead of ATP, which suggests Ck2 as upstream kinase instead of Ck1, at least in mouse myoblasts. However, no genetic loss-of-function experiments have been carried out in these studies. And the employed and rather unspecific drugs heparin and DRB are expected to also inhibit CK1 (Meggio et al., 1990).

In our kinome screen we identified CK1α but not CK2 to regulate PAX3-FOXO1 activity in aRMS cells. Furthermore, we demonstrated that CK1α is capable of phosphorylating S205 and S209 *in vitro* like it has been shown for Ck2 before (Dietz et al., 2009; Iyengar et al., 2012). This can be explained by overlapping recognition motifs of CK1

and CK2 at these positions (CK1: D/E-X-X-S/T; CK2: S/T-X-X-D/E; PAX3-FOXO1 sequence: DEG$\underline{S}_{205}$DID$\underline{S}_{209}$EPD), rather than by close relationship (Venerando et al., 2014). CK1 and CK2 actually belong to different branches of the kinome and share only weak structural similarities. Importantly, knockdown of CK1α was sufficient to reduce target gene expression, concluding that CK1α likely represents the phospho-mediating kinase in aRMS cells, although a role for CK2 cannot be excluded at the moment. Additional knockdown experiments will have to be carried out to clarify this issue.

Nevertheless, the most important finding of this study is the cooperating function of CK1α and PLK1 in PAX3-FOXO1 regulation. Both kinases phosphorylated the fusion protein at S205 and S503, at least *in vitro*. The impact of this observation becomes apparent considering that tumors often develop resistances to kinase inhibitors. In the case of aRMS, we previously observed escape from PLK1 inhibition (Chapter 7) and now actually found a negative correlation of CK1α and PLK1 expression in tumor biopsies indicating not only cooperating but also compensating capacities of the two kinases. In a next step, we will investigate if double depletion of CK1α and PLK1 could attain synergistic effects and if CK1α plays a superordinate role in resistant cells, which would demand for development of potential combination therapies.

In summary, our results highlight the particular importance to consider mechanistic biological interactions for therapeutic targeting as shown here for the cooperation of CK1α and PLK1 in PAX3-FOXO1 regulation.

8.6 Figure legends

Fig. 1. Mass spectrometric analyses detect phosphorylation sites of PAX3-FOXO1 purified from Rh4 cells

(A) Protein coverage achieved after trypsin and chymotrypsin digestions.

(B) Phospho-peptides identified by mass spectrometry.

(C) Summary of phospho-sites achieving the highest probability values within the according peptide based on MASCOT analyses.

Fig. 2. Kinome-wide siRNA screen identifies CK1α and PLK1 as regulators of PAX3-FOXO1

RNA silencing was carried out for 48h using 50 nM siRNA (Ambion Silencer® V3 Kinase siRNA Library). The luciferase readout (LF) was normalized to cell viability (V) measured by WST-1 assay. siRNAs targeting luciferase (pGL4) and PAX3-FOXO1 served as positive controls for reduced activity/cell viability ratio (LF/V), and siKIF11 for reduced cell viability. Reduced LF/V ratios upon CK1α silencing and PLK1 silencing are marked. *Data points*, mean of three independent experiments performed in triplicates; *threshold*, 1.5 SDs of mean of luciferase knockdown.

Fig. 3. CK1α and PLK1 phosphorylate PAX3-FOXO1 *in vitro*

(A) *In silico* analysis of PAX3-FOXO1 phosphorylation using the phospho-site prediction software GPS 2.1 for CK1α and GPS-Polo 1.0 for PLK (all isoforms).

(B and C) *In vitro* kinase assays. HEK293T cells were transfected with FLAG-tagged PAX3-FOXO1 expressing plasmid, purified, dephosphorylated by CIAP, and re-phosphorylated by recombinant CK1α and PLK1.

(B) Western blot analysis using anti phospho-S503+S506 antibody.

(C) Phospho-peptides identified by mass spectrometric analyses and most probable residues based on MASCOT analyses.

Fig. 4. CK1α stabilizes PAX3-FOXO1

(A) Quantification of exogenous PAX3-FOXO1 degradation by densitometry. Degradation of exogenous, wild type or phospho-mutant PAX3-FOXO1. RD cells were transfected with PAX3-FOXO1 wild type or PAX3-FOXO1-S503A expressing constructs and treated for 6h with DMSO or 35 µM cycloheximide (CHX). Levels were normalized to GAPDH. *Columns,* mean of three independent experiments; *bars,* SD Student's t-test ** p= 0.0052.

(B) Western blot analysis of endogenous PAX3-FOXO1 degradation after CK1α silencing. Rh4 cells were transfected with 8 nM of siRNA using three different sequences for 48h.

(C) Quantification of endogenous PAX3-FOXO1 degradation by densitometry upon CK1α silencing. *Bars,* SD; Student's t-test * p= 0.0257.

Fig. 5. CK1α activates PAX3-FOXO1

(A+B) RD cells were transduced with wild type PAX3-FOXO1 or mutant PAX3-FOXO1-6xA for 120h.

(A) Relative mRNA expression of PAX3-FOXO1 and target genes in RD cells. C_T values relative to wild type PAX3-FOXO1 were measured by qRT-PCR and normalized to GAPDH expression. *Columns,* two biological experiments performed in technical triplicates; *bars*, SD; no statistics due to lack of biological replicates.

(B) Western blot analysis of PAX3-FOXO1 expression.

(C) Relative mRNA expression of PAX3-FOXO1 and target genes in Rh4 cells after CK1α knockdown using three individual sequences at a concentration of 8 nM for 48h. C_T values relative to scrambled knockdown were measured by qRT-PCR and normalized to GAPDH expression. *Columns,* experiments performed with three independent siRNAs in technical triplicates; no statistics due to lack of biological replicates per siRNA.

Fig. 6. CK1α and PLK1 depletion reduce cell viability of aRMS cells

RNA silencing was carried out for 72h using 50 nM siRNA and three different sequences per target. Cell viability was measured by WST-1 assay and set relative to scrambled knockdown. *Columns*, mean of three independent experiments performed in triplicates; *bars,* SD; Student's t-test *** $p < 0.001$, ** $p < 0.01$, * $p < 0.025$.

(A) Cell viability of Rh4 cells.

(B) Cell viability of RMS13 cells.

Fig. 7. CK1α expression negatively correlates with the expression of PLK1 in aRMS tumor biopsies

CK1α and PLK1 gene expression in translocation positive aRMS patient-derived biopsies (n=54) measured by microarray (Affymetrix HG-U133A).

8.7 Figures

Fig. 1

A PAX3-FOXO1 purified from Rh4 cells

Coverage after trypsin digestion

Coverage after chymotrypsin digestion

Phospho-peptide found after trypsin digestion

Phospho-peptide found after chymotrypsin digestion

Phospho-peptide found only after purification from RMS13

Residue with the highest probability

S — Definite mapping of phospho-site not possible by MASCOT analysis

B

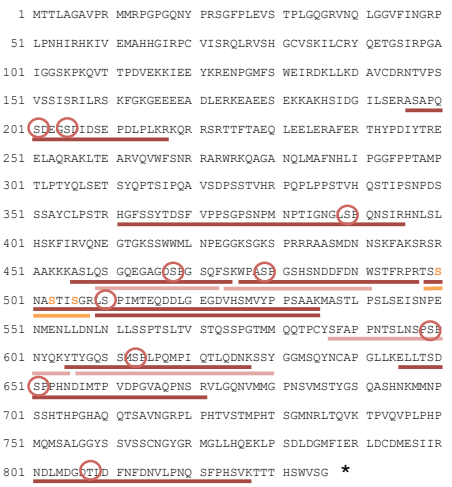

* The same phospho-peptides were identified after PAX3-FOXO1 purification from RMS13 cells (data not shown)

C

Phospho-site	Probability relative to other possible residues within the relevant phospho-peptide (MASCOT analysis)
S201 + S205	97.21% (T; for double phosphorylation)
S389	84.06% (T); alternative S393: 10.78%
S468	98.21% (T); 98,54% (C)
S479	95.36% (T); 76.41% (C)
S500/503/506	all sites possible
S510	92.72% (T, short peptide); 96.00% (T, long peptide)
S599	96.51% (C)
S613	87.96% (T); 64.16% (C); alternative S611: 8.05% (T); 12.48% (C)
S651	91.12% (T)
T807	100% (T)

(T) percentage after trypsin digestion; (C) percentage after chymotrypsin digestion

Fig. 2

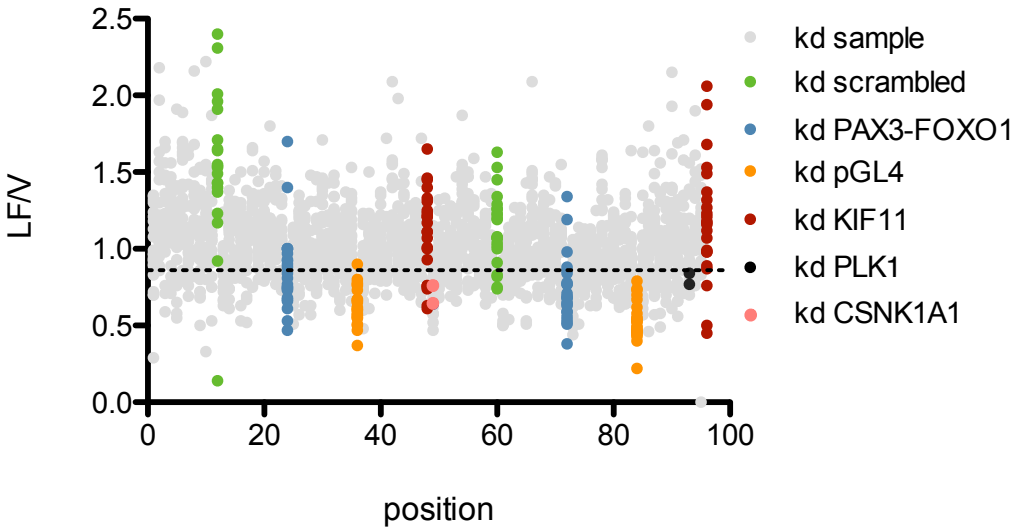
2.5
2.0
1.5
1.0
0.5
0.0
LF/V
0
20
40
60
80
100
position
kd sample
kd scrambled
kd PAX3-FOXO1
kd pGL4
kd KIF11
kd PLK1
kd CSNK1A1

Fig. 3

A

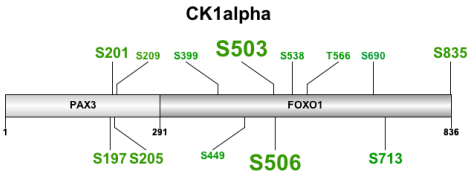

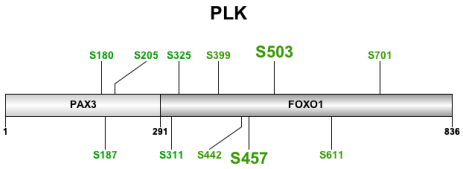

CK1α site	Peptide	Score	Cutoff
197	GILSERASAPQSDEG	1.706	1.235
201	ERASAPQSDEGSDID	2.294	1.235
205	APQSDEGSDIDSEPD	1.941	1.235
209	DEGSDIDSEPDLPLK	1.235	1.235
399	NSIRHNLSLHSKFIR	1.353	1.235
449	SKFAKSRSRAAKKKA	1.412	1.235
503	PRTSSNASTISGRLS	7.824	1.235
506	SSNASTISGRLSPIM	7.824	1.235
538	PSAAKMASTLPSLSE	1.235	1.235
566	LNLLSSPTSLTVSTQ	2.000	1.235
690	SVMSTYGSQASHNKM	1.235	1.235
713	PGHAQQTSAVNGRPL	1.765	1.235
835	TTTHSWVSG******	2.059	1.235

PLK site	Peptide	Score	Cutoff
180	ERKEAEESEKKAKHS	3.243	2.590
187	SEKKAKHSIDGILSE	3.091	2.590
205	APQSDEGSDIDSEPD	3.312	2.590
311	TYQLSETSYQPTSIP	3.112	2.590
325	PQAVSDPSSTVHRPQ	2.855	2.590
399	NSIRHNLSLHSKFIR	2.764	2.590
442	AASMDNNSKFAKSRS	3.069	2.590
457	RAAKKKASLQSGQEG	3.942	2.590
503	PRTSSNASTISGRLS	3.844	2.590
611	KYTYGQSSMSPLPQM	2.707	2.590
701	HNKMMNPSSHTHPGH	2.826	2.590

B

Kinase	Phospho-peptide	Probability relative to other possible residues within the relevant phospho-peptide (MASCOT analysis)	Residue in PAX3-FOXO1	Predicted site	Detected In aRMS cells
CK1α	HSIDGILSER	S8 100%	S197	yes	
CK1α	ASAPQSDEGSDIDSEPDLPLKR	S10 + S14 double 99.77%	S205 + S209	yes	yes (S205)
PLK1	AKHSIDGILSER	S4 100%	S187	yes	
PLK1	ASAPQSDEGSDIDSEPDLPLKR	S10 95.12%	S205	yes	yes

C

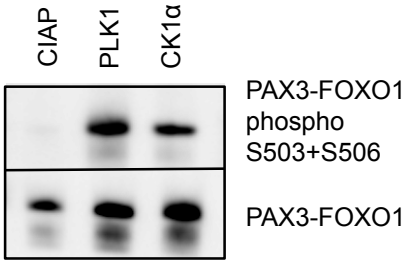

D

Phospho-sites detected in aRMS cells	Predicted kinases	*In vitro* kinase assay
S201	CK1α	
S205	PLK, CK1α	PLK1, CK1α
S389		PLK1 (Chapter 7)
S468		PLK1 (Chapter 7)
S479		
S500/503/506	PLK, CK1α	PLK1, CK1α
S510		PLK1 (Chapter 7)
S599		
S613		
S651		
T807		

Fig. 4

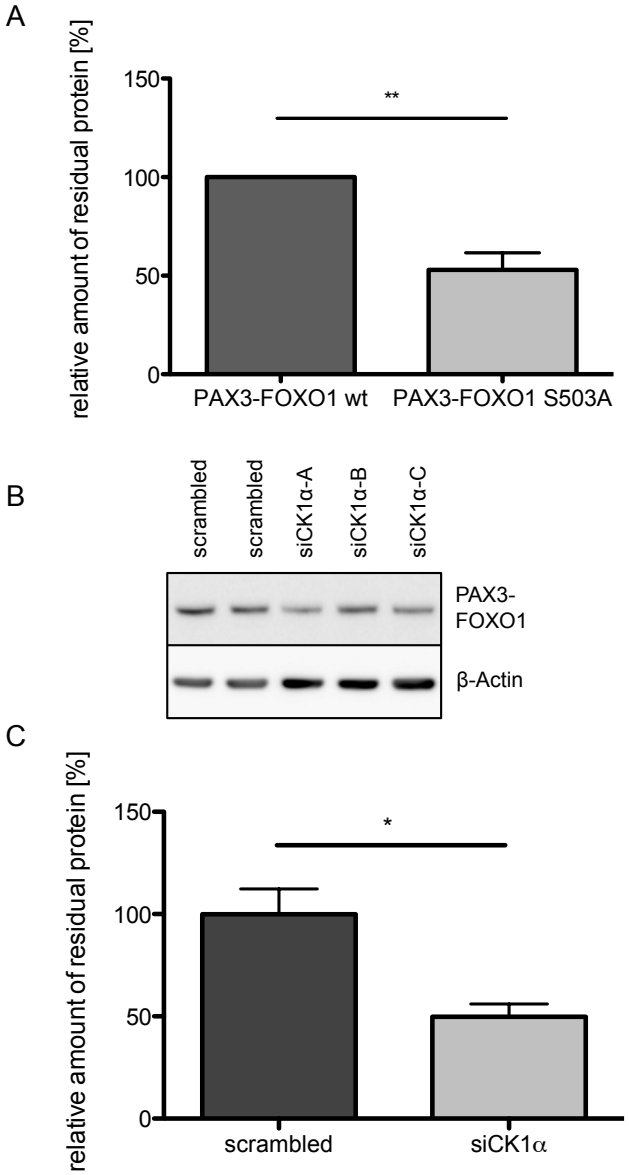
A
relative amount of residual protein [%]
150
100
50
0
**
PAX3-FOXO1 wt
PAX3-FOXO1 S503A
B
scrambled
scrambled
siCK1α-A
siCK1α-B
siCK1α-C
PAX3-FOXO1
β-Actin
C
relative amount of residual protein [%]
150
100
50
0
*
scrambled
siCK1α

Fig. 5

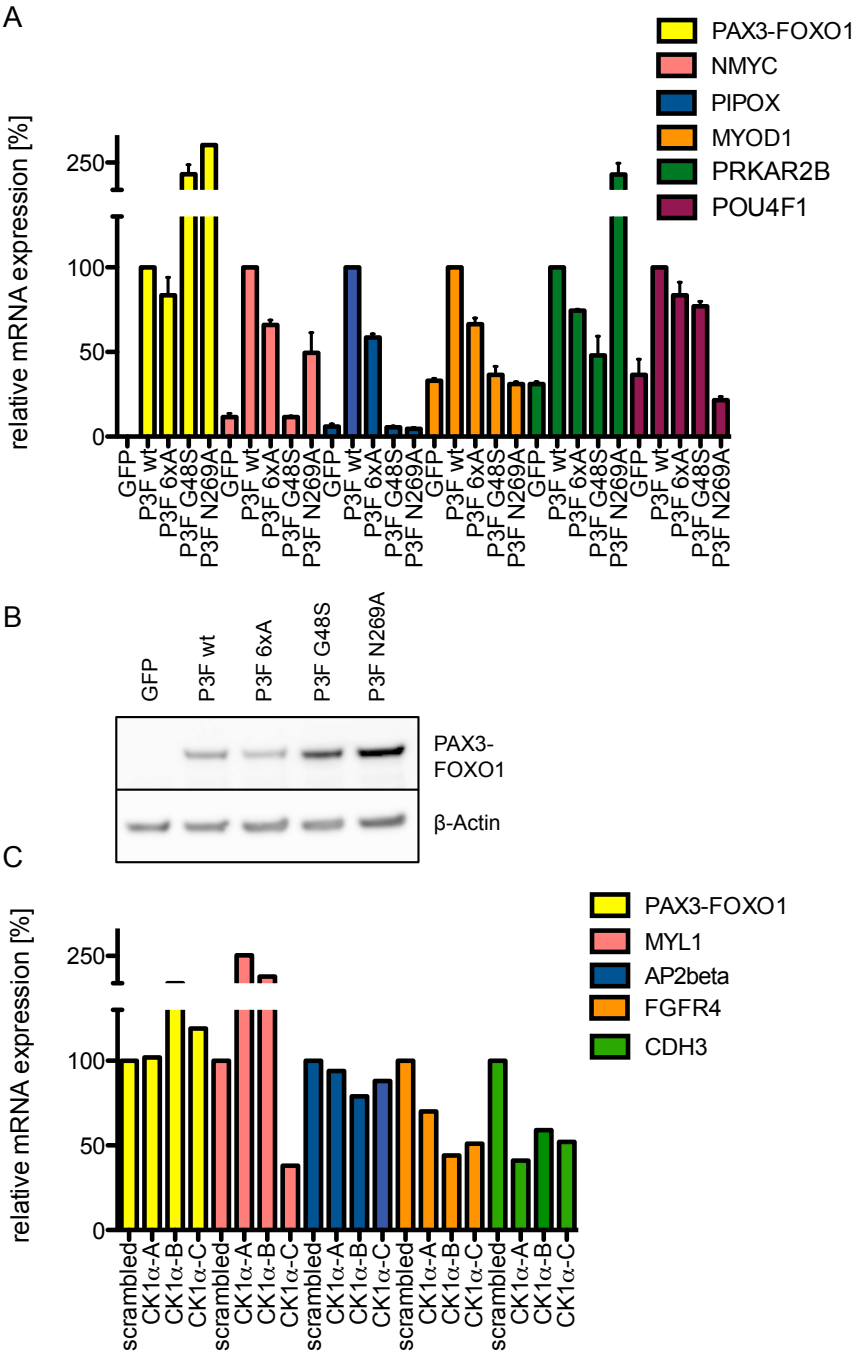
A
relative mRNA expression [%]
250
100
50
0
PAX3-FOXO1
NMYC
PIPOX
MYOD1
PRKAR2B
POU4F1
GFP
P3F wt
P3F 6xA
P3F G48S
P3F N269A
B
GFP
P3F wt
P3F 6xA
P3F G48S
P3F N269A
PAX3-FOXO1
β-Actin
C
relative mRNA expression [%]
250
100
50
0
PAX3-FOXO1
MYL1
AP2beta
FGFR4
CDH3
scrambled
CK1α-A
CK1α-B
CK1α-C

Fig. 6

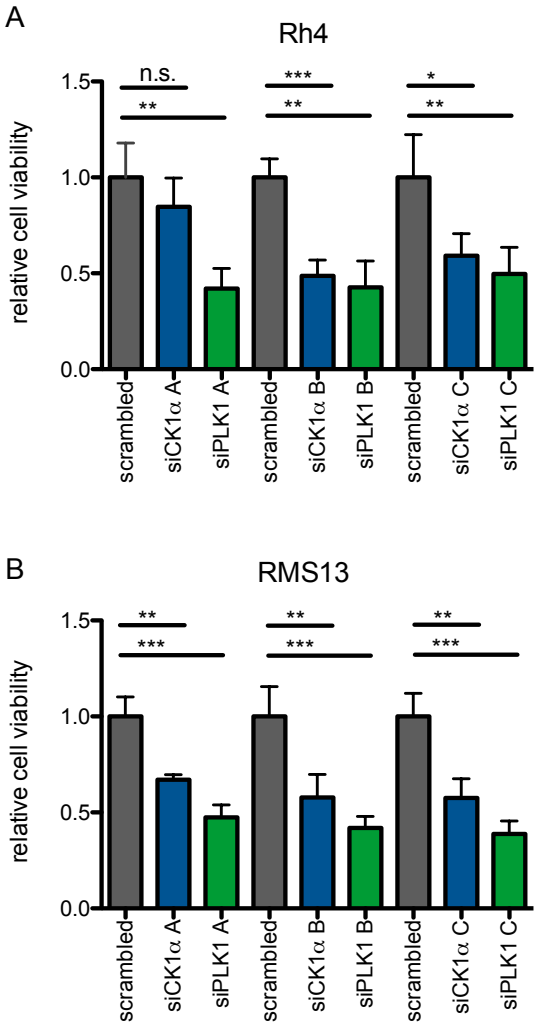
A
Rh4
relative cell viability
1.5
1.0
0.5
0.0
n.s.
**
***
**
*
**
scrambled
siCK1α A
siPLK1 A
scrambled
siCK1α B
siPLK1 B
scrambled
siCK1α C
siPLK1 C
B
RMS13
relative cell viability
1.5
1.0
0.5
0.0
**
***
**
***
**
***
scrambled
siCK1α A
siPLK1 A
scrambled
siCK1α B
siPLK1 B
scrambled
siCK1α C
siPLK1 C

Fig. 7

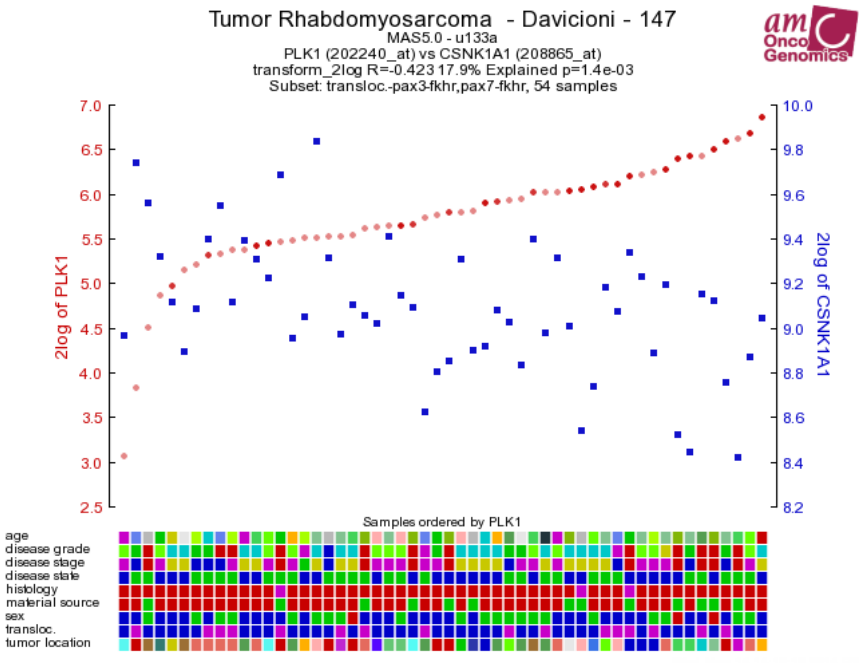
Tumor Rhabdomyosarcoma - Davicioni - 147
MAS5.0 - u133a
PLK1 (202240_at) vs CSNK1A1 (208865_at)
transform_2log R=-0.423 17.9% Explained p=1.4e-03
Subset: transloc.-pax3-fkhr,pax7-fkhr, 54 samples
2log of PLK1
2log of CSNK1A1
Samples ordered by PLK1
age
disease grade
disease stage
disease state
histology
material source
sex
transloc.
tumor location

9 Discussion

Performing a kinome-wide siRNA screen in an aRMS based reporter assay led to the identification of 47 upstream kinases of PAX3-FOXO1 with PLK1 and CK1α emerging as the most promising targets in terms of aRMS cytotoxicity. Grouping of the candidate kinases delineates a picture of the regulatory environment of PAX3-FOXO1 with a dominant influence of cell cycle regulators. Integration of our mechanistic data suggests a model of PAX3-FOXO1 regulation during cell cycle progression (Fig. 17). These novel findings allow targeting the fusion protein on top of the oncogenic machinery.

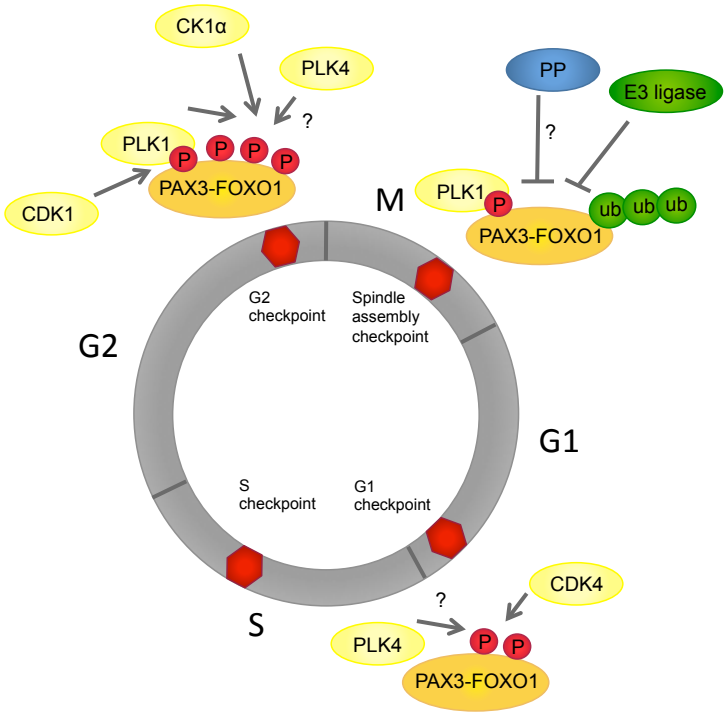

Fig. 17. PAX3-FOXO1 regulation during cell cycle. CDK1 phosphorylates PAX3-FOXO1 and primes for PLK1 binding and phosphorylation. On the one hand, PAX3-FOXO1 is activated by PLK1 in G2/M phase mediating checkpoint adaptation (Kikuchi et al., 2014). On the other hand, PAX3-FOXO1 activity is downregulated by ubiquitination and subsequent degradation during mitosis, potentially after dephosphorylation by an unknown protein phosphatase (PP) or due to spindle assembly checkpoint activation. The model also considers cooperating roles of CK1α and PLK4 in G2/M. PLK4 and previously reported CDK4 phosphorylation (Liu et al., 2013a) might additionally activate PAX3-FOXO1 during G1/S due to their cell cycle dependent activities in this phase.

With very potent PLK1 inhibitors currently investigated in clinical trials for treatment of different adult cancers, we first focused on mechanistic characterization of PLK1 inhibition in aRMS and successfully collected compelling and promising preclinical data suggesting PLK1 as a therapeutic target and prognostic marker in fusion positive RMS.

Although we have not yet identified CK1α specific inhibitors for *in vivo* treatment, we could actually demonstrate cooperation of CK1α and PLK1 in regard of phosphorylation of the fusion protein. This might be of special interest for future studies investigating escape mechanisms that have been indicated by our preliminary experiments.

Here, we discuss our strategy of transcription factor targeting, emerging challenges as well as future approaches. Our strategic but also novel mechanistic insights might be transferred to a variety of different tumors addicted to oncogenic transcription factors. As our strategy led to the successful identification and validation of PLK1 as a target in aRMS, we furthermore provide rationales for translating our results into clinical studies and discuss potential risks of PLK1 inhibitors and their application in aRMS therapy.

9.1 Strategies of transcription factor targeting

Many of the characterized PAX3-FOXO1 target genes contribute to tumor progression or maintenance, meaning that they are essential parts of the same oncogenic machinery. Therefore, most of them may be qualified as putative targets in aRMS therapy. However, involvement of several different target genes in tumorigenesis also suggests that single inhibition of any of these pathways might not be a sufficiently effective targeting strategy. Antagonizing single signaling cascades could moreover lead to activation of alternative pathways to overtake essential functions and could even exacerbate the disease by causing resistances (Kovar, 2014). In aRMS, preclinical activity was reported for several inhibitors targeting pathways downstream of PAX3-FOXO1. The most intensively studied target gene is IGF1R and its inhibition by the monoclonal antibody cixutumumab (IMC-A12) demonstrated significant *in vivo* activity in rhabdomyosarcoma xenografts (Houghton et al., 2010). However, in recent clinical phase 2 trials, monotherapies with cixutumumab did not meet the efficacy criteria for rhabdomyosarcoma treatments in a first study and showed only partial response in 1 out 20 RMS patients in a second investigation (Schoffski et al., 2013;

Weigel et al., 2014). This might be due to different resistance mechanisms acquired by IGF1R inhibition, including overexpression of PDGFRα, MAPK reactivation, HER2 overexpression, and downregulation of the IGF1R inhibitor IGFBP2 (Abraham et al., 2011; Huang et al., 2010; Kang et al., 2013).

Consequently, a more elegant strategy of choice implies direct targeting of PAX3-FOXO1 aiming at complete and definite elimination of the tumor. Therefore, we decided to exploit mechanisms of upstream PAX3-FOXO1 regulation. PAX3-FOXO1 function is the product of upstream enzymatic activities mediating posttranslational modifications and protein stability, protein-protein interactions, transcriptional as well as translational activities, and finally, epigenetic regulation. Based on studies that previously showed phosphorylation of PAX3-FOXO1 (see Introduction), our approach focused on kinase targeting.

9.1.1 Establishment of a functional screening system for upstream regulators

The first crucial step for identification of upstream regulators is the design and establishment of a screening system. We conducted a luciferase reporter assay and the resulting siRNA screening data suggest that this system recapitulates transcription factor activity and mirrors the function of the identified candidate kinases in primary aRMS tumors. Actually, eleven of the identified kinases showed an expression profile with significantly higher expression values in alveolar than in embryonal RMS, revealing a potential contribution to aRMS tumorigenesis (Hecker, 2010). A further group of seven candidates was represented within the target profile of the broad-spectrum kinase inhibitor PKC412, which represses PAX3-FOXO1 activity (Amstutz et al., 2008). Finally, five of the 47 candidates have been predicted to directly phosphorylate PAX3-FOXO1, indicating their impact on fusion protein activity. Hence, we think that the design of our screening system meets the requirements for the identification of upstream regulators of PAX3-FOXO1. However, limitations of such reporter assays are based on restriction to solely one target gene promoter in a context that does not recapitulate endogenous epigenetic landmarks and chromatin structure (Kovar, 2014). These technical limitations demand for substantial endogenous validation and request consequent expression analysis of various different endogenous target genes as we performed by qRT-PCR after PLK1 and CK1α depletion.

9.1.2 Complexity of posttranslational regulation

PAX3-FOXO1 was demonstrated to be highly phosphorylated indicating that its regulation might be orchestrated by multiple different phosphorylation events. Our mass spectrometry data showed at least eleven different phospho-sites in PAX3-FOXO1 purified from aRMS cells. Although we observed effects on protein stability by mutating S503, we predict that simultaneous site-specific mutagenesis of several residues might lead to an even more pronounced multilayered phenotypic change. This prediction is supported by the findings of Amstutz et al. (2008), who demonstrated that loss of function of six phospho-sites within the octapeptide has a greater impact on transactivation potency of PAX3-FOXO1 than single mutations. Thus, systematic site-specific mutagenesis might uncover the interplay of different phosphorylation sites in future studies.

Moreover, the overlapping functions of different kinases in phosphorylation of identical or additional sites in transcription factors as observed in PAX3-FOXO1 for PLK1 and CK1α, and potentially PLK1 and PLK4, might bear the risk of escape mechanisms induced by single agent targeting. Whether upregulation of CK1α and PLK4 activity after PLK1 inhibition occurs, remains to be investigated in future studies. Nevertheless, this illustrates that targeting posttranslational modifiers of oncogenic transcription factors might be compensated by alternative pathways, demanding awareness of escape mechanisms and undesired side effects.

9.1.3 Analysis of phospho-mutant transcription factors

We examined the S503 mutant and the 6xA octapeptide mutant by introducing them into fusion negative RD cells. Performing transient transfection, we were not able to modulate the expression signature of these cells (data not shown). Even viral transduction only resulted in partial upregulation of selected target genes. Using a proper cellular context, meaning in the case of aRMS either fusion positive cells after depletion of wild type PAX3-FOXO1 or cells resembling the cells of origin, might facilitate studies of mutant PAX3-FOXO1, as cellular context and chromatin accessibility determine transcription factor function. In fact, preliminary experiments demonstrated more efficient upregulation of several target genes in primary human MSC cells than in RD cells (data not shown), which might be a better approximation to the actual cell of origin and could be incorporated into future studies of PAX3-FOXO1

mutants. Taking together, this indicates that a careful choice of cell context is important for studying mutants of oncogenic transcription factors.

9.1.4 Cooperation of cell cycle arrest and impaired transcription factor activity

The identification of compounds specifically antagonizing PAX3-FOXO1 might be difficult because PAX3-FOXO1 activity and expression has been shown to be dynamic during cell cycle progression (Kikuchi et al., 2014). This is probably also the reason, why we identified many kinases involved in cell cycle regulation. Therefore, potentially any cell cycle arrest could affect PAX3-FOXO1 target gene expression. Also in the case of PLK1 inhibition, we did not fully succeed to distinguish fusion protein specific effects from those caused by mitotic arrest. In fact, we believe that drug induced apoptosis is the result of a combinational inhibition of several PLK1 dependent mechanisms including PAX3-FOXO1 regulation and cell cycle regulation. This interrelationship may not be surprising when considering the various different functions of PLK1 in cell division and in tumorigenesis (see Introduction). However, from a therapeutic point of view, targeting multiple tumor killing mechanism represents an advantage. Involving inhibition of multiple mechanisms does not only reach different compartments within a heterogeneous tumor, but also targets possible alternative pathways. Last but not least, a multiple approach enables the generation of a therapeutic window by reducing drug concentrations to protect healthy cells.

Summing up, the posttranslational regulation of the fusion protein is probably more complex than expected. Nevertheless, we were able to shed light on posttranslational regulation and cell cycle dependent dynamics of PAX3-FOXO1 function. Although strategies to directly target the oncogenic driver of aRMS are still impeded by insufficient knowledge about cell of origin and epigenetic regulation of PAX3-FOXO1, we successfully identified crucial upstream regulators of the fusion protein.

9.1.5 Future goals in transcription factor targeting

Studies investigating epigenetics of aRMS are still rare, but the low frequency of genetic alterations in aRMS indicates deregulation of epigenetic control, similar to other pediatric tumors (Huether et al., 2014). Mutations found in *BCOR,* encoding for a transcriptional repressor that interacts with histone deacetylases, support this notion (Shern et al., 2014). In addition, misbalance of different epigenetic modifiers has been reported for aRMS (Ciesla et al., 2014). For example, the overexpressed fusion target

gene and epigenetic regulator JARID2 maintains an undifferentiated state of fusion positive RMS (Walters et al., 2014). Also, the histone methyltransferase KMT1A arrests aRMS cells in myogenic differentiation (Lee et al., 2011). Last but not least, EZH2, a member of the polycomb group, is aberrantly expressed in aRMS. And importantly, EZH2 depletion resulted in apoptosis and its pharmacologic inhibitions prevented aRMS *in vivo* tumor growth (Ciarapica et al., 2014). Interestingly, it has furthermore been shown that histone deacetylase inhibitors potentiate the effects of PKC412 by p21 reactivation in aRMS (Hecker et al., 2010). To what extend epigenetic mechanisms also affect the expression of PAX3-FOXO1 itself and regulate its accessibility to chromatin, remains unresolved so far, although particular investigation of epigenetic mechanisms in relation to PAX3-FOXO1 expression will eventually lead to novel strategies of fusion protein targeting by epigenetic inhibition.

Surprisingly, two independent studies recently showed that BI 2536 and BI 6727 act as dual inhibitors against PLK1 kinase and against the bromodomain of BRD4 (Ciceri et al., 2014; Ember et al., 2014). Bromodomain and extra terminal (BET) family proteins are epigenetic readers that recruit transcriptional regulators, chromatin modulators and modifiers. Notably, in activity and binding studies against BRD4, BI 2536 was as potent as the prototypic BET inhibitor JQ1 (Ember et al., 2014). As we rather observed upregulation of PAX3-FOXO1 mRNA after BI 2536 treatment than repression of transcription, we could not identify inhibitory effects on PAX3-FOXO1 itself. However, different target genes such as NMYC might be affected by BRD4 inhibition as it has previously also been shown in neuroblastoma (Puissant et al., 2013). In this regard, we observed downregulation of NMYC after PLK1 inhibition, but we have not yet investigated the underlying mechanisms. In conclusion, we assume benefits for aRMS therapy by combining PLK1 inhibitors with epigenetic inhibitors and suggest future consideration of epigenetics for targeting of oncogenic transcription factors.

9.2 Rationales for clinical studies of PLK1 inhibitors in aRMS

9.2.1 Preclinical success of PLK1 inhibition in aRMS

We demonstrated a nearly complete tumor regression of aRMS xenografts by PLK1 inhibition, which has recently been confirmed by studies of the Pediatric Preclinical Testing Program investigating the second-generation PLK1 inhibitor BI 6727 (Gorlick et al., 2014). The authors did not provide any mechanistic model, but BI 6727 showed

potent activity against a panel of pediatric cancer cell lines *in vitro*. Two of the most responding cell lines included the aRMS lines Rh41 and Rh30 with a median relative IC_{50} of 6.9 nM and 8.2 nM after 96 hours. Across different pediatric tumor xenografts, objective *in vivo* responses were demonstrated for 4 out of 32 solid tumors (two neuroblastoma, one glioblastoma and one rhabdomyosarcoma model) and 1 out of 4 ALL xenografts (Gorlick et al., 2014). Concluding, the two independent studies proof that aRMS cells are highly prone to PLK1 inhibition in comparison to less responsive pediatric cell lines.

Besides the formation of mono-polar spindles, activation of the spindle assembly checkpoint, and mitotic arrest, additional factors might contribute to aRMS cell toxicity induced by PLK1 inhibitors.

9.2.1.1 Sensitization to PLK1 inhibition by PAX3-FOXO1 expression

Central to our study was the regulation of PAX3-FOXO1 by PLK1. Comparing drug induced cytotoxicity in different fusion positive and fusion negative rhabdomyosarcoma cell lines, we demonstrated PAX3-FOXO1 to sensitize to PLK1 inhibition. In agreement with investigations of BI 6727 by Gorlick et al. (2014), we measured lower IC_{50} values for BI 2536 in aRMS than in eRMS cells. Furthermore, we demonstrated that PLK1 expression significantly correlated with AP2β expression in human aRMS biopsies. This latter finding reveals that in aRMS PLK1 function is strongly reflected in PAX3-FOXO1 activity.

9.2.1.2 Sensitization to PLK1 inhibition by NMYC expression

Expression of the oncogenic transcription factor NMYC is common to the solid tumors that showed objective responses to BI 6727 in the study of Gorlick et al. (2014), suggesting a correlation of PLK1 function and NMYC levels. In accordance to this finding, our study provided the first evidence for reduced NMYC protein after BI 2536 and BI 6727 treatment. This reduction might be caused either by impaired PAX3-FOXO1 activity, by destabilization and active degradation of NMYC due to lack of PLK1 phosphorylation, or by a mechanism that also involves BI 2536/BI 6727 induced BRD4 inhibition. In any case, NMYC reduction is potentially contributing to the anti-tumor activity of PLK1 inhibitors in NMYC addicted tumors.

9.2.1.3 Sensitization to PLK1 inhibition by p53 repression

Various studies investigated whether non-functional p53 might influence cytotoxicity of PLK1 inhibition, obtaining different results that are still under debate. On the one

hand, treatment efficiencies in $p53^{-/-}$ in comparison to $p53^{+/+}$ cell lines including HCT116 colorectal cancer, MCF7 breast cancer and A549 non-small lung cancer, showed no dependency on p53 status upon treatment with different PLK1 inhibitors (Sanhaji et al., 2012; Sanhaji et al., 2013). On the other hand, several studies reported that mutant p53 is a marker of sensitivity (Craig et al., 2014). Based on the notion that mutant p53 cannot repress PLK1 expression, studies in pairs of isogenic cell lines showed that cells without functional p53 are more susceptible to PLK1 inhibition as they are addicted to overexpressed PLK1 (King et al., 2012; Sur et al., 2009). Sensitivity of Rh4 and RMS13 cells might also partially be the result of their p53 status. Our STR analysis demonstrated that the Rh4 cell line is derived from the same patient as Rh41 cells, and the RMS13 cell line from the same patient as Rh30 cells. Both Rh41 and Rh30 cells harbor mutations in the *p53* gene (Hinson et al., 2013) implying that also Rh4 and RMS13 cells express non-functional p53. In general, mutant p53 is often found in aRMS cell lines but has not been detected by sequencing of primary aRMS biopsies. However, *p53* loss of heterozygosity, copy number gain of *MDM2*, and *INK4/ARF* loss resulting in degradation of p53 are very common in aRMS tumors (Shern et al., 2014).

Summing up, the combination of these tumor-specific factors sensitizes to PLK1 inhibition. Nevertheless, it is important to conduct and evaluate toxicity in healthy cells before introducing PLK1 inhibitors into clinical trials.

9.2.2 Investigation and circumvention of PLK1 inhibitor toxicities in healthy cells

Despite great efficacy in preclinical *in vivo* studies, the clinical use of PLK1 inhibitors might be limited by undesired toxicities due to disturbance of pleiotropic PLK1 functions in mitosis. To exclude adverse effects on healthy cells, Plk1 depletion in non-cancer cell lines and primary cells has been performed *in vitro* and *in vivo*. Plk1 depletion in the mouse myoblast cell line C2C12 did neither cause any growth reduction nor any induction of apoptosis (Hu et al., 2009), whereas minor impact on proliferative activity was found in inducible knockdown mouse embryonic fibroblasts (MEFs) compared to wild type MEFs (Raab et al., 2011). Lentiviral targeting of PLK1 in retinal epithelial cells expressing human telomerase reverse transcriptase (hTERT-RPE1) and non-transformed breast epithelial cells (MCF10A) showed also only minor, respectively no impact on proliferation and kinetics as well as no effects on cell cycle profiles. Interestingly, p53 depletion sensitized MCF10A cells and resulted in cell cycle

arrest and induction of apoptosis (Liu et al., 2006). Also, PLK1 directed siRNA has been applied to test effects of PLK1 depletion in further human cells including human umbilical vein endothelial cells (HUVEC), fibroblasts and keratinocytes resulting in a non-significant growth inhibition below 5%. Cell cycle analysis of primary cells revealed only a moderate increase of cells in G2/M upon siRNA mediated knockdown of PLK1, which was, at least in keratinocytes, reflected by spindle assembly defects at a much lower frequencies than in cancer cell lines. Furthermore, a lack of activation of the spindle assembly checkpoint has been suggested in keratinocytes. In summary, induction of apoptosis was barely observed in primary cells, and in this latter study, not even upon silencing of p53 in contrast to the previously mentioned MCF10A cells (Raab et al., 2011). Overall, PLK1 depletion induced only minor effects in non-cancer cells.

However, it is indispensable to point out that treatment of MEFs with the PLK1 inhibitor BI 2536 showed different effects than Plk1 depletion. Growth inhibition was observed after 24 hours at elevated levels and was accompanied by altered cell cycle distribution at 50 nM as well as an induction of considerable apoptosis at 100 nM indicating the need for careful dose-finding studies (Raab et al., 2011). A further investigation compared fibroblasts to fully differentiated cells. Although BI 2536 treatment of primary neonatal rat cardiac fibroblasts for 24 hours either mitotically arrested cells with an IC_{50} of 43 nM leading to apoptosis or resulted in aneuploidy, treatment with 100 nM BI 2536 for 24 hours did not affect cardiomyocytes and their function. Importantly, this reveals that there is no impact of PLK1 inhibition on terminally differentiated cells (Lu et al., 2010).

The difference in apoptotic response to Plk1 depletion and BI 2536 treatment observed in MEFs might be due to unspecific inhibition of all Plk family members by the pharmaceutical compound. Plk1 depletion did not change Plk3 levels in MEFs. However, Plk2 and Plk4 levels have not been reported. It is likely that these PLK family members, in addition to other unrelated kinases, compensate PLK1 specific depletion in healthy cells, whereas this is not the case for BI 2536 treatment (Raab et al., 2011). While simultaneous inhibition of the oncogenes Plk1 and PLk4 in cancer cells, especially in aRMS, could be a therapeutic advantage, antagonizing the tumor suppressors PLK2 and PLK3 might be contra-productive for killing tumor cells and for persevering healthy cells. Thus, the development of more specific inhibitors is warranted. A first step has been made by the generation of polo-box binding domain

inhibitors such as poloxin, which leave kinases outside the PLK family unaffected by inhibition (Craig et al., 2014).

In addition to inhibitor specificity, also the p53 status might play a role in protecting healthy cells from apoptosis. The study of Sur et al. (2009) directly addressed reduction of side effects by combining BI 2536 with nutlin-3 in BALB/c xenograft models of HCT116 *p53*$^{-/-}$ cells, whereby nutlin-3 is supposed to stabilize p53 in healthy cells. While anti-tumor activity did not change, an immense reduction of neutropenia was observed because normal cells were protected from toxicity, a finding that is of high clinical relevance (Sur et al., 2009).

To also investigate *in vivo* functions of PLK1, an inducible knockdown of Plk1 in adult mice has been established receiving efficient but not complete Plk1 depletion. Mice underwent detailed phenotypic analysis. Neither histological, nor metabolic differences to wild type mice have been observed despite increased body weight and enhanced rectal temperature in males. In contrast to structural anti-mitotic drugs that interfere with spermatogenesis, no testis disorders have been reported for transgenic mice. Only a reduced proliferation index was detected in mucosal folds and ovarian follicles. Additionally, no significant induction of apoptosis was registered in any murine tissue. Despite reduced ferritin levels that could cause hematologic alterations, there was no evidence for disturbance in hematopoiesis without any abnormalities in white blood count, indication of neutropenia, or myelosuppression as it is often observed for anti-mitotic inhibition (Raab et al., 2011). With regard to our investigations and the evaluation of PLK1 inhibitors in pediatric malignancies, additional early stage induction of PLK1 inhibition during development and in very young mice might be important.

In summary, these data provide evidence that PLK1 inhibitors could succeed also in clinical trials without causing severe side effects. Genetic studies revealed only low dependency of primary non-transformed cells on Plk1 regarding proliferation, spindle assembly and apoptosis, whereas cancer cells were suggested to be addicted to Plk1. However, PLK1 inhibitors warrant further improvements in terms of specificity and it also needs to be considered for clinical studies that mice can tolerate higher drug concentrations than humans, a fact that demands an even more careful dosage evaluation (Gorlick et al., 2014).

9.2.3 Identification of escape mechanisms

Translation of preclinical results into clinical practice can fail due to evolving mechanisms of resistance often observed with kinase inhibitors. This effect might challenge kinase inhibitors more than other drugs, because they are main executers in cell metabolism, cellular function, and survival and therefore are opposed to strong selection pressure. Thus, cells mediate quick and efficient upregulation of compensatory pathways or counteracting mechanisms as logical reaction on kinase inhibition. Furthermore, their multiple interference points, which mediate interactions and structural dynamics for activation, are prone to mutations (Barouch-Bentov and Sauer, 2011). This can lead to clinical complications as for example observed in 7-15% of imatinib-treated CML patients that develop secondary resistance (Barouch-Bentov and Sauer, 2011). Besides few other studies that have already described escape from PLK1 inhibition, our preliminary results also indicate that aRMS tumors might be able to acquire resistance to BI 2536.

One common phenomenon observed in tumor resistance is overexpression of ATP-binding cassette (ABC) transporters, which mediate the efflux of many different compounds. Wu et al. (2013) provided first evidences that resistance towards BI 2536 might be mediated by drug efflux through ABCB1 and ABCG2. BI 2536 treatment per se did not lead to altered expression, but it was capable of enhancing the ATPase activity of these transporters.

Recently, the C67V mutation in the active site of PLK1 has been described to potentially cause drug insensitivity. In contrast to the gatekeeper mutation L130G, the C67V mutation did not interfere with function, but was able to occlude the PLK1 inhibitors BI 2536, BI 6727, GSK461364, and ZK-thiazolidone (TAL) from the ATP-binding pocket by steric hindrance resulting in drug resistance after PLK1-C67V compared to PLK1 wild type complementation of *PLK1*$^{-/-}$ cells (Burkard et al., 2012).

In aRMS, also mutations at PLK1 dependent phosphorylation sites within PAX3-FOXO1 might occur, leading to stabilization or constitutive activation of the fusion and thus to a less pronounced effect of PLK1 inhibition. Also, considering PLK1 crosstalk and feedback signaling might be of great value for further preclinical and clinical studies of aRMS and careful validation of resistance mechanisms could help to prevent disillusions.

9.2.4 Suggestion of reasonable data-based combination therapies in aRMS

Having identified crucial kinases, pathways and regulatory mechanisms in alveolar rhabdomyosarcoma, a first step and widely accepted strategy to circumvent resistance mechanisms is the combination of drugs targeting these different interconnected candidate networks. Based on our screening results, several candidate targets might be suitable for simultaneous inhibition with PLK1 in order to approach this challenge.

We observed overlapping functions of PLK1, PLK4 and CK1α, suggesting potential activation or upregulation of compensatory kinases and pathways upon PLK1 inhibition. Due to non-specific targeting within the PLK family, BI 2536 and BI 6727 probably simultaneously inhibit PLK1 and PLK4. Therefore, it could be interesting to also investigate anti-tumor activity of newly available PLK4 specific inhibitors such as CFI-400945 (Mason et al., 2014). Regarding specific CK1α targeting, we unfortunately could not identify suitable CK1α specific inhibitors so far.

In addition, our siRNA screening revealed phosphatidylinositol signaling and MAPK signaling as well as cell cycle regulation as essential pathways in fusion positive RMS. Importantly, all three pathways have already been suggested for treatment of rhabdomyosarcoma in previous studies. Activation of the PI3K/AKT/mTOR as well as the RAS/RAF/MEK/ERK pathway has been reported in rhabdomyosarcoma and high levels of AKT phosphorylation were associated with poor diagnosis (Cen et al., 2007; Petricoin et al., 2007). A further study even revealed co-activation of AKT and ERK in 36% of primary aRMS tumors (Renshaw et al., 2013). Finally, based on the linkage of the two signaling cascades and their ability to compensate for each other, Renshaw et al. (2013) proposed a combination therapy using an mTORC1/2 inhibitor (AZD8055) and a MEK inhibitor (AZD6244), while we propose additional co-administration of PLK1 directed compounds.

Involvement of cell cycle in the regulation of PAX3-FOXO1, as well as the fusion protein's own function in checkpoint adaptation, suggest combination of PLK1 targeting with further cell cycle inhibitors. Probably the most obvious combinations include standard chemotherapeutic regimens like vincristine. Moreover, the alternative mitotic inhibitor eribulin, which binds and inhibits microtubule plus ends, has recently been reported to achieve complete responses in five out of five aRMS xenografts demonstrating even superior activity to vincristine (Kolb et al., 2013). Also recent preclinical studies with nab-paclitaxel (abraxane), an albumin-stabilized nanoparticle formulation of paclitaxel, which stabilizes microtubules and induces

mitotic arrest, showed complete tumor regression in aRMS xenografts (Zhang et al., 2013). In terms of cell cycle kinase inhibition, the proposed PAX3-FOXO1 upstream regulators CDK1 and CDK4 (Liu et al., 2013a) may potentiate direct effects on the fusion protein. However, CDK4/6 inhibitors induce a G1 arrest, which might antagonize favorable effects of PLK1 inhibitor induced mitotic arrest, as it was already observed in pancreatic cancer by Franco et al. (2014).

Further candidate compounds for co-administration have been identified in our drug screen and importantly, some of the pathways and targets have already been proposed for therapeutic approaches in aRMS. These compounds include AKT (Cen et al., 2007), HSP90 (Lesko et al., 2007; Smith et al., 2008), FGFR (Crose et al., 2012; Li et al., 2013; Taylor et al., 2009), and SRC (Shor et al., 2007).

To round up, an additional targeting-layer of these oncogenic transcription factors that still requires validation might be realized by epigenetic inhibition.

9.2.5 Clinical studies of BI 2536 and BI 6727

The first clinical phase 1 trial of BI 2536 in adult patients with advanced solid tumors showed favorable efficacy and manageable toxicity (Mross et al., 2008), whereas respond rates could not be confirmed in a second part of the study (Frost et al., 2012). Also, phase 2 studies of relapsed or refractory solid tumors, non-small cell lung cancer, small cell lung cancer, chemotherapy-naive pancreatic cancer, and relapsed or refractory AML showed only modest to no activity of BI 2536, probably due to low intratumoral exposure and short half-life (Gjertsen and Schoffski, 2014). Thereupon, monotherapy with BI 2536 in clinical trials was terminated (Yim, 2013).

Nevertheless, the current focus of clinical development lies on the most advanced, second-generation PLK1 inhibitor volasertib (BI 6727) next to compounds from other companies like GSK461364 or NMS-P937 (Strebhardt et al., 2014). Volasertib has an improved pharmacokinetic profile and higher efficacy, which has been determined in a phase 1 trial in adults with advanced or metastatic solid tumors. In this study, reversible hematologic toxicity was the main side effect. Clinical phase 2 monotherapy and combination trials in advanced solid tumors, advanced or metastatic urothelial cancer, advanced ovarian cancer, advanced NSCLC, and AML have recently been completed or are currently ongoing (Gjertsen and Schoffski, 2014; Rudolph et al., 2009; Schoffski et al., 2012). Response rates in patients with solid tumors have been moderate, while monotherapy in AML patients resulted in a response rate of 13.3%,

and combination with low-dose cytarabine yielded a response rate of 31% (complete remission and complete remission with incomplete blood count recovery), leading to significant clinical benefits (Dohner et al., 2014; Gjertsen and Schoffski, 2014). Due to its impact on significantly improved survival rates, BI 6727 has also been granted a Breakthrough Therapy designation for treatment of AML by the FDA (Strebhardt et al., 2014). Based on these encouraging data in adult cancers, we believe that also children could benefit from volasertib therapy.

9.3 Conclusions and outlook

Despite a complex phosphorylation pattern and crosstalk between different signaling pathways, we were able to target PAX3-FOXO1 and NMYC by PLK1 inhibition. Validation of further candidate kinases might provide additional opportunities for PAX3-FOXO1 targeting, thus reduce drug dosing of PLK1 inhibitors and prevent compensatory mechanisms. Based on our studies, identification of compounds against CK1α and application of PLK4 and mitotic inhibitors would allow first combinational trials along these lines. In addition, we suggest investigations of PAX3-FOXO1 epigenetic regulation.

In general, our strategy can be easily transferred to other tumors addicted to oncogenic transcription factors, such as Ewing sarcoma. According to our proposed mechanism, NMYC/MYC expressing tumors like neuroblastoma might be sensitized to PLK1 inhibition, and possibly also PAX3 expressing cancers like melanoma might respond to PLK1 and/or CK1α inhibition.

We believe that transcription factor targeting is superior to inhibition of downstream pathways. Based on our data, PLK1 inhibitors might be able to confirm this for fusion positive RMS in clinical studies. Our preclinical studies of PLK1 inhibition in aRMS highly suggest clinical translation and promise encouraging prospects for improved therapy of alveolar rhabdomyosarcoma. Next to induction of mitotic arrest observed in different tumors treated with PLK1 inhibitors, expression of PAX3-FOXO1, NMYC and repressed p53 especially sensitize aRMS tumors. Referring to studies showing that healthy and terminally differentiated cells are not addicted to PLK1, risks of PLK1 inhibition for dividing cells persist but remain manageable as long as favorable therapeutic windows can be defined. Nevertheless, it is crucial to investigate potential resistance mechanisms in future studies. Prevention of escape of aRMS cells might be accomplished by proposed combination therapies, which needs to be proven by *in*

vitro and *in vivo* approaches. Importantly, anti-tumor activity and manageable side effects of volasertib observed in adult patients provide a good basis for future clinical studies in pediatric tumors like aRMS. Furthermore, we suggest prognostic value validation of PLK1 expression in a large-scale study to introduce routine PLK1 tissue staining for risk stratification of fusion positive RMS in clinical protocols.

10 References

Abraham, J., Prajapati, S. I., Nishijo, K., Schaffer, B. S., Taniguchi, E., Kilcoyne, A., McCleish, A. T., Nelon, L. D., Giles, F. G., Efstratiadis, A., et al. (2011). Evasion mechanisms to Igf1r inhibition in rhabdomyosarcoma. Mol Cancer Ther 10, 697-707.

Ackermann, S., Goeser, F., Schulte, J. H., Schramm, A., Ehemann, V., Hero, B., Eggert, A., Berthold, F., and Fischer, M. (2011). Polo-like kinase 1 is a therapeutic target in high-risk neuroblastoma. Clin Cancer Res 17, 731-741.

Adams, J., Palombella, V. J., Sausville, E. A., Johnson, J., Destree, A., Lazarus, D. D., Maas, J., Pien, C. S., Prakash, S., and Elliott, P. J. (1999). Proteasome inhibitors: a novel class of potent and effective antitumor agents. Cancer Res 59, 2615-2622.

Amstutz, R., Wachtel, M., Troxler, H., Kleinert, P., Ebauer, M., Haneke, T., Oehler-Janne, C., Fabbro, D., Niggli, F. K., and Schafer, B. W. (2008). Phosphorylation regulates transcriptional activity of PAX3/FKHR and reveals novel therapeutic possibilities. Cancer Res 68, 3767-3776.

Archambault, V., and Glover, D. M. (2009). Polo-like kinases: conservation and divergence in their functions and regulation. Nat Rev Mol Cell Biol 10, 265-275.

Aslam, M. I., Abraham, J., Mansoor, A., Druker, B. J., Tyner, J. W., and Keller, C. (2014). PDGFRbeta reverses EphB4 signaling in alveolar rhabdomyosarcoma. Proc Natl Acad Sci U S A 111, 6383-6388.

Ayyanathan, K., Fredericks, W. J., Berking, C., Herlyn, M., Balakrishnan, C., Gunther, E., and Rauscher, F. J., 3rd (2000). Hormone-dependent tumor regression in vivo by an inducible transcriptional repressor directed at the PAX3-FKHR oncogene. Cancer Res 60, 5803-5814.

Bakay, M., Wang, Z., Melcon, G., Schiltz, L., Xuan, J., Zhao, P., Sartorelli, V., Seo, J., Pegoraro, E., Angelini, C., et al. (2006). Nuclear envelope dystrophies show a transcriptional fingerprint suggesting disruption of Rb-MyoD pathways in muscle regeneration. Brain 129, 996-1013.

Barouch-Bentov, R., and Sauer, K. (2011). Mechanisms of drug resistance in kinases. Expert Opin Investig Drugs 20, 153-208.

Bennicelli, J. L., Advani, S., Schafer, B. W., and Barr, F. G. (1999). PAX3 and PAX7 exhibit conserved cis-acting transcription repression domains and utilize a common gain of function mechanism in alveolar rhabdomyosarcoma. Oncogene 18, 4348-4356.

Bennicelli, J. L., Edwards, R. H., and Barr, F. G. (1996). Mechanism for transcriptional gain of function resulting from chromosomal translocation in alveolar rhabdomyosarcoma. Proc Natl Acad Sci U S A 93, 5455-5459.

Bernasconi, M., Remppis, A., Fredericks, W. J., Rauscher, F. J., 3rd, and Schafer, B. W. (1996). Induction of apoptosis in rhabdomyosarcoma cells through down-regulation of PAX proteins. Proc Natl Acad Sci U S A 93, 13164-13169.

Breneman, J. C., Lyden, E., Pappo, A. S., Link, M. P., Anderson, J. R., Parham, D. M., Qualman, S. J., Wharam, M. D., Donaldson, S. S., Maurer, H. M., et al. (2003). Prognostic factors and clinical outcomes in children and adolescents with metastatic rhabdomyosarcoma--a report from the Intergroup Rhabdomyosarcoma Study IV. J Clin Oncol 21, 78-84.

Brunelli, S., Relaix, F., Baesso, S., Buckingham, M., and Cossu, G. (2007). Beta catenin-independent activation of MyoD in presomitic mesoderm requires PKC and depends on Pax3 transcriptional activity. Dev Biol 304, 604-614.

Burkard, M. E., Santamaria, A., and Jallepalli, P. V. (2012). Enabling and disabling polo-like kinase 1 inhibition through chemical genetics. ACS Chem Biol 7, 978-981.

Calhabeu, F., Hayashi, S., Morgan, J. E., Relaix, F., and Zammit, P. S. (2013). Alveolar rhabdomyosarcoma-associated proteins PAX3/FOXO1A and PAX7/FOXO1A suppress the transcriptional activity of MyoD-target genes in muscle stem cells. Oncogene 32, 651-662.

Cao, L., Yu, Y., Bilke, S., Walker, R. L., Mayeenuddin, L. H., Azorsa, D. O., Yang, F., Pineda, M., Helman, L. J., and Meltzer, P. S. (2010). Genome-wide identification of PAX3-FKHR binding sites in rhabdomyosarcoma reveals candidate target genes important for development and cancer. Cancer Res 70, 6497-6508.

Cen, L., Hsieh, F. C., Lin, H. J., Chen, C. S., Qualman, S. J., and Lin, J. (2007). PDK-1/AKT pathway as a novel therapeutic target in rhabdomyosarcoma cells using OSU-03012 compound. Br J Cancer 97, 785-791.

Chen, X., Stewart, E., Shelat, A. A., Qu, C., Bahrami, A., Hatley, M., Wu, G., Bradley, C., McEvoy, J., Pappo, A., et al. (2013). Targeting oxidative stress in embryonal rhabdomyosarcoma. Cancer Cell 24, 710-724.

Cheong, J. K., and Virshup, D. M. (2011). Casein kinase 1: Complexity in the family. Int J Biochem Cell Biol 43, 465-469.

Cholewa, B. D., Liu, X., and Ahmad, N. (2013). The role of polo-like kinase 1 in carcinogenesis: cause or consequence? Cancer Res *73*, 6848-6855.

Chopra, P., Sethi, G., Dastidar, S. G., and Ray, A. (2010). Polo-like kinase inhibitors: an emerging opportunity for cancer therapeutics. Expert Opin Investig Drugs 19, 27-43.

Ciarapica, R., De Salvo, M., Carcarino, E., Bracaglia, G., Adesso, L., Leoncini, P. P., Dall'Agnese, A., Walters, Z. S., Verginelli, F., De Sio, L., et al. (2014). The Polycomb group (PcG) protein EZH2 supports the survival of PAX3-FOXO1 alveolar rhabdomyosarcoma by repressing FBXO32 (Atrogin1/MAFbx). Oncogene 33, 4173-4184.

Ciceri, P., Muller, S., O'Mahony, A., Fedorov, O., Filippakopoulos, P., Hunt, J. P., Lasater, E. A., Pallares, G., Picaud, S., Wells, C., et al. (2014). Dual kinase-bromodomain inhibitors for rationally designed polypharmacology. Nat Chem Biol 10, 305-312.

Ciesla, M., Dulak, J., and Jozkowicz, A. (2014). MicroRNAs and epigenetic mechanisms of rhabdomyosarcoma development. Int J Biochem Cell Biol 53, 482-492.

Craig, S. N., Wyatt, M. D., and McInnes, C. (2014). Current assessment of polo-like kinases as anti-tumor drug targets. Expert Opin Drug Discov 9, 773-789.

Crose, L. E., Etheridge, K. T., Chen, C., Belyea, B., Talbot, L. J., Bentley, R. C., and Linardic, C. M. (2012). FGFR4 blockade exerts distinct antitumorigenic effects in

human embryonal versus alveolar rhabdomyosarcoma. Clin Cancer Res 18, 3780-3790.

Dasgupta, R., and Rodeberg, D. A. (2012). Update on rhabdomyosarcoma. Semin Pediatr Surg 21, 68-78.

Davicioni, E., Finckenstein, F. G., Shahbazian, V., Buckley, J. D., Triche, T. J., and Anderson, M. J. (2006). Identification of a PAX-FKHR gene expression signature that defines molecular classes and determines the prognosis of alveolar rhabdomyosarcomas. Cancer Res 66, 6936-6946.

Davis, R. J., and Barr, F. G. (1997). Fusion genes resulting from alternative chromosomal translocations are overexpressed by gene-specific mechanisms in alveolar rhabdomyosarcoma. Proc Natl Acad Sci U S A 94, 8047-8051.

De Giovanni, C., Landuzzi, L., Nicoletti, G., Lollini, P. L., and Nanni, P. (2009). Molecular and cellular biology of rhabdomyosarcoma. Future Oncol 5, 1449-1475.

De Pitta, C., Tombolan, L., Albiero, G., Sartori, F., Romualdi, C., Jurman, G., Carli, M., Furlanello, C., Lanfranchi, G., and Rosolen, A. (2006). Gene expression profiling identifies potential relevant genes in alveolar rhabdomyosarcoma pathogenesis and discriminates PAX3-FKHR positive and negative tumors. Int J Cancer 118, 2772-2781.

del Peso, L., Gonzalez, V. M., Hernandez, R., Barr, F. G., and Nunez, G. (1999). Regulation of the forkhead transcription factor FKHR, but not the PAX3-FKHR fusion protein, by the serine/threonine kinase Akt. Oncogene 18, 7328-7333.

Dietz, K. N., Miller, P. J., and Hollenbach, A. D. (2009). Phosphorylation of serine 205 by the protein kinase CK2 persists on Pax3-FOXO1, but not Pax3, throughout early myogenic differentiation. Biochemistry 48, 11786-11795.

Dietz, K. N., Miller, P. J., Iyengar, A. S., Loupe, J. M., and Hollenbach, A. D. (2011). Identification of serines 201 and 209 as sites of Pax3 phosphorylation and the altered phosphorylation status of Pax3-FOXO1 during early myogenic differentiation. Int J Biochem Cell Biol 43, 936-945.

Dohner, H., Lubbert, M., Fiedler, W., Fouillard, L., Haaland, A., Brandwein, J. M., Lepretre, S., Reman, O., Turlure, P., Ottmann, O. G., et al. (2014). Randomized,

phase 2 trial of low-dose cytarabine with or without volasertib in AML patients not suitable for induction therapy. Blood 124, 1426-1433.

Downing, J. R., Wilson, R. K., Zhang, J., Mardis, E. R., Pui, C. H., Ding, L., Ley, T. J., and Evans, W. E. (2012). The Pediatric Cancer Genome Project. Nat Genet 44, 619-622.

Duan, Z., Ji, D., Weinstein, E. J., Liu, X., Susa, M., Choy, E., Yang, C., Mankin, H., and Hornicek, F. J. (2010). Lentiviral shRNA screen of human kinases identifies PLK1 as a potential therapeutic target for osteosarcoma. Cancer Lett 293, 220-229.

Ebauer, M., Wachtel, M., Niggli, F. K., and Schafer, B. W. (2007). Comparative expression profiling identifies an in vivo target gene signature with TFAP2B as a mediator of the survival function of PAX3/FKHR. Oncogene 26, 7267-7281.

Ember, S. W., Zhu, J. Y., Olesen, S. H., Martin, M. P., Becker, A., Berndt, N., Georg, G. I., and Schonbrunn, E. (2014). Acetyl-lysine binding site of bromodomain-containing protein 4 (BRD4) interacts with diverse kinase inhibitors. ACS Chem Biol 9, 1160-1171.

Feng, Y. B., Lin, D. C., Shi, Z. Z., Wang, X. C., Shen, X. M., Zhang, Y., Du, X. L., Luo, M. L., Xu, X., Han, Y. L., et al. (2009). Overexpression of PLK1 is associated with poor survival by inhibiting apoptosis via enhancement of survivin level in esophageal squamous cell carcinoma. Int J Cancer 124, 578-588.

Franco, J., Witkiewicz, A. K., and Knudsen, E. S. (2014). CDK4/6 inhibitors have potent activity in combination with pathway selective therapeutic agents in models of pancreatic cancer. Oncotarget 5, 6512-6525.

Frost, A., Mross, K., Steinbild, S., Hedbom, S., Unger, C., Kaiser, R., Trommeshauser, D., and Munzert, G. (2012). Phase i study of the Plk1 inhibitor BI 2536 administered intravenously on three consecutive days in advanced solid tumours. Curr Oncol 19, e28-35.

Gjertsen, B. T., and Schoffski, P. (2014). Discovery and development of the Polo-like kinase inhibitor volasertib in cancer therapy. Leukemia. DOI: 10.1038/leu.2014.222.

Gorlick, R., Kolb, E. A., Keir, S. T., Maris, J. M., Reynolds, C. P., Kang, M. H., Carol, H., Lock, R., Billups, C. A., Kurmasheva, R. T., et al. (2014). Initial testing (stage 1) of

the polo-like kinase inhibitor volasertib (BI 6727), by the Pediatric Preclinical Testing Program. Pediatr Blood Cancer 61, 158-164.

Grass, B., Wachtel, M., Behnke, S., Leuschner, I., Niggli, F. K., and Schafer, B. W. (2009). Immunohistochemical detection of EGFR, fibrillin-2, P-cadherin and AP2beta as biomarkers for rhabdomyosarcoma diagnostics. Histopathology 54, 873-879.

Grinshtein, N., Datti, A., Fujitani, M., Uehling, D., Prakesch, M., Isaac, M., Irwin, M. S., Wrana, J. L., Al-Awar, R., and Kaplan, D. R. (2011). Small molecule kinase inhibitor screen identifies polo-like kinase 1 as a target for neuroblastoma tumor-initiating cells. Cancer Res 71, 1385-1395.

Guenther, M. K., Graab, U., and Fulda, S. (2013). Synthetic lethal interaction between PI3K/Akt/mTOR and Ras/MEK/ERK pathway inhibition in rhabdomyosarcoma. Cancer Lett 337, 200-209.

Hanahan, D., and Weinberg, R. A. (2000). The hallmarks of cancer. Cell 100, 57-70.

Hanahan, D., and Weinberg, R. A. (2011). Hallmarks of cancer: the next generation. Cell 144, 646-674.

Hatley, M. E., Tang, W., Garcia, M. R., Finkelstein, D., Millay, D. P., Liu, N., Graff, J., Galindo, R. L., and Olson, E. N. (2012). A mouse model of rhabdomyosarcoma originating from the adipocyte lineage. Cancer Cell 22, 536-546.

Hecker, R. (2010). Novel targeted approaches for rhabdomyosarcoma therapy. Ph.D thesis. University of Zurich.

Hecker, R. M., Amstutz, R. A., Wachtel, M., Walter, D., Niggli, F. K., and Schafer, B. W. (2010). p21 Downregulation is an important component of PAX3/FKHR oncogenicity and its reactivation by HDAC inhibitors enhances combination treatment. Oncogene 29, 3942-3952.

Hettmer, S., and Wagers, A. J. (2010). Muscling in: Uncovering the origins of rhabdomyosarcoma. Nat Med 16, 171-173.

Hinson, A. R., Jones, R., Crose, L. E., Belyea, B. C., Barr, F. G., and Linardic, C. M. (2013). Human rhabdomyosarcoma cell lines for rhabdomyosarcoma research: utility and pitfalls. Front Oncol 3, 183.

Holtrich, U., Wolf, G., Brauninger, A., Karn, T., Bohme, B., Rubsamen-Waigmann, H., and Strebhardt, K. (1994). Induction and down-regulation of PLK, a human serine/threonine kinase expressed in proliferating cells and tumors. Proc Natl Acad Sci U S A 91, 1736-1740.

Houghton, P. J., Morton, C. L., Gorlick, R., Kolb, E. A., Keir, S. T., Reynolds, C. P., Kang, M. H., Maris, J. M., Wu, J., and Smith, M. A. (2010). Initial testing of a monoclonal antibody (IMC-A12) against IGF-1R by the Pediatric Preclinical Testing Program. Pediatr Blood Cancer 54, 921-926.

Hu, K., Lee, C., Qiu, D., Fotovati, A., Davies, A., Abu-Ali, S., Wai, D., Lawlor, E. R., Triche, T. J., Pallen, C. J., and Dunn, S. E. (2009). Small interfering RNA library screen of human kinases and phosphatases identifies polo-like kinase 1 as a promising new target for the treatment of pediatric rhabdomyosarcomas. Mol Cancer Ther 8, 3024-3035.

Huang, F., Hurlburt, W., Greer, A., Reeves, K. A., Hillerman, S., Chang, H., Fargnoli, J., Graf Finckenstein, F., Gottardis, M. M., and Carboni, J. M. (2010). Differential mechanisms of acquired resistance to insulin-like growth factor-i receptor antibody therapy or to a small-molecule inhibitor, BMS-754807, in a human rhabdomyosarcoma model. Cancer Res 70, 7221-7231.

Huart, A. S., MacLaine, N. J., Meek, D. W., and Hupp, T. R. (2009). CK1alpha plays a central role in mediating MDM2 control of p53 and E2F-1 protein stability. J Biol Chem 284, 32384-32394.

Huether, R., Dong, L., Chen, X., Wu, G., Parker, M., Wei, L., Ma, J., Edmonson, M. N., Hedlund, E. K., Rusch, M. C., et al. (2014). The landscape of somatic mutations in epigenetic regulators across 1,000 paediatric cancer genomes. Nat Commun 5, 3630.

Iyengar, A. S., Loupe, J. M., Miller, P. J., and Hollenbach, A. D. (2012). Identification of CK2 as the kinase that phosphorylates Pax3 at Ser209 in early myogenic differentiation. Biochem Biophys Res Commun 428, 24-30.

Jothi, M., and Mal, A. K. (2012). Too much AKT turns PAX3-FKHR dead: a prospect of novel therapeutic strategy for alveolar rhabdomyosarcoma. Oncotarget 3, 1064-1065.

Jothi, M., Mal, M., Keller, C., and Mal, A. K. (2013). Small molecule inhibition of PAX3-FOXO1 through AKT activation suppresses malignant phenotypes of alveolar rhabdomyosarcoma. Mol Cancer Ther *12*, 2663-2674.

Jothi, M., Nishijo, K., Keller, C., and Mal, A. K. (2012). AKT and PAX3-FKHR cooperation enforces myogenic differentiation blockade in alveolar rhabdomyosarcoma cell. Cell Cycle 11, 895-908.

Kaatsch, P. (2010). Epidemiology of childhood cancer. Cancer Treat Rev 36, 277-285.

Kang, Z., Yu, Y., Zhu, Y. J., Davis, S., Walker, R., Meltzer, P. S., Helman, L. J., and Cao, L. (2013). Downregulation of IGFBP2 is associated with resistance to IGF1R therapy in rhabdomyosarcoma. Oncogene. DOI: 10.1038/onc.2013.509.

Kasahara, K., Goto, H., Izawa, I., Kiyono, T., Watanabe, N., Elowe, S., Nigg, E. A., and Inagaki, M. (2013). PI 3-kinase-dependent phosphorylation of Plk1-Ser99 promotes association with 14-3-3gamma and is required for metaphase-anaphase transition. Nat Commun 4, 1882.

Keller, C., Arenkiel, B. R., Coffin, C. M., El-Bardeesy, N., DePinho, R. A., and Capecchi, M. R. (2004). Alveolar rhabdomyosarcomas in conditional Pax3:Fkhr mice: cooperativity of Ink4a/ARF and Trp53 loss of function. Genes Dev 18, 2614-2626.

Keller, C., and Capecchi, M. R. (2005). New genetic tactics to model alveolar rhabdomyosarcoma in the mouse. Cancer Res 65, 7530-7532.

Keller, C., and Guttridge, D. C. (2013). Mechanisms of impaired differentiation in rhabdomyosarcoma. Febs J 280, 4323-4334.

Kettenbach, A. N., Wang, T., Faherty, B. K., Madden, D. R., Knapp, S., Bailey-Kellogg, C., and Gerber, S. A. (2012). Rapid determination of multiple linear kinase substrate motifs by mass spectrometry. Chem Biol 19, 608-618.

Khan, J., Simon, R., Bittner, M., Chen, Y., Leighton, S. B., Pohida, T., Smith, P. D., Jiang, Y., Gooden, G. C., Trent, J. M., and Meltzer, P. S. (1998). Gene expression profiling of alveolar rhabdomyosarcoma with cDNA microarrays. Cancer Res 58, 5009-5013.

Khan, J., Wei, J. S., Ringner, M., Saal, L. H., Ladanyi, M., Westermann, F., Berthold, F., Schwab, M., Antonescu, C. R., Peterson, C., and Meltzer, P. S. (2001). Classification

and diagnostic prediction of cancers using gene expression profiling and artificial neural networks. Nat Med 7, 673-679.

Kikuchi, K., Hettmer, S., Aslam, M. I., Michalek, J. E., Laub, W., Wilky, B. A., Loeb, D. M., Rubin, B. P., Wagers, A. J., and Keller, C. (2014). Cell-cycle dependent expression of a translocation-mediated fusion oncogene mediates checkpoint adaptation in rhabdomyosarcoma. PLoS Genet 10, e1004107.

Kikuchi, K., Tsuchiya, K., Otabe, O., Gotoh, T., Tamura, S., Katsumi, Y., Yagyu, S., Tsubai-Shimizu, S., Miyachi, M., Iehara, T., and Hosoi, H. (2008). Effects of PAX3-FKHR on malignant phenotypes in alveolar rhabdomyosarcoma. Biochem Biophys Res Commun 365, 568-574.

King, S. I., Purdie, C. A., Bray, S. E., Quinlan, P. R., Jordan, L. B., Thompson, A. M., and Meek, D. W. (2012). Immunohistochemical detection of Polo-like kinase-1 (PLK1) in primary breast cancer is associated with TP53 mutation and poor clinical outcom. Breast Cancer Res 14, R40.

Kolb, E. A., Gorlick, R., Reynolds, C. P., Kang, M. H., Carol, H., Lock, R., Keir, S. T., Maris, J. M., Billups, C. A., Desjardins, C., et al. (2013). Initial testing (stage 1) of eribulin, a novel tubulin binding agent, by the pediatric preclinical testing program. Pediatr Blood Cancer 60, 1325-1332.

Kovar, H. (2014). Blocking the road, stopping the engine or killing the driver? Advances in targeting EWS/FLI-1 fusion in Ewing sarcoma as novel therapy. Expert Opin Ther Targets, 1-14.

Lae, M., Ahn, E. H., Mercado, G. E., Chuai, S., Edgar, M., Pawel, B. R., Olshen, A., Barr, F. G., and Ladanyi, M. (2007). Global gene expression profiling of PAX-FKHR fusion-positive alveolar and PAX-FKHR fusion-negative embryonal rhabdomyosarcomas. J Pathol 212, 143-151.

Lee, M. H., Jothi, M., Gudkov, A. V., and Mal, A. K. (2011). Histone methyltransferase KMT1A restrains entry of alveolar rhabdomyosarcoma cells into a myogenic differentiated state. Cancer Res 71, 3921-3931.

Lee, K. S., Park, J. E., Kang, Y. H., Kim, T. S., and Bang, J. K. (2014). Mechanisms underlying Plk1 polo-box domain-mediated biological processes and their physiological significance. Mol Cells 37, 286-294.

Lenart, P., Petronczki, M., Steegmaier, M., Di Fiore, B., Lipp, J. J., Hoffmann, M., Rettig, W. J., Kraut, N., and Peters, J. M. (2007). The small-molecule inhibitor BI 2536 reveals novel insights into mitotic roles of polo-like kinase 1. Curr Biol 17, 304-315.

Lesko, E., Gozdzik, J., Kijowski, J., Jenner, B., Wiecha, O., and Majka, M. (2007). HSP90 antagonist, geldanamycin, inhibits proliferation, induces apoptosis and blocks migration of rhabdomyosarcoma cells in vitro and seeding into bone marrow in vivo. Anticancer Drugs 18, 1173-1181.

Li, S. Q., Cheuk, A. T., Shern, J. F., Song, Y. K., Hurd, L., Liao, H., Wei, J. S., and Khan, J. (2013). Targeting Wild-Type and Mutationally Activated FGFR4 in Rhabdomyosarcoma with the Inhibitor Ponatinib (AP24534). PLoS One 8, e76551.

Linabery, A. M., and Ross, J. A. (2008). Childhood and adolescent cancer survival in the US by race and ethnicity for the diagnostic period 1975-1999. Cancer 113, 2575-2596.

Linardic, C. M. (2008). PAX3-FOXO1 fusion gene in rhabdomyosarcoma. Cancer Lett 270, 10-18.

Lisboa, S., Cerveira, N., Vieira, J., Torres, L., Ferreira, A. M., Afonso, M., Norton, L., Henrique, R., and Teixeira, M. R. (2008). Genetic diagnosis of alveolar rhabdomyosarcoma in the bone marrow of a patient without evidence of primary tumor. Pediatr Blood Cancer 51, 554-557.

Liu, L., Wu, J., Ong, S. S., and Chen, T. (2013a). Cyclin-dependent kinase 4 phosphorylates and positively regulates PAX3-FOXO1 in human alveolar rhabdomyosarcoma cells. PLoS One 8, e58193.

Liu, X., Choy, E., Harmon, D., Yang, S., Yang, C., Mankin, H., Hornicek, F. J., and Duan, Z. (2011). Inhibition of polo-like kinase 1 leads to the suppression of osteosarcoma cell growth in vitro and in vivo. Anticancer Drugs 22, 444-453.

Liu, X., and Erikson, R. L. (2003). Polo-like kinase (Plk)1 depletion induces apoptosis in cancer cells. Proc Natl Acad Sci U S A 100, 5789-5794.

Liu, X., Lei, M., and Erikson, R. L. (2006). Normal cells, but not cancer cells, survive severe Plk1 depletion. Mol Cell Biol 26, 2093-2108.

Liu, Z., Ren, J., Cao, J., He, J., Yao, X., Jin, C., and Xue, Y. (2013b). Systematic analysis of the Plk-mediated phosphoregulation in eukaryotes. Brief Bioinform 14, 344-360.

Lu, B., Mahmud, H., Maass, A. H., Yu, B., van Gilst, W. H., de Boer, R. A., and Sillje, H. H. (2010). The Plk1 inhibitor BI 2536 temporarily arrests primary cardiac fibroblasts in mitosis and generates aneuploidy in vitro. PLoS One 5, e12963.

Lu, L. Y., Wood, J. L., Minter-Dykhouse, K., Ye, L., Saunders, T. L., Yu, X., and Chen, J. (2008). Polo-like kinase 1 is essential for early embryonic development and tumor suppression. Mol Cell Biol 28, 6870-6876.

Malempati, S., and Hawkins, D. S. (2012). Rhabdomyosarcoma: review of the Children's Oncology Group (COG) Soft-Tissue Sarcoma Committee experience and rationale for current COG studies. Pediatr Blood Cancer 59, 5-10.

Marshall, A. D., and Grosveld, G. C. (2012). Alveolar rhabdomyosarcoma - The molecular drivers of PAX3/7-FOXO1-induced tumorigenesis. Skelet Muscle 2, 25.

Marshall, A. D., van der Ent, M. A., and Grosveld, G. C. (2012). PAX3-FOXO1 and FGFR4 in alveolar rhabdomyosarcoma. Mol Carcinog 51, 807-815.

Mason, J. M., Lin, D. C., Wei, X., Che, Y., Yao, Y., Kiarash, R., Cescon, D. W., Fletcher, G. C., Awrey, D. E., Bray, M. R., et al. (2014). Functional Characterization of CFI-400945, a Polo-like Kinase 4 Inhibitor, as a Potential Anticancer Agent. Cancer Cell 26, 163-176.

Meggio, F., Shugar, D., and Pinna, L. A. (1990). Ribofuranosyl-benzimidazole derivatives as inhibitors of casein kinase-2 and casein kinase-1. Eur J Biochem 187, 89-94.

Miller, P. J., and Hollenbach, A. D. (2007). The oncogenic fusion protein Pax3-FKHR has a greater post-translational stability relative to Pax3 during early myogenesis. Biochim Biophys Acta 1770, 1450-1458.

Miller, P. J., Dietz, K. N., and Hollenbach, A. D. (2008). Identification of serine 205 as a site of phosphorylation on Pax3 in proliferating but not differentiating primary myoblasts. Protein Sci 17, 1979-1986.

Missiaglia, E., Williamson, D., Chisholm, J., Wirapati, P., Pierron, G., Petel, F., Concordet, J. P., Thway, K., Oberlin, O., Pritchard-Jones, K., et al. (2012). PAX3/FOXO1 fusion gene status is the key prognostic molecular marker in rhabdomyosarcoma and significantly improves current risk stratification. J Clin Oncol 30, 1670-1677.

Mross, K., Frost, A., Steinbild, S., Hedbom, S., Rentschler, J., Kaiser, R., Rouyrre, N., Trommeshauser, D., Hoesl, C. E., and Munzert, G. (2008). Phase I dose escalation and pharmacokinetic study of BI 2536, a novel Polo-like kinase 1 inhibitor, in patients with advanced solid tumors. J Clin Oncol 26, 5511-5517.

Naini, S., Etheridge, K. T., Adam, S. J., Qualman, S. J., Bentley, R. C., Counter, C. M., and Linardic, C. M. (2008). Defining the cooperative genetic changes that temporally drive alveolar rhabdomyosarcoma. Cancer Res 68, 9583-9588.

Ognjanovic, S., Linabery, A. M., Charbonneau, B., and Ross, J. A. (2009). Trends in childhood rhabdomyosarcoma incidence and survival in the United States, 1975-2005. Cancer 115, 4218-4226.

Olanich, M. E., and Barr, F. G. (2013). A call to ARMS: targeting the PAX3-FOXO1 gene in alveolar rhabdomyosarcoma. Expert Opin Ther Targets 17, 607-623.

Paulson, V., Chandler, G., Rakheja, D., Galindo, R. L., Wilson, K., Amatruda, J. F., and Cameron, S. (2011). High-resolution array CGH identifies common mechanisms that drive embryonal rhabdomyosarcoma pathogenesis. Genes Chromosomes Cancer 50, 397-408.

Petricoin, E. F., 3rd, Espina, V., Araujo, R. P., Midura, B., Yeung, C., Wan, X., Eichler, G. S., Johann, D. J., Jr., Qualman, S., Tsokos, M., et al. (2007). Phosphoprotein pathway mapping: Akt/mammalian target of rapamycin activation is negatively associated with childhood rhabdomyosarcoma survival. Cancer Res 67, 3431-3440.

Puissant, A., Frumm, S. M., Alexe, G., Bassil, C. F., Qi, J., Chanthery, Y. H., Nekritz, E. A., Zeid, R., Gustafson, W. C., Greninger, P., et al. (2013). Targeting MYCN in neuroblastoma by BET bromodomain inhibition. Cancer Discov 3, 308-323.

Raab, M., Kappel, S., Kramer, A., Sanhaji, M., Matthess, Y., Kurunci-Csacsko, E., Calzada-Wack, J., Rathkolb, B., Rozman, J., Adler, T., et al. (2011). Toxicity

modelling of Plk1-targeted therapies in genetically engineered mice and cultured primary mammalian cells. Nat Commun 2, 395.

Reinhardt, H. C., and Yaffe, M. B. (2013). Phospho-Ser/Thr-binding domains: navigating the cell cycle and DNA damage response. Nat Rev Mol Cell Biol 14, 563-580.

Rena, G., Woods, Y. L., Prescott, A. R., Peggie, M., Unterman, T. G., Williams, M. R., and Cohen, P. (2002). Two novel phosphorylation sites on FKHR that are critical for its nuclear exclusion. Embo J 21, 2263-2271.

Renshaw, J., Taylor, K. R., Bishop, R., Valenti, M., De Haven Brandon, A., Gowan, S., Eccles, S. A., Ruddle, R. R., Johnson, L. D., Raynaud, F. I., et al. (2013). Dual Blockade of the PI3K/AKT/mTOR (AZD8055) and RAS/MEK/ERK (AZD6244) Pathways Synergistically Inhibits Rhabdomyosarcoma Cell Growth In Vitro and In Vivo. Clin Cancer Res 19, 5940-5951.

Rizki, A., Mott, J. D., and Bissell, M. J. (2007). Polo-like kinase 1 is involved in invasion through extracellular matrix. Cancer Res 67, 11106-11110.

Roeb, W., Boyer, A., Cavenee, W. K., and Arden, K. C. (2007). PAX3-FOXO1 controls expression of the p57Kip2 cell-cycle regulator through degradation of EGR1. Proc Natl Acad Sci U S A 104, 18085-18090.

Roeb, W., Boyer, A., Cavenee, W. K., and Arden, K. C. (2008). Guilt by association: PAX3-FOXO1 regulates gene expression through selective destabilization of the EGR1 transcription factor. Cell Cycle 7, 837-841.

Rubin, B. P., Nishijo, K., Chen, H. I., Yi, X., Schuetze, D. P., Pal, R., Prajapati, S. I., Abraham, J., Arenkiel, B. R., Chen, Q. R., et al. (2011). Evidence for an unanticipated relationship between undifferentiated pleomorphic sarcoma and embryonal rhabdomyosarcoma. Cancer Cell 19, 177-191.

Rudolph, D., Steegmaier, M., Hoffmann, M., Grauert, M., Baum, A., Quant, J., Haslinger, C., Garin-Chesa, P., and Adolf, G. R. (2009). BI 6727, a Polo-like kinase inhibitor with improved pharmacokinetic profile and broad antitumor activity. Clin Cancer Res 15, 3094-3102.

Salvi, M., Trashi, E., Cozza, G., Franchin, C., Arrigoni, G., and Pinna, L. A. (2012). Investigation on PLK2 and PLK3 substrate recognition. Biochim Biophys Acta 1824, 1366-1373.

Sanhaji, M., Kreis, N. N., Zimmer, B., Berg, T., Louwen, F., and Yuan, J. (2012). p53 is not directly relevant to the response of Polo-like kinase 1 inhibitors. Cell Cycle 11, 543-553.

Sanhaji, M., Louwen, F., Zimmer, B., Kreis, N. N., Roth, S., and Yuan, J. (2013). Polo-like kinase 1 inhibitors, mitotic stress and the tumor suppressor p53. Cell Cycle 12, 1340-1351.

Schoffski, P. (2009). Polo-like kinase (PLK) inhibitors in preclinical and early clinical development in oncology. Oncologist 14, 559-570.

Schoffski, P., Adkins, D., Blay, J. Y., Gil, T., Elias, A. D., Rutkowski, P., Pennock, G. K., Youssoufian, H., Gelderblom, H., Willey, R., and Grebennik, D. O. (2013). An open-label, phase 2 study evaluating the efficacy and safety of the anti-IGF-1R antibody cixutumumab in patients with previously treated advanced or metastatic soft-tissue sarcoma or Ewing family of tumours. Eur J Cancer 49, 3219-3228.

Schoffski, P., Awada, A., Dumez, H., Gil, T., Bartholomeus, S., Wolter, P., Taton, M., Fritsch, H., Glomb, P., and Munzert, G. (2012). A phase I, dose-escalation study of the novel Polo-like kinase inhibitor volasertib (BI 6727) in patients with advanced solid tumours. Eur J Cancer 48, 179-186.

Scholl, F. A., Betts, D. R., Niggli, F. K., and Schafer, B. W. (2000). Molecular features of a human rhabdomyosarcoma cell line with spontaneous metastatic progression. Br J Cancer 82, 1239-1245.

Shapiro, D. N., Sublett, J. E., Li, B., Downing, J. R., and Naeve, C. W. (1993). Fusion of PAX3 to a member of the forkhead family of transcription factors in human alveolar rhabdomyosarcoma. Cancer Res 53, 5108-5112.

Shern, J. F., Chen, L., Chmielecki, J., Wei, J. S., Patidar, R., Rosenberg, M., Ambrogio, L., Auclair, D., Wang, J., Song, Y. K.*, et al.* (2014). Comprehensive genomic analysis of rhabdomyosarcoma reveals a landscape of alterations affecting a common genetic axis in fusion-positive and fusion-negative tumors. Cancer Discov *4*, 216-231.

Shor, A. C., Keschman, E. A., Lee, F. Y., Muro-Cacho, C., Letson, G. D., Trent, J. C., Pledger, W. J., and Jove, R. (2007). Dasatinib inhibits migration and invasion in diverse human sarcoma cell lines and induces apoptosis in bone sarcoma cells dependent on SRC kinase for survival. Cancer Res 67, 2800-2808.

Shukla, N., Ameur, N., Yilmaz, I., Nafa, K., Lau, C. Y., Marchetti, A., Borsu, L., Barr, F. G., and Ladanyi, M. (2012). Oncogene mutation profiling of pediatric solid tumors reveals significant subsets of embryonal rhabdomyosarcoma and neuroblastoma with mutated genes in growth signaling pathways. Clin Cancer Res 18, 748-757.

Smith, M. A., Morton, C. L., Phelps, D. A., Kolb, E. A., Lock, R., Carol, H., Reynolds, C. P., Maris, J. M., Keir, S. T., Wu, J., and Houghton, P. J. (2008). Stage 1 testing and pharmacodynamic evaluation of the HSP90 inhibitor alvespimycin (17-DMAG, KOS-1022) by the pediatric preclinical testing program. Pediatr Blood Cancer 51, 34-41.

Smith, M. A., Seibel, N. L., Altekruse, S. F., Ries, L. A., Melbert, D. L., O'Leary, M., Smith, F. O., and Reaman, G. H. (2010). Outcomes for children and adolescents with cancer: challenges for the twenty-first century. J Clin Oncol 28, 2625-2634.

Smith, M. R., Wilson, M. L., Hamanaka, R., Chase, D., Kung, H., Longo, D. L., and Ferris, D. K. (1997). Malignant transformation of mammalian cells initiated by constitutive expression of the polo-like kinase. Biochem Biophys Res Commun 234, 397-405.

Sorensen, P. H., Lynch, J. C., Qualman, S. J., Tirabosco, R., Lim, J. F., Maurer, H. M., Bridge, J. A., Crist, W. M., Triche, T. J., and Barr, F. G. (2002). PAX3-FKHR and PAX7-FKHR gene fusions are prognostic indicators in alveolar rhabdomyosarcoma: a report from the children's oncology group. J Clin Oncol 20, 2672-2679.

Spankuch-Schmitt, B., Bereiter-Hahn, J., Kaufmann, M., and Strebhardt, K. (2002a). Effect of RNA silencing of polo-like kinase-1 (PLK1) on apoptosis and spindle formation in human cancer cells. J Natl Cancer Inst 94, 1863-1877.

Spankuch-Schmitt, B., Wolf, G., Solbach, C., Loibl, S., Knecht, R., Stegmuller, M., von Minckwitz, G., Kaufmann, M., and Strebhardt, K. (2002b). Downregulation of human polo-like kinase activity by antisense oligonucleotides induces growth inhibition in cancer cells. Oncogene 21, 3162-3171.

Steegmaier, M., Hoffmann, M., Baum, A., Lenart, P., Petronczki, M., Krssak, M., Gurtler, U., Garin-Chesa, P., Lieb, S., Quant, J., et al. (2007). BI 2536, a potent and selective inhibitor of polo-like kinase 1, inhibits tumor growth in vivo. Curr Biol 17, 316-322.

Stegmaier, S., Poremba, C., Schaefer, K. L., Leuschner, I., Kazanowska, B., Bekassy, A. N., Bielack, S. S., Klingebiel, T., and Koscielniak, E. (2011). Prognostic value of PAX-FKHR fusion status in alveolar rhabdomyosarcoma: a report from the cooperative soft tissue sarcoma study group (CWS). Pediatr Blood Cancer 57, 406-414.

Strebhardt, K. (2010). Multifaceted polo-like kinases: drug targets and antitargets for cancer therapy. Nat Rev Drug Discov 9, 643-660.

Strebhardt, K., Becker, S., and Matthess, Y. (2014). Thoughts on the current assessment of Polo-like kinase inhibitor drug discovery. Expert Opin Drug Discov, 1-8.

Strebhardt, K., and Ullrich, A. (2006). Targeting polo-like kinase 1 for cancer therapy. Nat Rev Cancer 6, 321-330.

Sultan, I., Qaddoumi, I., Yaser, S., Rodriguez-Galindo, C., and Ferrari, A. (2009). Comparing adult and pediatric rhabdomyosarcoma in the surveillance, epidemiology and end results program, 1973 to 2005: an analysis of 2,600 patients. J Clin Oncol 27, 3391-3397.

Sur, S., Pagliarini, R., Bunz, F., Rago, C., Diaz, L. A., Jr., Kinzler, K. W., Vogelstein, B., and Papadopoulos, N. (2009). A panel of isogenic human cancer cells suggests a therapeutic approach for cancers with inactivated p53. Proc Natl Acad Sci U S A 106, 3964-3969.

Tan, J., Li, Z., Lee, P. L., Guan, P., Aau, M. Y., Lee, S. T., Feng, M., Lim, C. Z., Lee, E. Y., Wee, Z. N., et al. (2013). PDK1 signaling toward PLK1-MYC activation confers oncogenic transformation, tumor-initiating cell activation, and resistance to mTOR-targeted therapy. Cancer Discov 3, 1156-1171.

Taylor, J. G. t., Cheuk, A. T., Tsang, P. S., Chung, J. Y., Song, Y. K., Desai, K., Yu, Y., Chen, Q. R., Shah, K., Youngblood, V., et al. (2009). Identification of FGFR4-

activating mutations in human rhabdomyosarcomas that promote metastasis in xenotransplanted models. J Clin Invest 119, 3395-3407.

Thuault, S., Hayashi, S., Lagirand-Cantaloube, J., Plutoni, C., Comunale, F., Delattre, O., Relaix, F., and Gauthier-Rouviere, C. (2013). P-cadherin is a direct PAX3-FOXO1A target involved in alveolar rhabdomyosarcoma aggressiveness. Oncogene 32, 1876-1887.

Tomasetti, C., Vogelstein, B., and Parmigiani, G. (2013). Half or more of the somatic mutations in cancers of self-renewing tissues originate prior to tumor initiation. Proc Natl Acad Sci U S A 110, 1999-2004.

Triscott, J., Lee, C., Foster, C., Manoranjan, B., Pambid, M. R., Berns, R., Fotovati, A., Venugopal, C., O'Halloran, K., Narendran, A., et al. (2013). Personalizing the Treatment of Pediatric Medulloblastoma: Polo-like Kinase 1 as a Molecular Target in High-Risk Children. Cancer Res 73, 6734-6744.

Van Gaal, J. C., De Bont, E. S., Kaal, S. E., Versleijen-Jonkers, Y., and van der Graaf, W. T. (2012a). Building the bridge between rhabdomyosarcoma in children, adolescents and young adults: the road ahead. Crit Rev Oncol Hematol 82, 259-279.

van Gaal, J. C., Flucke, U. E., Roeffen, M. H., de Bont, E. S., Sleijfer, S., Mavinkurve-Groothuis, A. M., Suurmeijer, A. J., van der Graaf, W. T., and Versleijen-Jonkers, Y. M. (2012b). Anaplastic lymphoma kinase aberrations in rhabdomyosarcoma: clinical and prognostic implications. J Clin Oncol 30, 308-315.

van Vugt, M. A., van de Weerdt, B. C., Vader, G., Janssen, H., Calafat, J., Klompmaker, R., Wolthuis, R. M., and Medema, R. H. (2004). Polo-like kinase-1 is required for bipolar spindle formation but is dispensable for anaphase promoting complex/Cdc20 activation and initiation of cytokinesis. J Biol Chem 279, 36841-36854.

Venerando, A., Ruzzene, M., and Pinna, L. A. (2014). Casein kinase: the triple meaning of a misnomer. Biochem J 460, 141-156.

Vogel, K. S., Klesse, L. J., Velasco-Miguel, S., Meyers, K., Rushing, E. J., and Parada, L. F. (1999). Mouse tumor model for neurofibromatosis type 1. Science 286, 2176-2179.

Vogelstein, B., Papadopoulos, N., Velculescu, V. E., Zhou, S., Diaz, L. A., Jr., and Kinzler, K. W. (2013). Cancer genome landscapes. Science 339, 1546-1558.

Wachtel, M., Dettling, M., Koscielniak, E., Stegmaier, S., Treuner, J., Simon-Klingenstein, K., Buhlmann, P., Niggli, F. K., and Schafer, B. W. (2004). Gene expression signatures identify rhabdomyosarcoma subtypes and detect a novel t(2;2)(q35;p23) translocation fusing PAX3 to NCOA1. Cancer Res 64, 5539-5545.

Wachtel, M., Runge, T., Leuschner, I., Stegmaier, S., Koscielniak, E., Treuner, J., Odermatt, B., Behnke, S., Niggli, F. K., and Schafer, B. W. (2006). Subtype and prognostic classification of rhabdomyosarcoma by immunohistochemistry. J Clin Oncol 24, 816-822.

Walters, Z. S., Villarejo-Balcells, B., Olmos, D., Buist, T. W., Missiaglia, E., Allen, R., Al-Lazikani, B., Garrett, M. D., Blagg, J., and Shipley, J. (2014). JARID2 is a direct target of the PAX3-FOXO1 fusion protein and inhibits myogenic differentiation of rhabdomyosarcoma cells. Oncogene 33, 1148-1157.

Ward, E., DeSantis, C., Robbins, A., Kohler, B., and Jemal, A. (2014). Childhood and adolescent cancer statistics, 2014. CA Cancer J Clin 64, 83-103.

Weigel, B., Malempati, S., Reid, J. M., Voss, S. D., Cho, S. Y., Chen, H. X., Krailo, M., Villaluna, D., Adamson, P. C., and Blaney, S. M. (2014). Phase 2 trial of cixutumumab in children, adolescents, and young adults with refractory solid tumors: a report from the Children's Oncology Group. Pediatr Blood Cancer 61, 452-456.

Williamson, D., Missiaglia, E., de Reynies, A., Pierron, G., Thuille, B., Palenzuela, G., Thway, K., Orbach, D., Lae, M., Freneaux, P., et al. (2010). Fusion gene-negative alveolar rhabdomyosarcoma is clinically and molecularly indistinguishable from embryonal rhabdomyosarcoma. J Clin Oncol 28, 2151-2158.

Wu, C. P., Hsiao, S. H., Sim, H. M., Luo, S. Y., Tuo, W. C., Cheng, H. W., Li, Y. Q., Huang, Y. H., and Ambudkar, S. V. (2013). Human ABCB1 (P-glycoprotein) and ABCG2 mediate resistance to BI 2536, a potent and selective inhibitor of Polo-like kinase 1. Biochem Pharmacol 86, 904-913.

Xue, Y., Ren, J., Gao, X., Jin, C., Wen, L., and Yao, X. (2008). GPS 2.0, a tool to predict kinase-specific phosphorylation sites in hierarchy. Mol Cell Proteomics 7, 1598-1608.

Yang, Z., MacQuarrie, K. L., Analau, E., Tyler, A. E., Dilworth, F. J., Cao, Y., Diede, S. J., and Tapscott, S. J. (2009). MyoD and E-protein heterodimers switch rhabdomyosarcoma cells from an arrested myoblast phase to a differentiated state. Genes Dev 23, 694-707.

Yeh, J. E., Toniolo, P. A., and Frank, D. A. (2013). Targeting transcription factors: promising new strategies for cancer therapy. Curr Opin Oncol 25, 652-658.

Yim, H. (2013). Current clinical trials with polo-like kinase 1 inhibitors in solid tumors. Anticancer Drugs 24, 999-1006.

Yuan, C., Wang, L., Zhou, L., and Fu, Z. (2014). The function of FOXO1 in the late phases of the cell cycle is suppressed by PLK1-mediated phosphorylation. Cell Cycle *13*, 807-819.

Zeng, F. Y., Dong, H., Cui, J., Liu, L., and Chen, T. (2010). Glycogen synthase kinase 3 regulates PAX3-FKHR-mediated cell proliferation in human alveolar rhabdomyosarcoma cells. Biochem Biophys Res Commun 391, 1049-1055.

Zhang, L., Marrano, P., Kumar, S., Leadley, M., Elias, E., Thorner, P., and Baruchel, S. (2013). Nab-paclitaxel is an active drug in preclinical model of pediatric solid tumors. Clin Cancer Res 19, 5972-5983.

Zhang, X. G., Lu, X. F., Jiao, X. M., Chen, B., and Wu, J. X. (2012). PLK1 gene suppresses cell invasion of undifferentiated thyroid carcinoma through the inhibition of CD44v6, MMP-2 and MMP-9. Exp Ther Med 4, 1005-1009.

11 Curriculum Vitae

Personal Details

Name:	THALHAMMER, Verena
Date of Birth	August 12, 1984
Nationality:	German
E-mail:	verena.thalhammer@gmx.ch

Education

Jul 2010 - Dec 2014	**University of Zurich, Switzerland** Life Science Graduate School Zurich Cancer Biology PhD Program Department of Oncology and Children's Research Center, University Children's Hospital Zurich
Oct 2007 - Mar 2010	**University of Regensburg, Germany** Biochemistry; Semester 7 – 9 Degree: Diplom, Jan 2010 Department of Biochemistry Thesis "DNA Methyltransferase 1: Regulation and Mechanisms of DNA Methylation"
Aug 2007 - May 2008	**University of Colorado, USA** Molecular, Cellular and Developmental Biology
Oct 2004 - Aug 2007	**University of Regensburg, Germany** Biochemistry; Semester 1 – 6
Sep 1995 - Jun 2004	**Comenius Gymnasium Deggendorf, Germany** Type: natural sciences General qualification for university entrance, Jun 2004

Interdisciplinary and Advanced Education

Courses

Oct 2013 - May 2014	**Graduate Campus, University of Zurich**
	Know-how in economics
	Project management for research
	Resource-focused stress management
	Negotiation and moderation techniques
Aug 2012 - Jan 2013	**Clinical Trials Center, University Hospital Zurich**
	GCP course I - III
Aug 2010	**University of Zurich**
	Course in laboratory animal science

Conferences

Apr 2014	American Association for Cancer Research Annual Meeting 2014, San Diego, CA
Jan 2013	Charles Rodolphe Brupbacher Symposium on Breakthroughs in Cancer Research and Therapy, Zurich
Apr 2012	American Association for Cancer Research Annual Meeting 2012, Chicago, IL
Feb 2011	Charles Rodolphe Brupbacher Symposium on Cancer Genome and DNA Repair, Zurich
Nov 2010	EORTC-NCI-AACR Symposium on Molecular Targets and Cancer Therapeutics, Berlin

Presentations

Oral Presentations

- Kolloquium in angewandter Krebsforschung, Zurich, May 2014

  Validation of PLK1 as a novel therapeutic target in alveolar rhabdomyosarcoma

- SPOG Meeting, Lugano, Jan 2014

  PLK1 as a novel therapeutic target in alveolar rhabdomyosarcoma

- Cancer Network Student's Retreat, Mar 2012

  Validation of PLK1 as a novel therapeutic target in alveolar rhabdomyosarcoma

- Kolloquium in angewandter Krebsforschung, Zurich, Apr 2011

  Regulators of PAX3-FKHR: PLK1 as a therapeutic target in alveolar rhabdomyosarcoma

Posters

- AACR Annual Meeting, San Diego, Apr 2014

  PLK1 regulates PAX3-FOXO1 stability and its inhibition mediates regression of alveolar rhabdomyosarcoma xenograft tumors

- Brupbacher Symposium, Zurich, Jan 2013

  Targeting of the oncogenic transcription factor PAX3-FKHR through inhibition of Polo-like kinase 1

- AACR Annual Meeting, Chicago, Apr 2012

  Validation of Polo-like kinase 1 as a novel therapeutic target in alveolar rhabdomyosarcoma

- FZK/CRC Retreat, Au, Oct 2012

  Validation of Polo-like kinase 1 as a novel therapeutic target in alveolar rhabdomyosarcoma

- Brupbacher Symposium, Zurich, Feb 2011

  Regulators of the oncogenic transcription factor PAX3-FKHR: Is PLK1 a new therapeutic target in alveolar rhabdomyosarcoma?

Publications

Thalhammer V, Lopez-Garcia LA, Herrero-Martin D, Hecker R, Laubscher D, Gierisch ME, Wachtel M, Bode P, Nanni P, Blank B, Koscielniak E, Schäfer BW. PLK1 phosphorylates PAX3-FOXO1 inhibition of which triggers regression of alveolar rhabdomyosarcoma. Accepted in Cancer Res 2014.

Boro A, Pretre K, Rechfeld F, Thalhammer V, Oesch S, Wachtel M, Schäfer BW, Niggli FK. Small-molecule screen identifies modulators of EWS/FLI1 target gene expression and cell survival in Ewing's sarcoma. Int J Cancer 2012; 131: 2153-64.

Felle M, Joppien S, Nemeth A, Diermeier S, Thalhammer V, Dobner T, Kremmer E, Kappler R, Längst G. The USP7/Dnmt1 complex stimulates the DNA methylation activity of Dnmt1 and regulates the stability of UHRF1. Nucleic Acids Res 2011; 39: 8355-65.

Van Blerkom J, Davis P, Thalhammer V. Regulation of mitochondrial polarity in mouse and human oocytes: the influence of cumulus derived nitric oxide. Mol Hum Reprod 2008; 14: 431-44.

12 Acknowledgements

First of all, I would like to thank Prof. Dr. Beat Schäfer for accepting me in his laboratory and giving me the opportunity to pursue my Ph.D. project, for his good advice and trust in my work.

I may also express my gratitude to the thesis committee members Prof. Dr. Alex Hajnal, Prof. Dr. Ian Frew, and Prof. Dr. Carola Ponzetto for their scientific suggestions and helpful discussions during our meetings.

I am thankful to Dr. Regina Hecker for introducing me into the research topic and Dr. Marco Wachtel for answering all my questions during my stay in the RMS lab. I would also like to thank PD Dr. Stefano Ferrari for his advice.

Big thanks also go to Dr. Laura Lopez, Dr. David Herrero and Dr. med. Peter Bode for great cooperation and all the good times we spent together in the lab.

Furthermore, I thank my master student Dominik Laubscher, and my colleagues Sabrina Steiert and Maria Gierisch for their help and contributions to my work.

I enjoyed being part of the AFS community and many thanks go to all former and current colleagues, especially to Anna, David, Elisa, Jürgen, Laura, Lucie, Melle, Nurhak, Patricia, and Sam for being great friends.

Last but not least, I would like to thank my parents, my brothers Manuel and Lukas, Jamina, and Piero for all their absolute, continuous support, for always cheering me up and putting things into perspective.